Stephen F. Austin State University

# SFA ScholarWorks

Spring 5-11-2024

# Depositional Facies Analysis of the Cotton Valley Group Sandstones of the Blackburn Field, Northern Louisiana using Well Logs and Cores; Implications for Carbon Sequestration

Frederick Owusu
*Stephen F Austin State University*, fredowusuqx@yahoo.com

Depositional Facies Analysis of the Cotton Valley Group Sandstones of the Blackburn Field, Northern Louisiana using Well Logs and Cores; Implications for Carbon Sequestration

Creative Commons License

Depositional Facies Analysis of the Cotton Valley Group Sandstones of the Blackburn

Field, Northern Louisiana using Well Logs and Cores; Implications for Carbon

Sequestration


By

FREDERICK OWUSU, Bachelor of Science


Presented to the Faculty of the Graduate School of

Stephen F. Austin State University

In Partial Fulfillment

Of the Requirements


For the Degree of

Master of Science Geology

STEPHEN F. AUSTIN STATE UNIVERSITY

May, 2024

Depositional Facies Analysis of the Cotton Valley Group Sandstones of the Blackburn

Field, Northern Louisiana using Well Logs and Cores; Implications for Carbon

Sequestration



By



FREDERICK OWUSU, Bachelors of Science



APPROVED:


_____
Dr. Julie Bloxson, Thesis Director


_____
Dr. R. LaRell Nielson, Committee Member


_____
Dr. Mindy Faulkner, Committee Member


_____
Dr. Robert Friedfeld, Committee Member


_____
Dr. Forrest Lane
Dean of Research and Graduate Studies

ABSTRACT

The Cotton Valley Group (CVG) consists of tight sandstones with heterogeneous reservoir properties due to variations in depositional environments and diagenesis, spanning across eastern Texas through the Florida panhandle. It has served as a hydrocarbon target since the 1940s, and with recent technological advances, there is renewed exploration of the tight reservoirs within the group. Across northern Louisiana, the CVG has moderate to good reservoir properties, whereas those south extending westward across the Sabine uplift into east Texas decrease in porosity and permeability. With reservoir depletion coupled with its relatively simple mineralogy, these sandstone units may serve as good, localized carbon capture, utilization, and storage (CCUS) reservoirs or benefit from secondary gas recovery.

This research is focused on the depositional conditions and reservoir characteristics, within the CVG, Claiborne Parish, Louisiana to create a preliminary geologic assessment for carbon sequestration in the Blackburn Field. This research utilizes both geophysical and sedimentological analyses, centered on core from the Worley Estate 29H-1 well, particularly focusing on the lower sandstone units. A combination of core descriptions, thin section analysis, x-ray diffraction and x-ray fluorescence are used to characterize reservoir properties. The CVG was divided into six units based upon changes in lithology in the core, correlated to the well log, and extrapolated across the Blackburn Field, northwest Claiborne Parish.

Overall, this group represents deposition ranging from tidal flats to lagoon to reworked barrier islands and reefal slope environments. The lithologies are comprised of sequences of quartz wackes, thinly bedded silty mudstones, quartz arenites, and wackestones. Porosity within the CVG Sandstones was mostly secondary in origin caused by fractures, dissolution of cements and fossils (bivalves), and minor primary intergranular pores. The porosity and permeability vary throughout the reservoir, restricted mainly by detrital clays, carbonate cementation, or protected by chlorite pore coatings. The sandstones of the CVG in the Blackburn Field may not be regarded as ideal $CO_2$ storage reservoirs due to their low porosity-permeability characteristics resulting from the clays and extensive carbonate cementation restricting pore throats.

# AKNOWLEDGEMENT

# Table of Contents

## LIST OF FIGURES

# LIST OF TABLES

# LIST OF APPENDICES

# 1.0 INTRODUCTION

The exploitation of fossil fuels for energy production has caused an increase in the emission of carbon dioxide ($CO_2$) gases into the atmosphere. This enhances greenhouse effects resulting in global warming (Bryant, 1997). The sources of these $CO_2$ emissions include power plants, petrochemical plants and refineries, and industrial processes (Bachu, 2003). About half of these $CO_2$ emissions are naturally sequestered into oceans and the terrestrial biosphere (plants and soils) each year, while the rest are accumulated in the atmosphere contributing to global warming (UNFCCC, 2015). Other forms of intervention, such as carbon sequestration, are needed to balance these increasing $CO_2$ emissions into the atmosphere (Duncan and Morrissey, 2011). To reduce these anthropogenic $CO_2$ emissions in the atmosphere, carbon sequestration or storage in geological media provides the best alternative to this effect (Bachu, 2003).

Carbon sequestration is defined as the method of storing carbon dioxide ($CO_2$) in the subsurface in deep geological formations to prevent its release into the atmosphere (Duncan and Morrissey, 2011). Underground carbon dioxide sequestration in sedimentary formations and carbon mineralization are considered the two methods for the long-term storage of carbon dioxide (NASEM, 2019). The formation of carbonate minerals such as calcite, dolomite, ankerite, or siderite from the dissolved cations and $CO_2$, also known as mineral trapping, is considered the safest and most effective long-term storage of $CO_2$ (Xu et al., 2005).

Sedimentary basins are favorable for the storage of $CO_2$ emissions due to their intrinsic characteristics. These include porosity, permeability, and geothermal regimes. Igneous and volcanic terranes are unsuitable for carbon storage due to a lack of porosity, permeability, and potential extensive fracture networks. Geologic media for carbon storage can include oil and gas reservoirs, sandstone and carbonate aquifers, coal beds, salt beds, and salt domes. An impermeable rock layer must overlie these formations to prevent the $CO_2$ gases from escaping (Bachu, 2003). Reservoir properties, fluid retention capacity, and cap-rock sealing strength are the critical parameters of concern (key issues) in $CO_2$ sequestration (Bachu et al., 2007). Deep saline reservoirs offer huge potential for the sequestration of larger volumes of $CO_2$ (Leetaru et al., 2009). In the United States, the Environmental Potential Agency considers aquifers with salinities less than 10,000 mg/L total dissolved solids as underground drinking water sources, excluding those with salinities above 10,000mg/L total dissolved solids, thereby serving as targets for the sequestration of $CO_2$ (Xu et al., 2005).

The sandstone reservoir within the Cotton Valley Group is a tight sandstone with variable porosity and permeability attributed to the diagenetic processes and the depositional environment. The Cotton Valley Group were a target for hydrocarbons in the 1940s but were considered uneconomical due to their low permeability and porosity (Dyman and Condon, 2006). Based on facies and reservoir properties, the Cotton Valley Group has been divided into blanket sandstones across northern Louisiana and down-dip massive sandstones to the south of blanket sandstones, extending westward across the

Sabine uplift into east Texas. The blanket sandstone has moderate to good reservoir properties, whereas the massive sandstones have low porosity and permeability (Dyman and Condon, 2006). This research aims to characterize the depositional conditions both temporally and spatially within the Cotton Valley Group, Claiborne Parish, Louisiana, to create a preliminary geologic assessment for carbon sequestration in the area. In addressing the global concerns of climate change, especially in the oil and gas sector, CCUS has proven to effectively reduce emissions into the atmosphere.

1.2 Objectives

The main objective of this research is to create a subsurface model for deposition and diagenesis of the Cotton Valley Group in Claiborne Parish, LA. This will be done by analyzing core via descriptions, XRF, XRD, and thin sections.

1. Assess the porosity and permeability controls on the Cotton Valley Group in Claiborne Parish. This will be conducted via thin section analysis to determine what is restricting porosity in the Cotton Valley.

2. Correlate the core data to the well log data, and extrapolate across the study area. This allows for the extrapolation of high-spatial resolution data (core) to geophysical proxies (well logs). Lithofacies and their corresponding controls on porosity and permeability from the core will be correlated to the log signatures and then mapped across the area to determine their extent.

3. Assess the $CO_2$ storage capacity and ability of the Cotton Valley Group in Claiborne Parish, LA.

## 2.0 CARBON SEQUESTRATION

2.1 Carbon sequestration in sandstones

Globally, experimental studies of geological sequestration of $CO_2$ in subsurface reservoirs have been conducted both on small scale (field) and larger scale (basins) (Xu et al., 2005). At the global scale, the deployment of large-scale carbon capture and storage projects is mainly based on enhanced oil recovery, which involves the injection of gaseous, liquid, or supercritical $CO_2$ in a subsurface reservoir to extract the oil remains from the field. Eventually, the injected $CO_2$ becomes trapped in the subsurface in the form of structural trapping, in the pore space (residual trapping), in fluids in the form of solubility trapping, or precipitates into a carbonate mineral (mineral trapping) as shown in Figure 1 (Snæbjörnsdóttir et al., 2020).
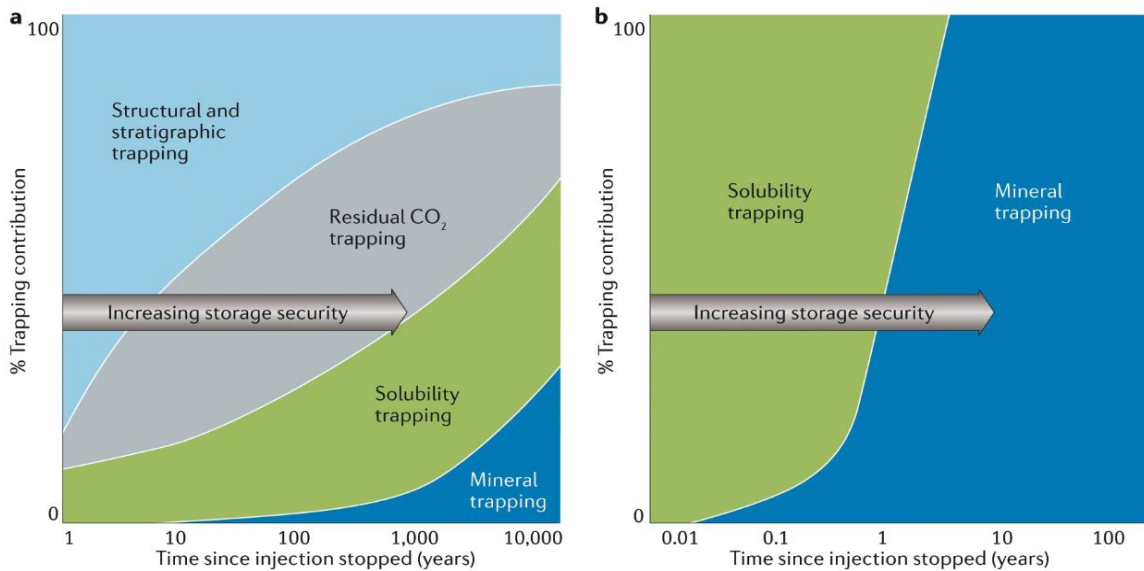


Figure 1 A) The change in carbon trapping mechanism of $CO_2$ storage over time when injecting pure supercritical $CO_2$ into sedimentary basins, B) When injecting water-dissolved $CO_2$ for mineralization (from Snæbjörnsdóttir et al., 2020).

Sandstone is ideal for capturing and storing $CO_2$, due to its high permeability, widespread distribution, and mineralogical and geochemical characteristics. Experimental studies conducted in the laboratory and in-situ under stimulation conditions on sandstones have shown a variance from fair to promising results. This depends on the nature of sandstones under analysis, due to factors such as micro-pores, mineral composition, and participation percentage (Christopoulou et al., 2022).

In the mid-western United States, the Cambrian-aged Mt. Simon sandstone, a saline reservoir, is used to store gas in the shallow parts of the Illinois basin. This sandstone, comprised of fine to coarser grains with interbeds of shale, has a potential sequestration capacity between 27 and 109 billion metric tonnes of $CO_2$, with the overlying Eau Claire Formation acting as the seal (Leetaru et al., 2009).

## 2.2 Geochemistry of mineral carbonation

One of the main factors that control the geochemical reactions of $CO_2$ in storage reservoirs is the pH. As $CO_2$ is injected into saline aquifers or reservoirs, the $CO_2$ is dissolved in water producing an acidic medium as shown in Equations 1 - 4 (Wang et al., 2017).

$$CO_2 \text{ (g)} \leftrightharpoons CO_2 \text{ (aq)} \ldots \text{Eqn (1)}$$

$$CO_2 \text{ (aq)} + H_2O \leftrightharpoons H_2CO_3 \text{ (aq)} \ldots \text{Eqn (2)}$$

$$H_2CO_3 \text{ (aq)} \leftrightharpoons HCO_3^- \text{ (aq)} + H^+ \text{ (aq)} \ldots \text{Eqn (3)}$$

$$\text{HCO}_3^- \text{ (aq)} \leftrightharpoons \text{CO}_3^{2-} \text{ (aq)} + \text{H}^+ \text{ (aq)} \dots \text{Eqn (4)}$$
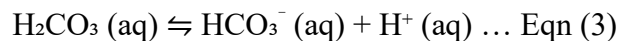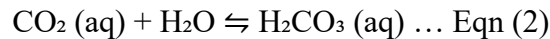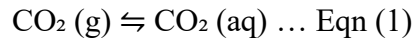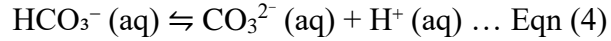
This facilitates the dissolution of silicate and oxide minerals resulting in an increase of ions (both cations and anions) such as $Ca^{2+}$, $Mg^{2+}$, $Na^+$, $SiO_4^{4-}$, or $Fe^{2+}$ in solution, thereby inducing secondary precipitation of minerals such as silica, silicates, and carbonates (Wang et al., 2019). Some examples of dissolution and precipitation are shown below in Equations 5 - 8:

$$\text{NaAlSi}_3\text{O}_8 \text{ (Na-feldspar)} + 4\text{H}^+ + 4\text{H}_2\text{O} \leftrightarrow \text{Na}^+ + \text{Al}^{3+} + 3\text{H}_4\text{SiO}_4 \text{ (aq)} \dots \text{Eqn (5)}$$

$$\text{CaAl}_2\text{Si}_2\text{O}_8 \text{ (Ca-feldspar)} + 8\text{H}^+ \leftrightarrow \text{Ca}^{2+} + 2\text{Al}^{3+} + 2\text{H}_4\text{SiO}_4 \text{ (aq)} \dots \text{Eqn (6)}$$

$$\text{Ca}^{2+} + \text{HCO}_3^- \leftrightarrow \text{CaCO}_3 \text{ (calcite)} + \text{H}^+ \dots \text{Eqn (7)}$$

$$\text{Fe}^{2+} + \text{HCO}_3^- \leftrightarrow \text{FeCO}_3 \text{ (siderite)} + \text{H}^+ \dots \text{Eqn (8)}$$
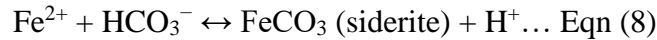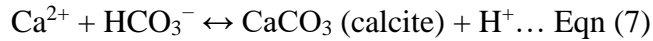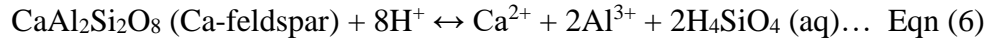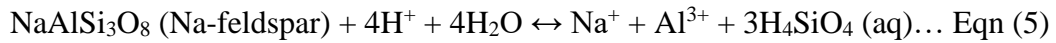
The main factors that control the extent of mineral dissolution and secondary mineral precipitation are the rock type, the distribution of reactive mineral phases, and diffusive mass transport conditions. In limestone reservoirs, the presence of minerals such as calcite and dolomite limits the acidity of the pore-water due to its strong pH buffering capacity, thereby altering the effects of the $CO_2$-brine interaction. Basalts are more reactive to $CO_2$-brine medium because they contain larger amounts of reactive minerals such as olivine, feldspars, and pyroxene, which result in significant reservoir alteration (Zhang et al., 2019). In sandstones, the $CO_2$-brine interaction is dependent on the mineral content; sandstones predominantly composed of quartz with less reactive minerals such as feldspar, chlorite, and hematite have limited $CO_2$-brine sandstone interactions and vice-versa for sandstones, with higher reactive minerals (Zhang et al., 2019).

The precipitation of carbonate and secondary minerals can clog the pathways, thereby affecting porosity and permeability. This is because these precipitated minerals tend to have larger volumes than the primary source minerals (Snæbjörnsdóttir et al., 2020).

Although CCUS may help reduce greenhouse emissions into the atmosphere, there are some key challenges in the storage of $CO_2$ in sedimentary basins. There is a tendency for the injected $CO_2$ (gaseous, liquid, or supercritical phase) to migrate back to the surface without an adequate seal. Also, achieving the climate goals may require identifying new storage reservoirs to accommodate the larger $CO_2$ volumes in the atmosphere. Lastly, the mineral trapping mechanism that results in carbonate minerals depends on silicate-bound divalent metals (Snæbjörnsdóttir et al., 2020).

# 3.0 GEOLOGIC SETTING

This study focuses on Jurassic-Aged sedimentary rocks in the Gulf of Mexico Basin. During the Triassic the area that would become the Gulf of Mexico Basin was situated along the equator as a part of the Pangea Supercontinent. Along the Gulf Coast Plain, rifting and segmentation of Pangea started in the Late Triassic and continued through to the Late Jurassic. The Yucatan Block moved away by a counterclockwise rotation and southerly drift, from the southeastern margin of the North American craton. This resulted in the opening of the Proto Gulf of Mexico, with flooding of marine waters from the Pacific into the depressed areas from the Middle to Late Jurassic (Atwell et al., 2008).

A thick accumulation of salt deposits within the basin occurred during this time, and subsequently, the development of carbonate ramps during the peak of transgression at the western and central margins of the Gulf of Mexico in the Late Jurassic (Atwell et al., 2008) as shown in Figure 2 below.
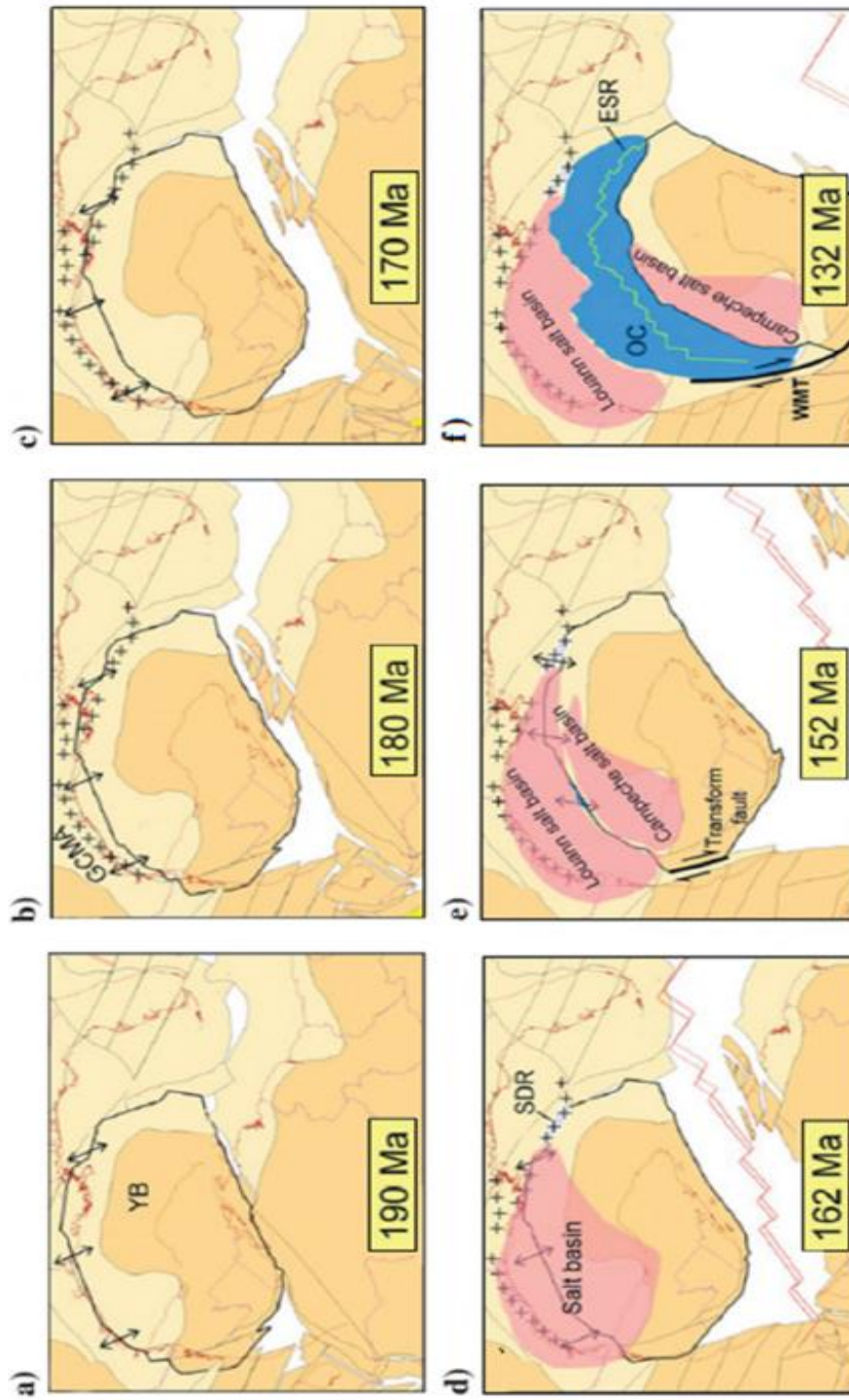
Figure 2 Late Triassic to Early Jurassic continental rifting occurred in a NW to SE direction between North America and the combined Yucatan-South American plate, starting from (a) 190 Ma when rifting was initiated through (f) 132 Ma where the Louann salt basin was separated by oceanic crust (OC). YB indicates the Yucatan block, and its counterclockwise rotation. GCMA indicates Gulf Coast Magnetic Anomaly (Cornelius S., 2023).

Sawyer et al. (1991) characterized the tectonic evolution of the Gulf of Mexico and related salt basins into three phases based on the distribution of crust type. First, the early rifting stage from the Late Triassic to the Early Jurassic was associated with the development of grabens bounded by listric normal faults and the deposition of non-marine siliciclastic sediments and volcanics. Continuous rifting through the Middle Jurassic was characterized by crustal thinning, formation of transitional crust, and accumulation of thick salt deposits. Lastly, the development of seafloor spreading and the formation of oceanic crust in the Late Jurassic phase. This phase was associated with crustal cooling, subsidence, and regional marine transgression.

The tectonic subsidence rates in the northern Gulf of Mexico during the Late Jurassic were 40m/my (130ft/my). The high stratigraphic base level during the Late Jurassic resulted in the creation of large accommodation space. The tectonic subsidence rates from the early Cretaceous to the Late Cretaceous were 22m/my (72ft/my) and 14m/my (46ft/my), respectively. This change in subsidence rate from high to low represents the evolution from syn-rift to post-rift passive margin development (Mancini et al., 2003).

The Jurassic deposits of the northern Gulf of Mexico represent early post-rift sediments, whereas the Upper Cretaceous deposits represent late post-rift sediments. The Jurassic sediments were deposited during a time of maximum accommodation due to thermal cooling and subsidence. The Upper Cretaceous was a period of less tectonic activity and less accommodation space. At the time, the stratal patterns were mainly controlled by sea-level changes. The post-rift deposits of the Lower Cretaceous represent

a change from a thermal subsidence event in the Late Jurassic to a period of highstand of the global sea level during the Late Cretaceous (Mancini et al., 2005).

The Cotton Valley Group is composed of terrigenous clastic sediment deposited in the northern Gulf of Mexico basins during the continental extension from the Late Triassic to Early Jurassic time (Eoff et al., 2015). These deposits represent a major influx of clastic sediments into the Gulf of Mexico. The south-central Mississippi, Louisiana-Mississippi border, and northeast Texas served as the major depocenters of the Cotton Valley Group (Dyman and Condon, 2006). During the initial phases of rifting, the Gulf of Mexico, East Texas, North Louisiana, and Mississippi salt basins were formed over thinned crust. This resulted in thick salt being deposited across the region, known as the Jurassic-aged Louann Salt, across the region. These basins are divided by a series of arches/uplifts (Eoff et al., 2015). The East Texas Basin is separated from the northern Louisiana Salt Basin by a basement arch known as the Sabine Uplifts (Dyman and Condon, 2006). In the Late Jurassic, these basins were flooded with marine waters due to the region's newly formed oceanic crust. This ended the salt deposits of the middle Jurassic (Eoff et al., 2015).

The Cotton Valley Group underlies most of the northern coastal plain of the Gulf of Mexico, extending from east Texas to Alabama (Figure 3). It is comprised of sandstones, shales, and limestone. It forms a sedimentary wedge that thickens and deepens southwards towards the Gulf of Mexico basins and pinches out (towards a zero edge) in southern Arkansas, central Mississippi, southern Alabama, and east Texas (Dyman and Condon, 2006). The Cotton Valley Group is present in East Texas basins, northern Louisiana salt

basins, and the Mississippi salt basins (Dyman and Condon, 2006). The Cotton Valley units reflect variations in depositional environments, extending southwards in a deepening basin (Forgotson, 1954). In northern Louisiana, the Cotton Valley Group represents a regressive depositional sequence, with three stratigraphic units, the Bossier Shales, Terryville Sandstone, and the Hico Shale. These are bounded on top by a carbonate unit known as the Knowles Limestone (Eversull, 1985).
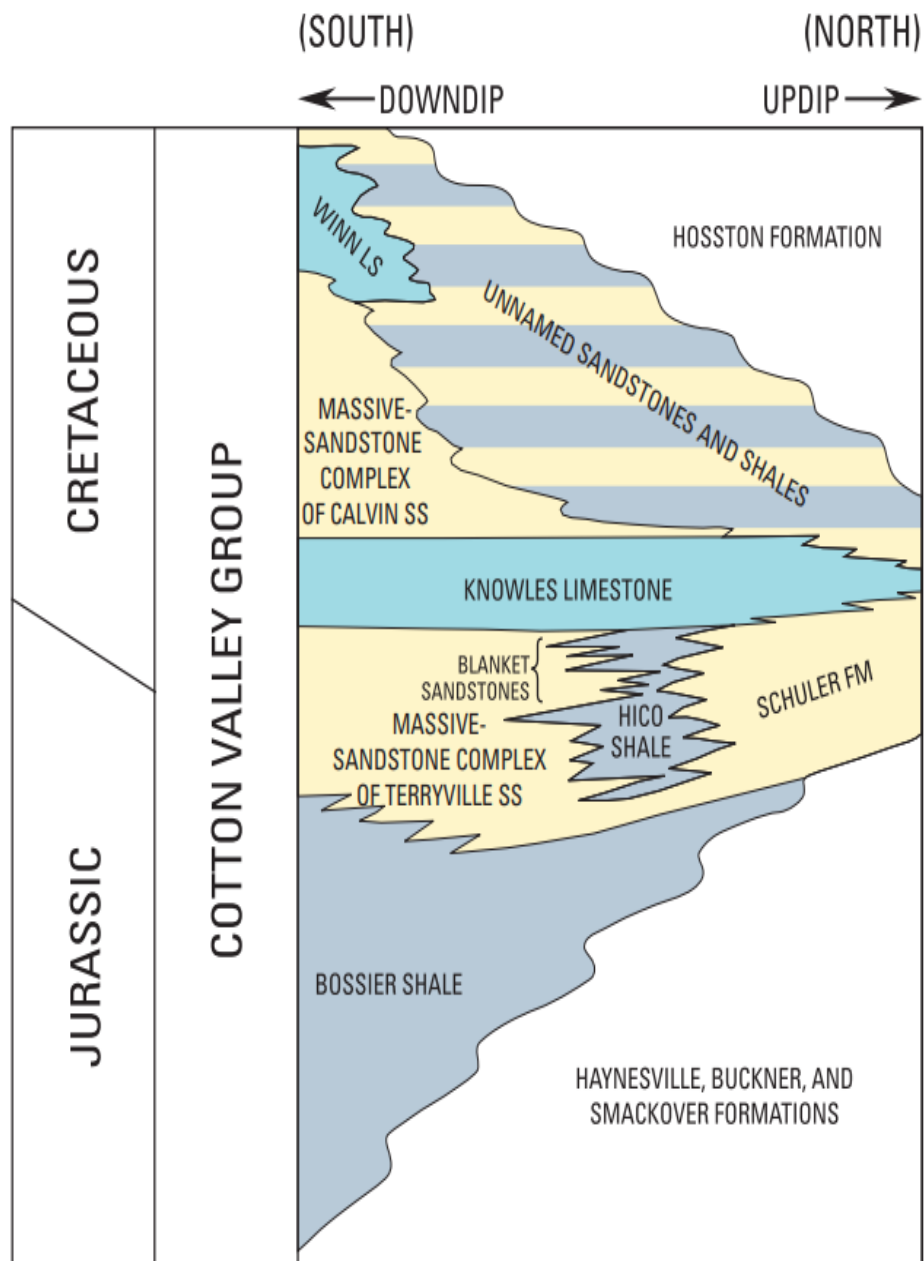
Figure 3 Generalized stratigraphic column of the Cotton Valley Group in northern Louisiana (Bartberger et al., 2002).

## 4.0 STRATIGRAPHY

Different interpretations have been published regarding the formation level subdivisions within Cotton Valley Group. These subdivisions are not universally accepted. In East Texas, an informal unit referred to as Taylor Sandstone is named within the Cotton Valley Sandstones, but is insignificant in northern Louisiana (Ewing, 2001). Also, regarding the upper bounding units within the Cotton Valley Group, Saucier (1985) interpreted the Knowles Limestone as the uppermost unit, whereas Coleman and Coleman (1981) included the Calvin Sandstone and the Winn Limestone as the uppermost bounding units of the CVG (Dyman and Condon, 2006).

### 4.1 Bossier Shale

The Bossier Shale forms the lowermost unit of the Cotton Valley Group. This comprises thick shale unit that conformably overlies the Haynesville Formation (Dyman and Condon, 2006). The Bossier Shale units are dark-grey, calcareous, fossiliferous, and of marine origin, ranging in thickness from ~250ft (76.2m) to ~2,000ft (609.6m) (Montgomery, 2001). The Bossier Shale was deposited during periods of low energy, and grades into the Terryville Sandstone. It overlies the Haynesville Formation, and the Smackover Formation in areas where the Haynesville Formation is absent (Mancini et al., 2008).

### 4.2 Terryville Sandstone

The Terryville Sandstone is a massive white quartz-arenite that overlies the Bossier Shale unit. It may reach a maximum thickness of about 1,400ft (426m). The Terryville Sandstone is interbedded with a few thin dark grey shales (Mancini, 2008). It is a very fine

to medium-grained quartz sandstone with several thin dark limestones and limey shales (Eversull, 1985). Based on the reservoir quality, it is subdivided into two units: the massive sandstones and the blanket sandstones. In northern Louisiana, the Terryville Sandstones are comprised of stacked barrier islands, offshore bars, strand-plains, and fluvial-deltaic units (Dyman and Condon, 2006).

The ancestral Mississippi River served as a source of large volumes of sand deposition into the Gulf of Mexico, in the form of a delta in northeastern Louisiana and adjacent Mississippi. These deltaic sands were reworked by the longshore current in a westward direction forming east-west barrier islands/strand-plain complexes along the shore, which resulted in the accumulation of Terryville Sandstones massive-sandstones complex (Dyman and Condon, 2006). These barrier islands/strand plains formed a boundary that separated the open marine water to the south from the lagoon to the north (landwards). The blanket sandstones were deposited from a period of transgression (relative sea level rise), that transported sediments northwards from the Terryville Sandstones massive-sandstones (barrier complex) into the Hico lagoon as shown in Figure 4.

These transgressive blanket sandstones comprise about 20 distinct tongues that extend northwards from the barrier complex, and thins upwards/pinches out into the Hico Shale. Generally, the transgressive blanket sandstone ranges in thickness from 30ft (9.1m) to 70 ft (21.3m) but may reach 140ft (42.7m) towards the south, where they thicken and deepen, merging into the Terryville Sandstones massive-sandstones complex (Dyman and Condon, 2006).
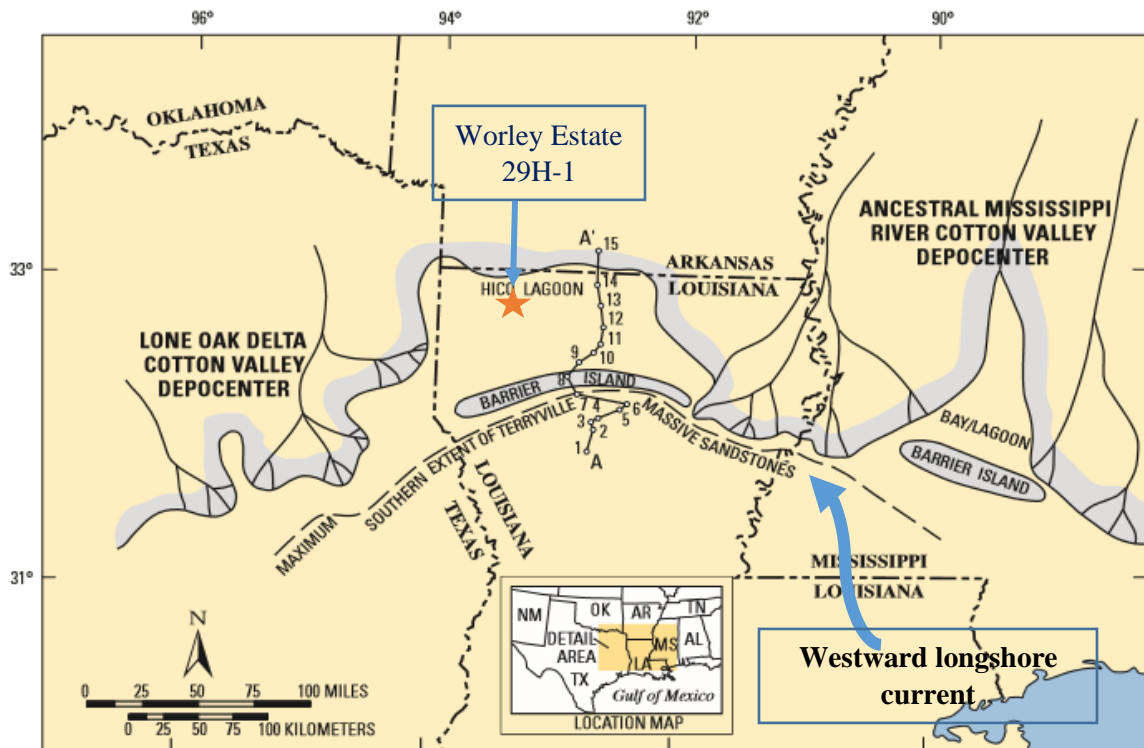
Figure 4 Paleogeography of the Uppermost Cotton Valley Group Sandstones (Modified from Coleman and Coleman, 1981). The study area is marked with an orange star, and was located in the Hico Lagoon during the time of deposition.

In East Texas, the stratigraphic equivalent of the Terryville Sandstone is referred to as the Cotton Valley Sandstones. This consists of braided-stream, fan-delta, and wave-dominated deltaic sandstones (Figure 5). The Terryville/Cotton Valley Sandstones average thickness ranges from 330-450m (1000–1400ft) in east Texas and northern Louisiana. In the east Texas basin, the Cotton Valley Sandstones are characterized by fan delta deposition along the western margin of the basin, and a wave-dominated deltaic system along the northern flanks due to the progradation of the fan deltas basinward by a mature

drainage system. The lower unit of these Cotton Valley Group Sandstones forms the Taylor Sands (Dyman and Condon, 2006).
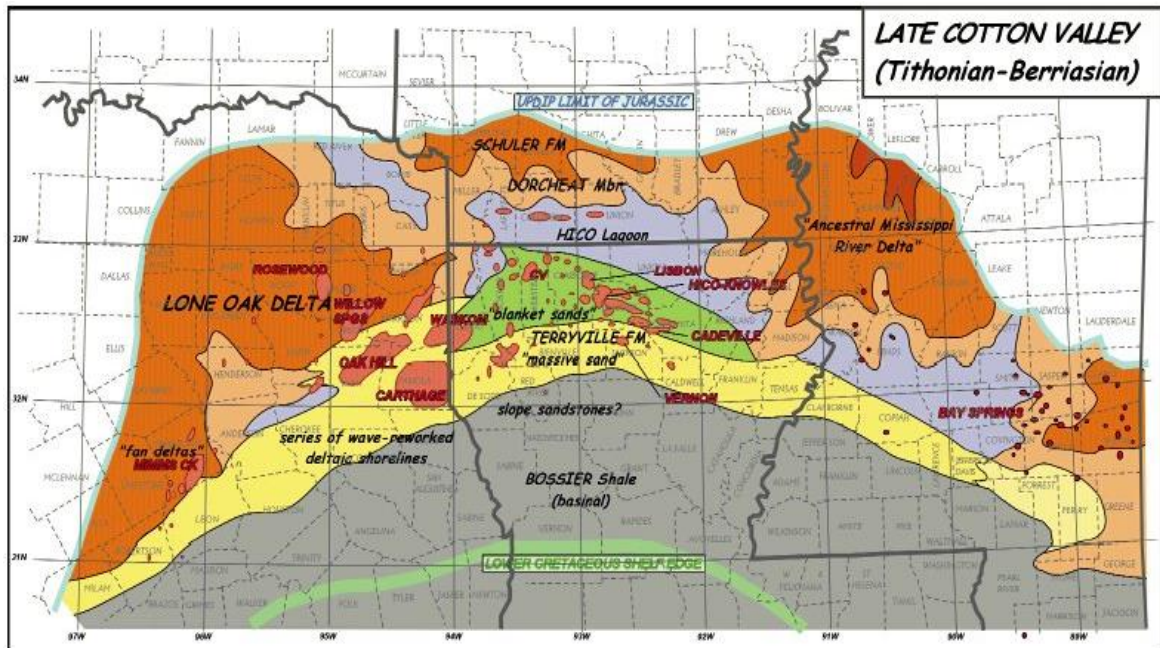


Figure 5 Map of depositional systems, late Cotton Valley (Tithonian — Berriasian) (Ewing, 2001).

4.3 Hico Shale

The Hico Shale was deposited in a lagoon environment (lagoonal facies) separated from the open marine by the barrier complex of the Terryville Sandstones massive-sandstones complex (Dyman and Condon, 2006). It is comprised of dark grey shales with thin beds of silty limestone, siltstone, and sandstone (Mancini, 2008). The Hico Shale interfingers the Schuler Formation towards the north.

4.4 Schuler Formation

The Schuler Formation is a progradational fluvial-deltaic sequence composed of siltstone, sandstone, and some shales (Mancini, 2010). The Schuler Formation was deposited in a continental environment, north of the Hico lagoon (landwards). It is comprised of fluvial and coastal plain sandstones and shales (Dyman and Condon, 2006), distinguished as a terrestrial red bed that grades downdip into the Hico, Bossier, Terryville, and Knowles formations (Eversull, 1985).

The Schuler Formation is subdivided into the Shongaloo and Dorcheat Members in the northeastern Gulf Coast lithostratigraphy, as shown in Figure 3. The Schongaloo is made of coastal sandstone deposits, whereas the Dorcheat Member is composed of sandstones, sandy shales, and conglomerates (Mancini, 2010). Further up-dip (northwards), the Schuler Formation is overlain by the Hosston Formation (Mancini, 2008).

4.5 Knowles Limestone

The Knowles Limestone is a 300-400ft (91.4m – 121.9m) thick carbonate unit that overlies the Schuler Formation across most parts of the US Gulf Coast. The Knowles Limestone represents a major sea level transgression phase (Mancini, 2010) during the Early Cretaceous which interrupted the deposition of sands allowing carbonate deposition (Figure 6) (Dyman and Condon, 2006). The Knowles Limestone is comprised of alternating beds of dark-grey argillaceous limestones and dark-grey shales that grade northwards into the red shales and sands of the Schuler Formation and forms the upper unit

of the Cotton Valley Group. It overlies the Terryville Sandstone, and Hico Shale (Thomas and Mann, 1966).

The deposition of the Knowles Limestone is followed by an unconformity, a sequence boundary in the Early Cretaceous. This hiatus was subsequently overlain by the Calvin Sandstones deposited on the shelf in Louisiana, followed by Winn Limestone, a transgressive carbonate unit (Ewing, 2001).
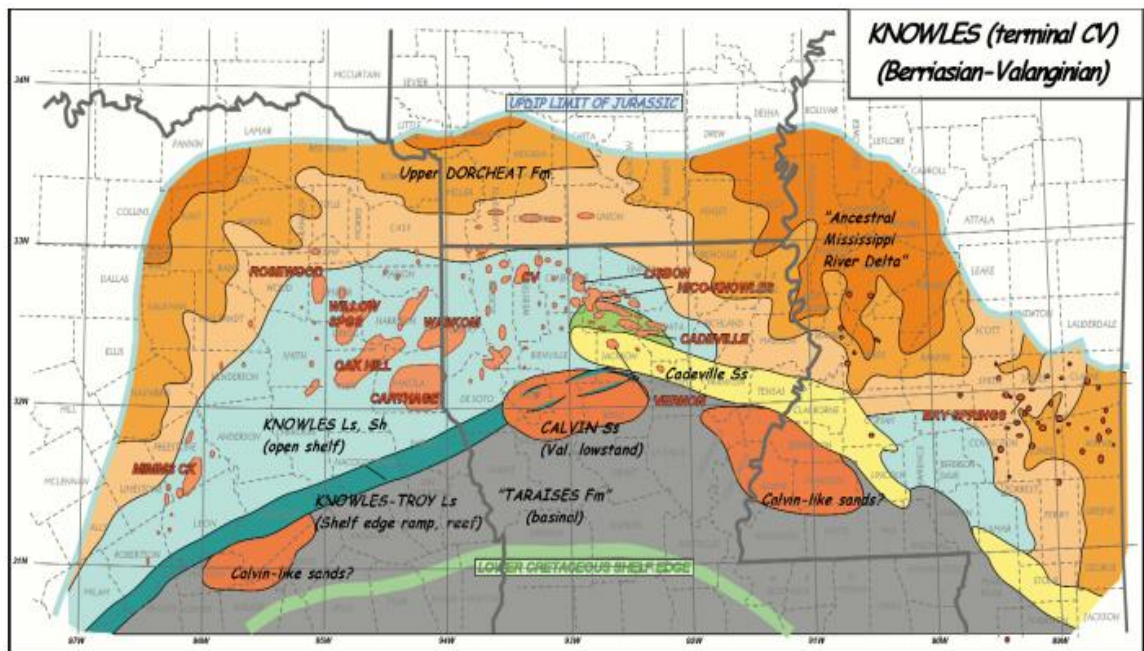


Figure 6 Map of depositional systems, Knowles Limestone (terminal Cotton Valley; Berriasian-Valanginian) (Ewing, 2001).

# 6.0 DATA AND METHODS

The methods used in this study involve core and well log analysis. The objectives are to create a high-level reservoir characterization for potential carbon sequestration efforts in the northern Louisiana area in the Cotton Valley Group Sandstones, and also to understand depositional characteristics so they could be extrapolated across the region at a later date if the sandstone is deemed suitable for injection.

## 6.1 Core analysis

The core used for this research study is from Worley Estate 29H-1 well, with API number 1702722589, from Claiborne Parish, Louisiana, donated by Buffco (Table 1). The core is housed at the Stephen F. Austin State University East Texas Core Repository (Core No. 206). This well is located in the Blackburn Field of the northeastern flank of the Sabine uplift. The core is 278ft (84.7m) long and drilled from depths of 9,877ft to 10,155ft (3,010.5m – 3,095.2m) within the Cotton Valley Group. A detailed description of the cores was made including color, grain sizes, lithofacies, sedimentary structures, fossils, and types of cement and veins. It was presented on a 1 inch = 1 ft scale. The sandstones were classified using Dott's (1964) classification whereas the limestones were classified using Dunham's (1962) classification. The rock color and grain sizes were described using the Geological Society of America rock color chart and Wentworth scale, respectively. An acid test (10% HCl) was used to distinguish calcite cement and veins from quartz, as calcite effervesces readily with an acid. Core lithologies were then correlated to the well logs, and

21

these core characteristics were then extrapolated throughout the field and just beyond the

field limits using well log analysis.

Table 1: Worley Estate 29H-1 well data.

| Core number | 206 |
|---|---|
| Location | Cage |
| District code | LA |
| API number | 1702722589 |
| County parish | Claiborne Parish |
| Top depth (ft) | 9877 |
| Bottom depth (ft) | 10155 |
| Coordinates | WGS 84 |
| SH _Latitude | 32.87421401 |
| SH _longitude | -93.2194444 |
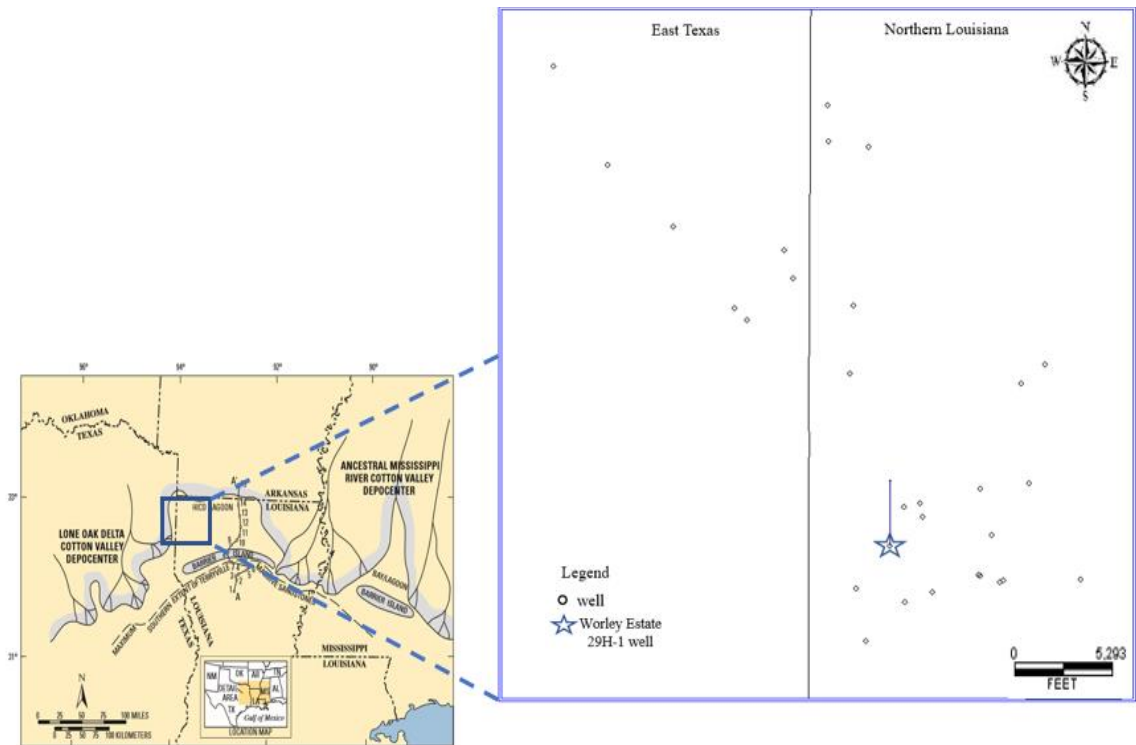


Figure 7 Map showing the location of Worley Estate 29H-1 well in northern Louisiana.

6.2 X-ray Fluorescence spectroscopy

X-ray fluorescence (XRF) spectroscopy was completed at a 1ft (30 cm) interval down the core face using a hand-held Thermo-Fisher Niton XLT3 GOLDD+. The XRF method measures the elemental concentration of a sample. The instrument emits X-radiation, which is absorbed by the electrons within a sample. This energy absorption by the electrons causes the excitation of electrons, resulting in the ejection of the electrons from their atomic shells and ultimately creating a vacancy. An electron of a higher orbital state fills the vacancy. The atoms of specific elements are characterized by their emitted fluorescence energy and wavelength spectra, recorded as a relative abundance or counts. The XRF can determine magnesium through uranium. The advantages of the XRF method are that it is non-destructive where element intensities are easily obtained on the sediment core surface, and the spatial resolution of the XRF is usually higher compared to ICP-MS or XRD (Weltje and Tjallingii, 2008).

First, the core was cleaned with deionized water to remove drilling mud, debris, and brine from the surface and allowed to air dry. For a standardized data control measurement, every 20th sample analyzed was a silica standard. Elemental concentrations were recorded on the instrument, downloaded, and placed in an Excel spreadsheet. This study focused on the bulk elements, such as Fe, Ca, K, Al, Si, Cl, and S. Statistics were run on the mineralogy determined via bulk elemental concentrations.

## 6.3 X-ray diffraction

   X-ray powder diffraction data was provided by WD Von Goten Laboratories (2016), previously run on 30 samples throughout the core. The mineralogy was used as a qualitative assessment of the XRF to determine variations down the core at a finer resolution compared to what can be obtained from XRD. Main elements of the mineral composition were used as indicators of relative change; for example, Si was used as a siliciclastic indicator (specifically, quartz and clay minerals), while Ca was used as a calcite indicator.

   XRD is classified as " semi-destructive" because a part of the core needs to be sampled and crushed. Each sample takes several hours to prepare, run, and analyze. XRF requires cleaning of the core surface with deionized water, and approximately 3 minutes a sample to run.

## 6.4 Thin section microscopy

   Twenty-five samples were sent to the Grindstone Laboratory for thin sections. These were polished to about 30 micrometers. The pores in the sample rocks were impregnated with blue epoxy to maintain the pores spaces after which thin sections were prepared. The thin sections were analyzed under the microscope with plane-polarized and cross-polarized light, using a Labomed Lx POL compound microscope at the SFA Department of Earth Sciences and Geologic Resources lab. Petrographic analysis was used to determine the mineralogical content, and describe the various textural compositions and diagenetic history.

6.5 Well log analysis and mapping

The well data used for this research project were gathered from wells drilled into Cotton Valley Group Sandstones using Enverus software online database (Prism) and S&P Global (IHS lognet). A total of 30 wells that penetrated the Cotton Valley Group Sandstones in both the Claiborne and Webster Parishes were selected, located in northern Louisiana and East Texas. This consisted of wells from three fields: Blackburn, Blackburn East (northern Louisiana), and the Dykesville fields (East Texas). The well data extracted from Prism software (Enverus) included well names, API numbers, coordinates (longitude and latitude), elevation, and true vertical depth in CSV format. Well logs (digital and rasta images) and shapefiles including Louisiana state, county, and township grids were obtained from S&P Global. These well data were then imported into IHS Petra software, using the coordinate system (US State Plane ft Louisiana North), and datum (NAD 83).

The well logs for this research study area consisted mainly of spontaneous potential (SP) logs, resistivity logs, and gamma ray. A few wells contained additional logs such as photoelectric effect (PE) and density, as shown in Figure 8. Gamma ray (GR) logs are used to distinguish between different rock lithologies and correlate across an area. For example, shales are usually associated with radioactive elements such as potassium, uranium and thorium. Therefore, they tend to have a very high gamma ray response due to the emission of natural gamma radiation. Other lithologies such as sandstones/carbonates may contain fewer radioactive elements and therefore report lower gamma ray values. The Spontaneous potential (SP) response complements the gamma ray logs. Sandstones usually contain high

saline fluids (brines) compared to the drilling fluids (mud) and the SP logs show a strong deflection to the left, and vice versa for shaly formation (right deflection).

In this project, the type log used was the Worley Estate 29H-1 well (API 1702722589) provided by Buffco. The core was divided into six units based on lithologies observed in the core and gamma ray, spontaneous potential, and resistivity log responses. This was used to describe the lithological facies, their spatial variations within the basin, as well as the porosity and permeability assessment of individual facies. These stratigraphic units were correlated with other well logs in the area to build cross-sections, structural and isopach maps within the study area. Structure and isopach maps were generated in IHS Petra for these six defined units across the study area.
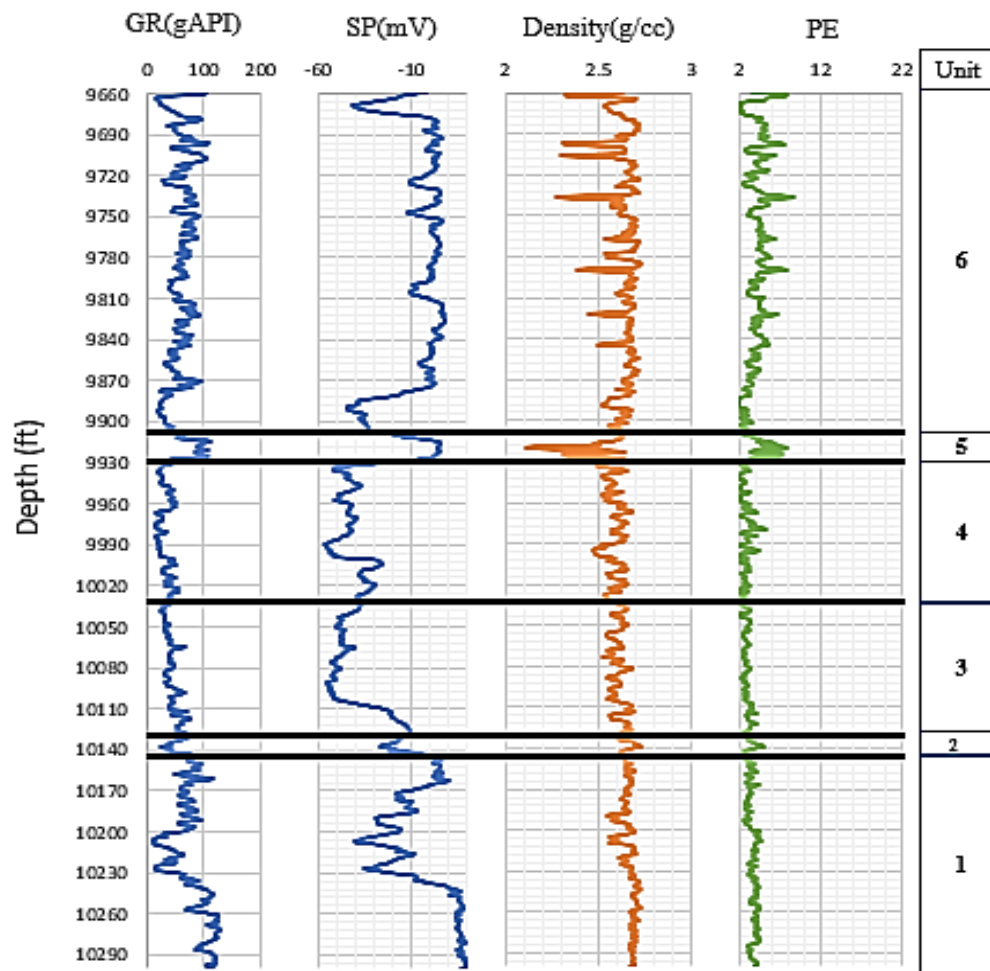
Figure 8 Worley Estate 29H-1 well logs of the Cotton Valley Group Sandstones.

# 7.0 RESULTS AND INTERPRETATION

## 7.1 Units and lithofacies

The core of the Worley Estate 29H-1 well was divided into six distinct units based on the well logs and lithology observed in the core (Figure 9). Each unit comprises either a singular lithology or multiple lithologies. Each unit represents a mappable unit across the study area and a change in depositional environment. Their corresponding porosity and permeability values are also shown.
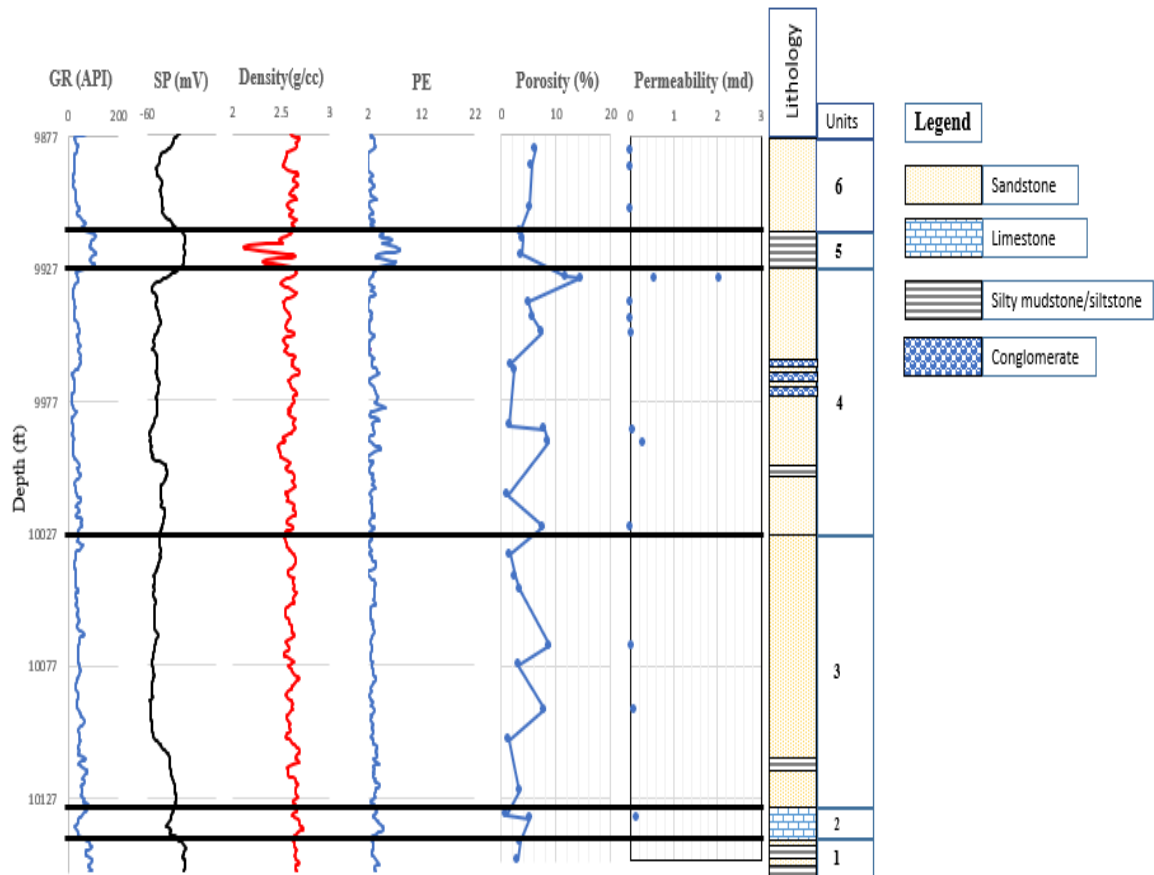


Figure 9 Lithofacies, porosity and permeability within the Cotton Valley Group Sandstones.

28

### 7.1.1 Unit 1

### 7.1.1.1 Quartz arenite

This quartz arenite is a sandstone and silty clay unit ranging from 10,140ft -10,154ft (3091m – 3095m). It has a density of 2.65g/cc, an average gamma ray value of 80 API and a photoelectric effect value of ~ 3.5. The sandstone unit is medium grey to dark grey in color, medium-grained to fine grained in texture, and comprises well-sorted and rounded grains. Some sedimentary structures observed in this unit include very thin to thin parallel laminations, cross-stratifications, and fractures which are a result of differential compaction. The measured total porosity ranged from 2% to 4%.

### 7.1.1.2 Lithofacies: Silty mudstone

The silty mudstone were dark grey to black in color, well sorted, and comprised of angular to rounded grains. Some of the observed structures include laminations and pelletal accumulations. At depths of 10,153ft – 10,154.5ft (3094.6m - 3095.1m), there are accumulation of broken and dissolved bivalves which have been replaced by sparry calcite.
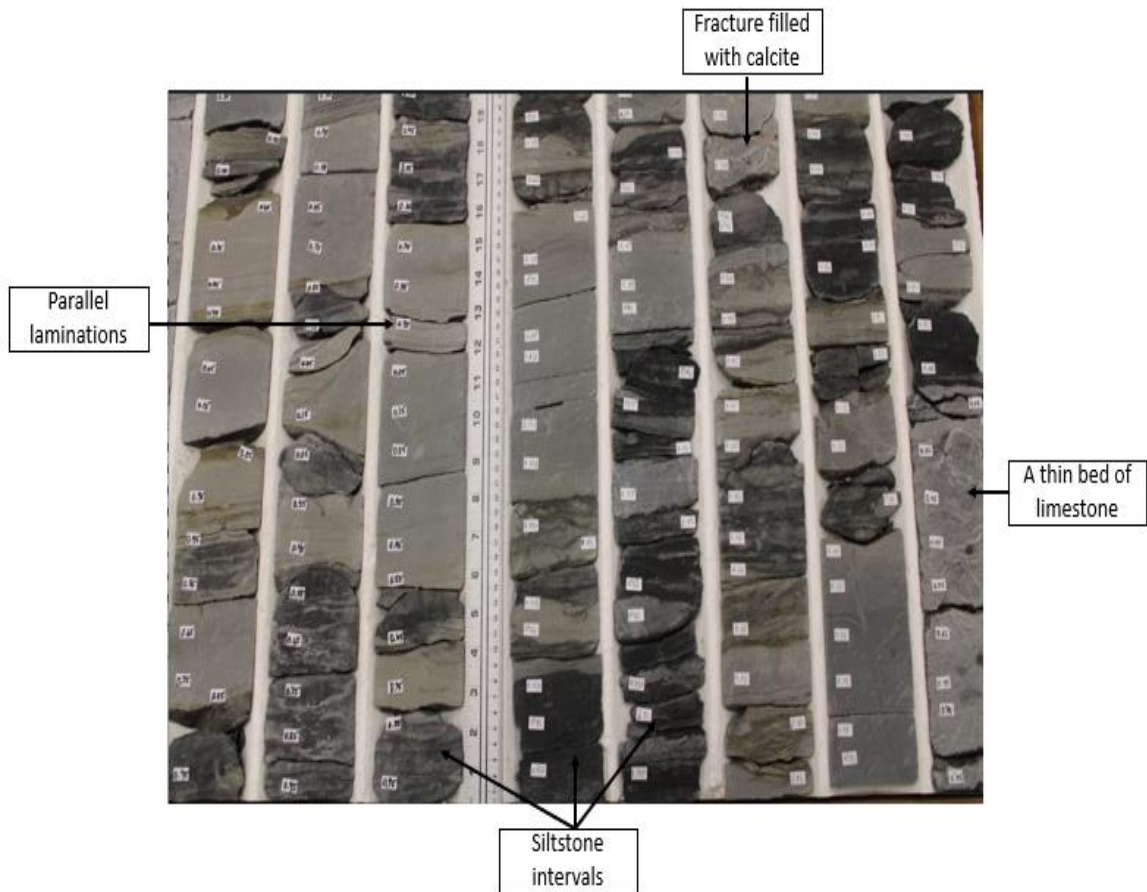
Figure 10 Image of the quartz arenite laminated with siltstone lithofacies in unit 1 from depths of 10,138ft (3090.1m) to 10,154ft (3094.9m).

## 7.1.2 Unit 2

### 7.1.2.1 Wackestone

This layer of wackestone ranges from 10,133ft to 10,140ft (3088.5m-3090.7m). Typical well log responses are a neutron density value of 2.8g/cc, gamma ray value of 25 API, and a photoelectric effect value of ~ 4, and corresponds to a negative deflection on the SP curve.

This unit is light to medium grey in color. It consists of abundant fossils that include bivalves and gastropods. Sedimentary structures observed include fractures that have been filled by calcite and secondary porosity because of the dissolution of some bivalve shells (moldic pores). This unit coarsens upwards into a silty fossiliferous mudstone comprised of angular quartz grains. The measured total porosity ranged from 0.8% to 5.2%, and a permeability of 0.14md.
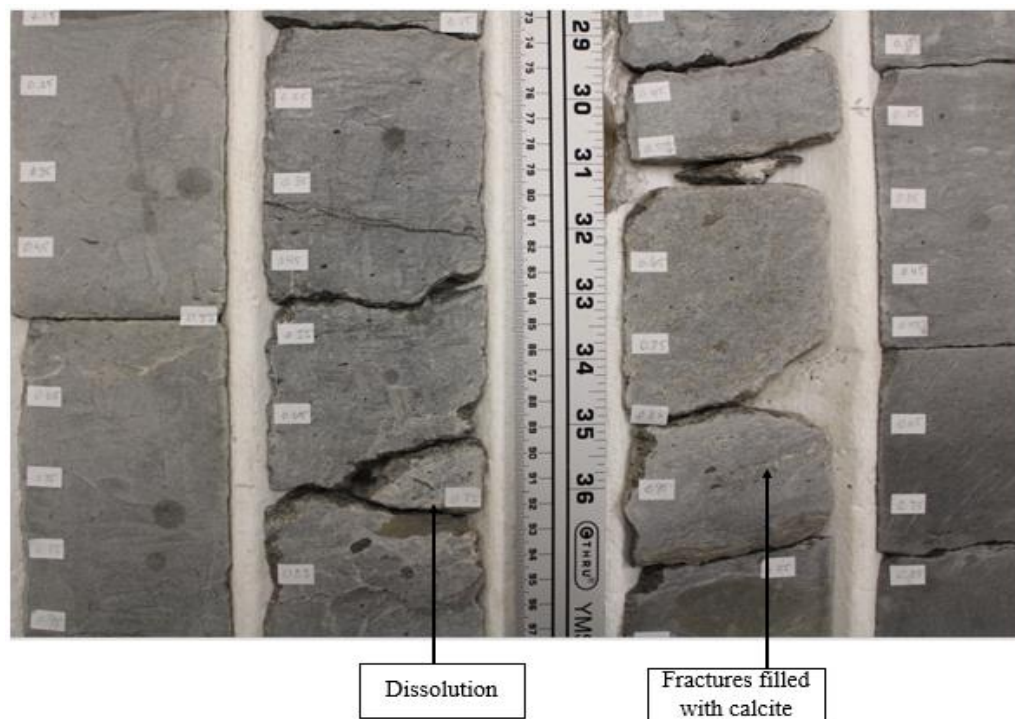


Figure 11 Image of wackestone lithofacies from depths 10,131ft (3087.9m) to 10,138ft (3090.1m).

7.1.3 Unit 3

7.1.3.1 Quartz arenite

This sandstone unit ranges from 10,033ft to 10,130ft (3058.1m - 3087.6m). Well log
responses in this interval consist of an average neutron density of 2.65g/cc, an average
gamma ray value of 40 API, and a photoelectric effect value of ~ 3. These are light grey in
color, fine-grained in texture and consists of well rounded to sub-angular grains. Some of
the sedimentary structures within this facies include parallel laminations tilted at a lower
angle ($< 5^0$), cross stratifications, and bioturbations (horizontal burrows). These
laminations contained organic-rich materials which are darker in color as well as lenses
outlined by organic-rich materials occurring at specific intervals within this unit. Also,
fractures were present throughout this interval. This is a potential reservoir unit with
porosity ranging from 1.2% to 8.8%, and permeability ranging from 0.009md to 0.1md.

7.1.3.2 Siltstone

The sandstone facies were intercalated with silty intervals mostly at the bottom of this unit.
These silts occurred at depths ranging from 10,110ft -10,133ft (3081.5m – 3088.5m). The
silts are medium grey to dark grey in color, fine-grained in texture, and comprised of well
sorted and angular grains. Some sedimentary structures observed in this unit include very
thin to thin parallel laminations and cross-stratifications.

Figure 12 Image of quartz arenites laminated with siltstone from depths of 10,014ft (3052.3m) to 10,022ft (3054.7m).
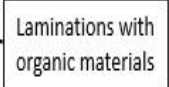
7.1.4 Unit 4

7.1.4.1 Quartz arenite

This unit is about 104ft (31.6m) in thickness, ranging from depths 9,929ft to about 10,033ft (3026.4m – 3058.1m). This has an average density of 2.65g/cc, an average gamma ray value of 40 API, and a photoelectric effect of ~3. This is predominantly a sandstone unit. These sandstones consist of well sorted, sub-rounded to rounded grains, and are light grey in color. Some of the sedimentary structures observed included parallel laminations, cross-stratification, and fractures filled with calcite. The cross-stratifications were observed to be truncated at very low angles at the top and the bottom. This is a potential reservoir unit with measured total porosity ranging from 1.2% to 14.5%, and a permeability ranging from 0.009md to 2.04md.

7.1.4.2 Conglomerate

Intervals of thin conglomerate beds (rounded pebble clasts) occurred within the quartz arenite at depths ranging from 9,970ft (3038.9m) – 9,971ft (3039.2m), 9,972ft (3039.5m)-9,973ft (3039.8) and 9,974ft (3040.1m) – 9,975ft (3040.4m), which have been heavily cemented by calcite. The dissolution of calcite enhances secondary porosity in this unit.
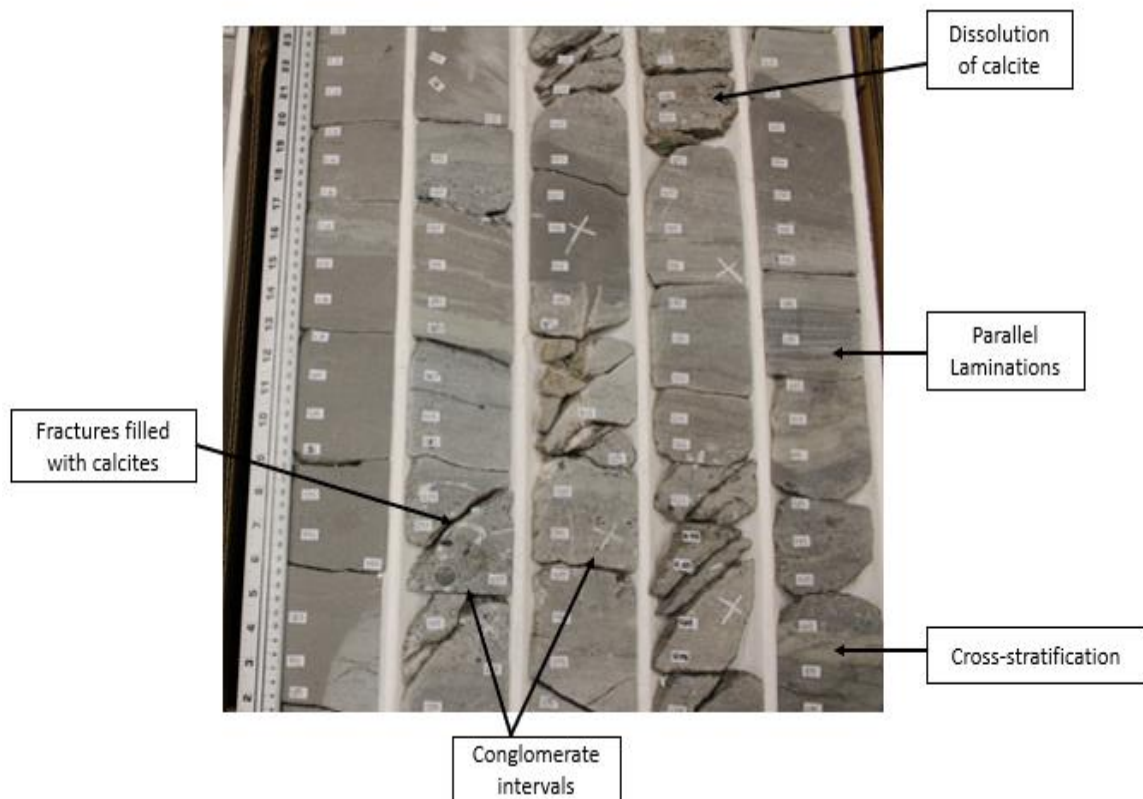
Figure 13 Quartz arenites intercalated with conglomerate lithofacies from depths 9,967ft (3037.9m) to 9,975ft (3040.4m).

7.1.5 Unit 5

7.1.5.1 Silty mudstone/siltstone

From the cores, there is a gradual change in facies from medium to light grey sandstones in the upper section of the core (Lithofacies 4) to a dark grey/black silty clay unit at an interval of 9,912ft to 9,929ft (3021.2m – 3026.4m). On the well logs, Unit 5 is characterized by a high gamma ray (100 API), an average density of about 2.4g/cc, photoelectric effect of ~ 6, and a strong deflection to the right on the SP curve. These dark

grey/black silty mudstone facies are comprised of silt to clay sized grains and very fissile. Sedimentary structures observed include very thin (<1mm) to thin (1-3mm) horizontal laminae and cross laminations. The upper and lower contacts of these cross laminations are gradational. Thick accumulations of pellets are sparsely distributed within specific intervals of the cores. This is a potential seal with measured total porosity ranging from 3% to 4%.
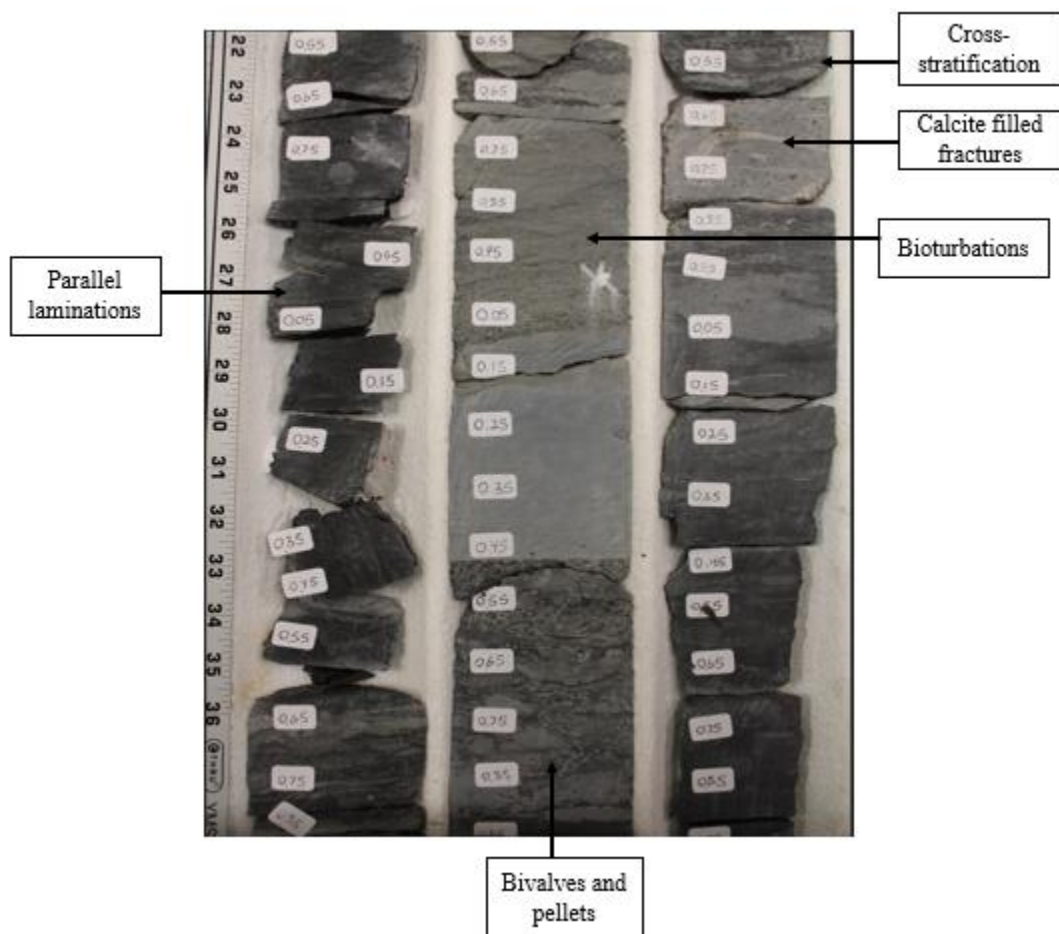


Figure 14 Silty mudstone/siltstone lithofacies from depths 9,917ft (3022.7m) to 9,923ft (3024.5m).

7.1.6 Unit 6

7.1.6.1 Quartz wacke

This sandstone unit is distinguished by a low gamma ray value of 20 API, density of about 2.65g/cc, and photoelectric effect of ~ 2.5. These correspond to a negative deflection to the left as shown by the SP curve in Figure 9. This sandstone lithofacies is about 35ft (10.6m) thick, ranging from the depths of 9,877ft to about 9,912ft (3010.51m - 3021.2m). It is medium grey to light grey in color. It is predominantly coarse-grained in texture and consists of sub-angular, sub-rounded, and sorted grains. Sedimentary structures observed include parallel laminations, herringbone cross-stratifications with sharp basal and top contacts, soft sediment deformation, vertical and horizontal bioturbations (burrows), fractures filled with calcite, and channels. Some of these bioturbations were very extensive giving it a mottled appearance. The fossils present include bivalve shells, gastropods, and pieces of intraclasts. Tiny layers of black organic materials occurred at a depth of 9,889ft (3014.3m) as well as organic materials draped in thin laminations at 9,907.5ft (3019.8m). This is a potential reservoir unit with measured total porosity ranging from 5.1% to 6.3%, and permeability ranging from 0.003 to 0.004md.
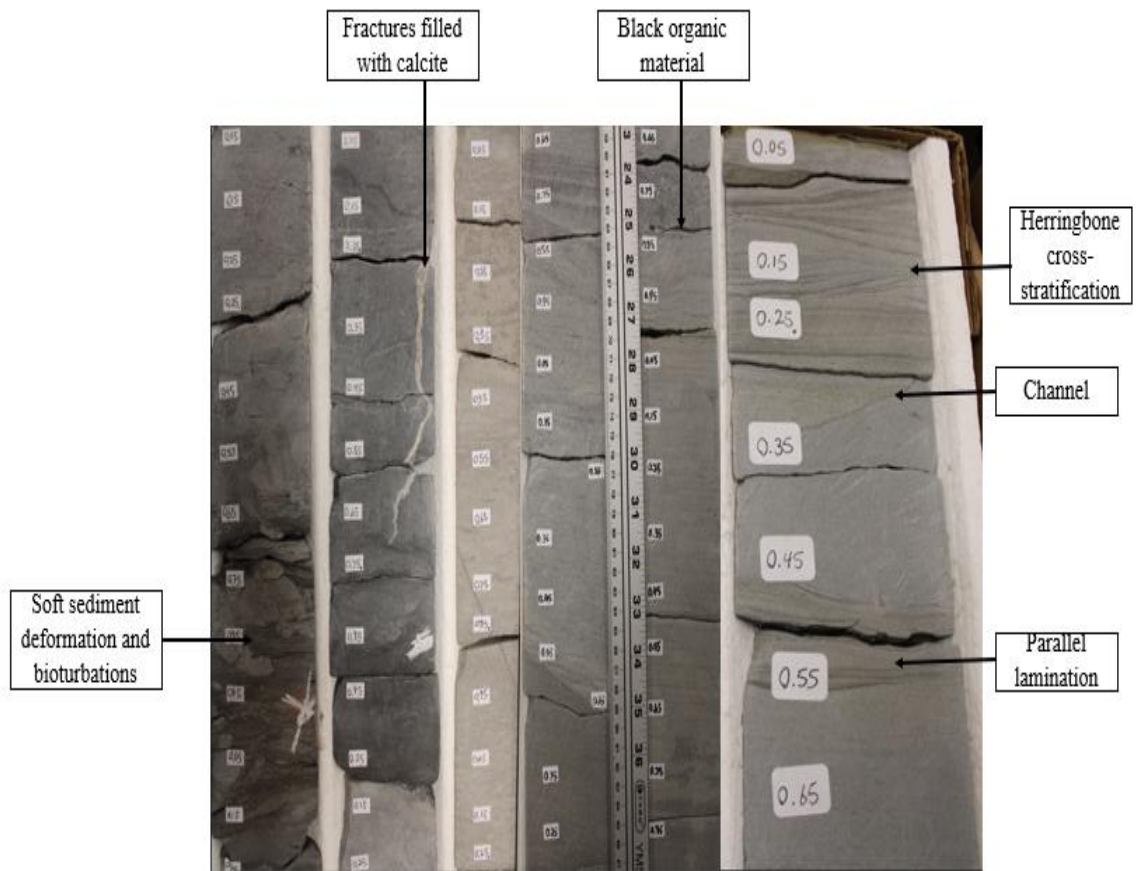
Figure 15 Quartz wacke lithofacies from depths from 9,877ft (3010.5m) to 9,907ft (3019.7m).

7.2 Thin section analyses

7.2.1 Unit 1

7.2.1.1 Lithofacies: Quartz arenite

Sample 1 (10,149.8ft, 3093.7m) is a quartz arenite, comprised of about 99% quartz grains and 1% feldspar (Figure 16 A). It is coarse-grained, with sub-rounded to rounded grains and moderate sphericity. It is grain-supported and mostly silica cemented. The grain contacts are mostly concavo-convex contact. Dead oil occurs as black stains and are sparsely distributed in it. No grain orientation is observed in this sample. This sample is texturally mature.

Sample 2 (10,143.29ft, 3091.7m) is a quartz arenite, comprised of about 99% quartz grains and 1% feldspar (Figure 16 B). It is coarse-grained, with sub-rounded to rounded grains and moderate sphericity. It is grain-supported, and mostly silica cemented. The grain contacts are mostly concavo-convex contact. Dead oil occurs as black stains in it. It is texturally mature.

7.2.1.2 Lithofacies: Siltstone

Sample 3 (10,138.5ft, 3090.2m) is a siltstone with about 10% clay. It is comprised mainly of quartz grains with sub-angular to sub-rounded grains and low sphericity. This is mainly grain-supported with point contacts. The cement is mostly quartz overgrowths. Fractured porosity is observed which is as a result of pressure compaction.
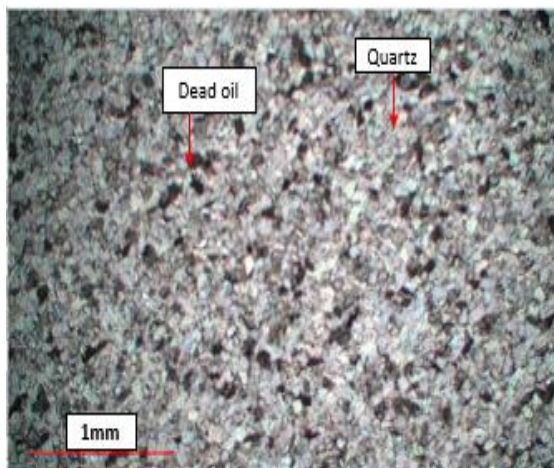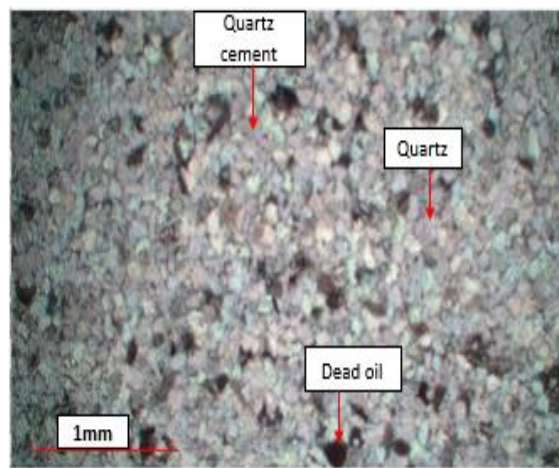
a. Sample 1 (10,149.8ft, 3093.7m)     b. Sample 2 (10,143.29ft, 3091.7m)
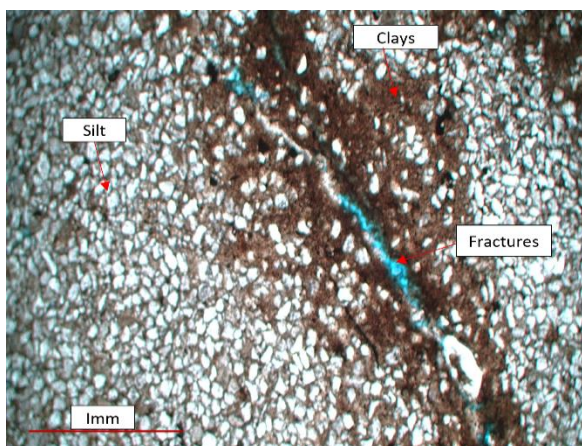


c.   Sample 3 (10,138.5ft, 3090.2m)

Figure 16 Samples of Unit 1 at 4X magnification under cross-polarized light.

### 7.2.2 Unit 2

### 7.2.2.1 Lithofacies: Wackestone

Sample 4 (10,134.52ft, 3089m) is a poorly washed, poorly sorted, pelletal, fossiliferous wackestone, comprised of 95% fossils and about 5% pellets (Figure 17A). It is

predominantly made of sparry calcite cement. Secondary porosity in the form of moldic porosity occurs throughout this sample. The diagenetic history involved compaction, followed by sparry calcite cementation and dissolution.

Sample 5 (10,133.2ft, 3088.6m) is a silty pelletal fossiliferous wackestone. This sample consists of about 90% fossils and 10% pellets, with a poorly sorted and poorly washed matrix (Figure 17B). The cement is predominantly made of sparry calcite. The fossils present include bivalves and echinods with striations. The silty pelletal fossiliferous wackestone was subjected to pressure compaction and subsequently an infill of secondary calcite cements.
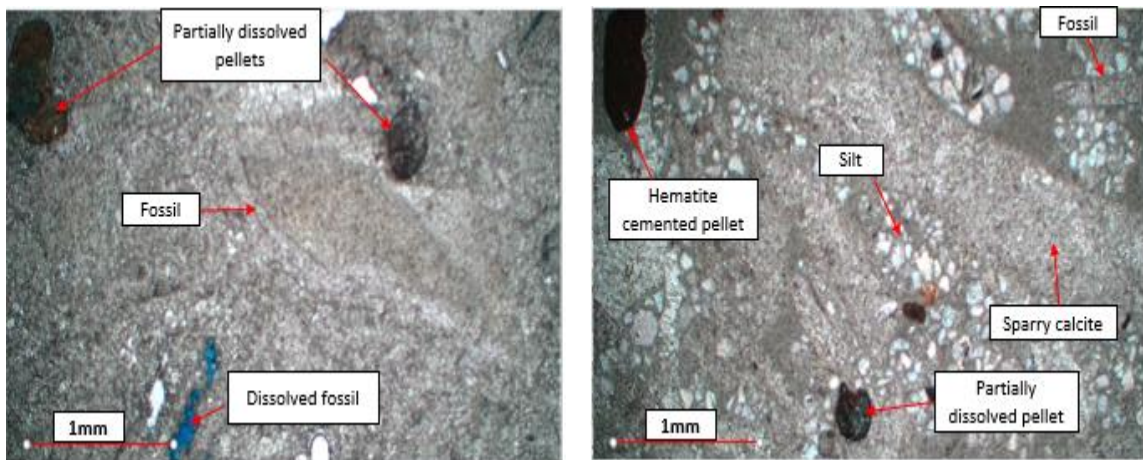


a. Sample 4 (10,134.52ft, 3089m)          b. Sample 5 (10,133.2ft, 3088.6m)

Figure 17 Samples of Unit 2 at 4X magnification under cross-polarized light.

### 7.2.3 Unit 3

#### 7.2.3.1 Lithofacies: Siltstone

Sample 6 (10,124.8ft, 3086m) is a siltstone consisting of ~10% clay minerals and 90% silt-size quartz grains (Figure 19a). It is predominantly made of sub-angular to sub-rounded quartz grains and low sphericity. This is mainly grain-supported with mostly point contacts. The types of cement include quartz overgrowths, patches of calcite cement, and a minor amount of hematite. Fractured porosity with dead oil flows along the fractures was observed. It is texturally mature.

#### 7.2.3.2 Lithofacies: Quartz arenite

Sample 7 (10,104.98ft, 3080m) is a quartz arenite, with about 95% quartz grains and 3-5% fossil fragments (bivalves). This sample is coarse-grained, sub-rounded and mostly has concavo-convex and sutured contacts. It is grain supported. The cement includes quartz overgrowths, calcite, and sporadic hematite cements. The bivalves (fossils) have been recrystallized. This sample is texturally mature and shows moderate porosity (Figure 19b & 19d).

Sample 8 (10,089.3ft, 3075.2m) is a fossiliferous quartz arenite (Figure 19c) comprised of 90% quartz grains and 10% fossil fragments. It is grain supported with mostly sub-angular grains. This sample is heavily calcite cemented with some amounts of quartz overgrowths. This sample is classified as texturally mature.

Sample 9 (10,076.68ft, 3071.4m) is a quartz arenite, with about 95% quartz grains and 3-5% fossil fragments (bivalves). It is coarse-grained, sub-rounded, and has concavo-convex and sutured contacts. This sample is grain-supported. The cement includes quartz overgrowths, calcite, and hematite cements. Some of the bivalves (fossils) have been recrystallized, and others dissolved resulting in large moldic pores. It is texturally mature and shows good porosity (Figure 19d).

Sample 10 (10,069.6ft, 3069.2m) is a quartz arenite, comprised of 100% quartz grains (Figure 19e). This is also coarse-grained with sub-angular grains. There are abundant quartz overgrowths in this sample. It is grain-supported with both concavo-convex and sutured contacts. This has silica cement and calcite cement. No hematite cement and clay pore filling is observed. There is a weak orientation of grains. Patches of dead oil stains occurred as black stains throughout the sample. This sample is classified as texturally mature.

Sample 11 (10,048.23ft, 3062.7m) is a quartz arenite, with about 97% quartz and 3% of fossil fragments (bivalves). This sample is coarse-grained, sub-rounded to rounded grains with moderate to high sphericity (Figure 19f). This is grain-supported. Concavo-convex and sutured contacts are observed between the grains. Calcite cement is the principal cement, with a few quartz overgrowth and patches of hematite cement.

Sample 12 (10,043.6ft, 3061.3m) is a quartz arenite. This sample is comprised of ~94% quartz grains, 1% feldspar, and 6% fossil fragments (bivalves). This is also coarse-grained,

43

sub-rounded to rounded grains with moderate porosity, and rhombohedral packing (Figure 19g). This sample is grain-supported with both concavo-convex and sutured contacts. The principal cement is calcite, with patches of hematite cement and a minor amount of quartz overgrowth. This sample has good porosity. It is texturally mature.

Sample 13 (10,035.28ft, 3058.8m) is a quartz arenite. This contains ~93% quartz, 2% feldspar, and 5% rock fragments (bivalves). This sample is coarse-grained with mostly sub-angular, sub-rounded to rounded exhibiting moderate sphericity (Figure 19h). It is grain-supported with both concave-convex and sutured contacts. It is mostly calcite cemented with very little hematite cement. The bivalves are encased with sparry calcite cement. No grain orientation or sedimentary structure is observed. This sample has a moderate porosity (interparticle porosity). It is texturally mature.
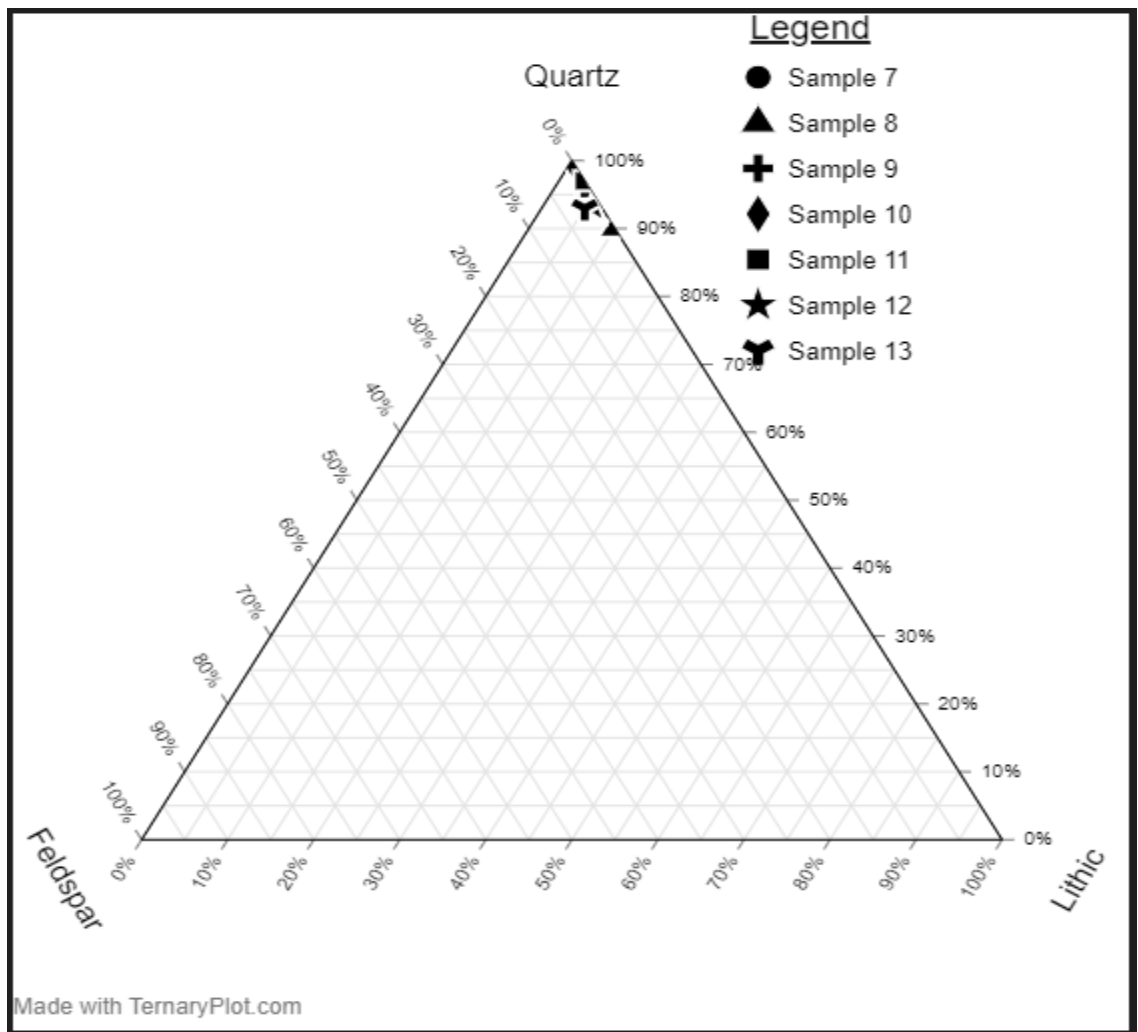
Figure 18 Ternary plot of samples of Lithofacies 4.
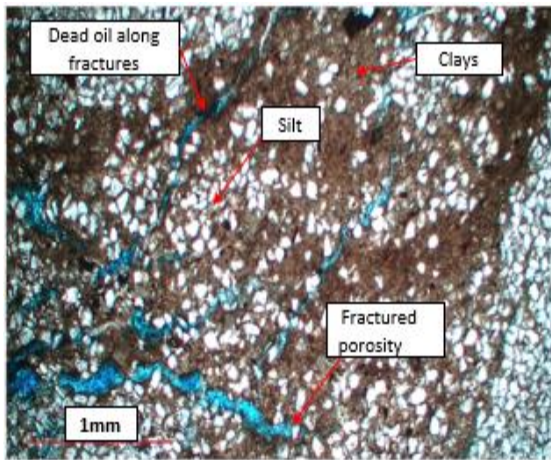
a. Sample 6 (10,124.8ft, 3086m)
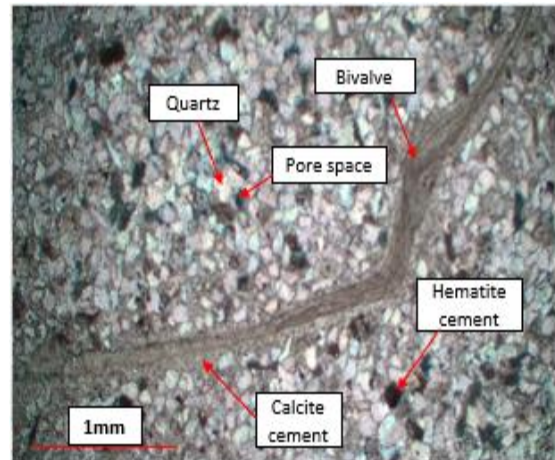


b. Sample 7 (10,104.98ft, 3080m)
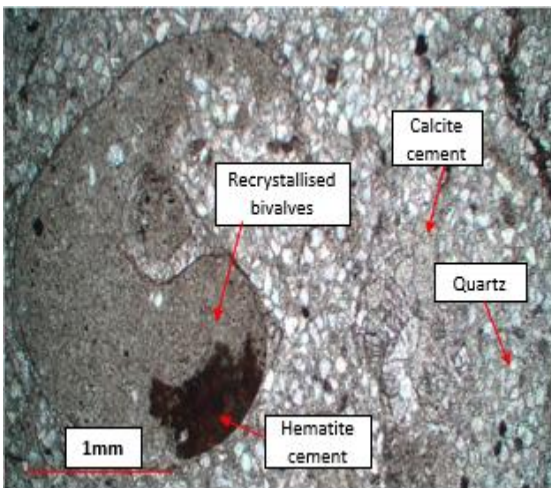


c. Sample 8 (10,089.3ft, 3075.2m)
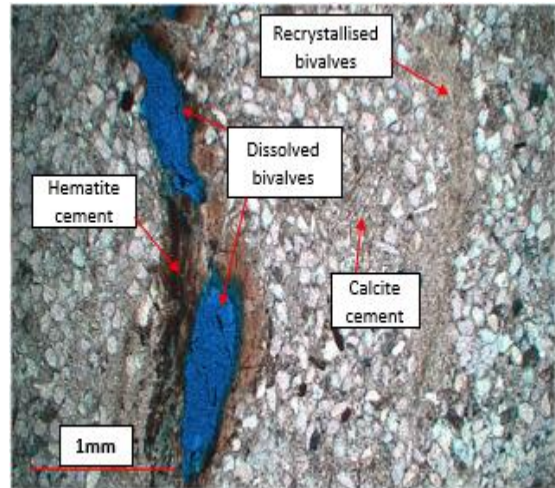


d. Sample 9 (10,076.68ft, 3071.4m)
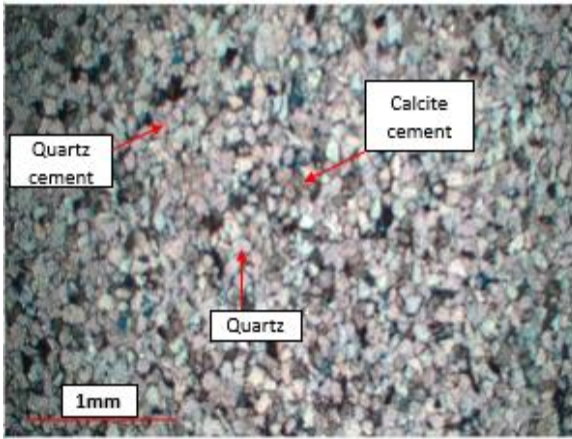
e. Sample 10 (10,069.6ft, 3069.2m)
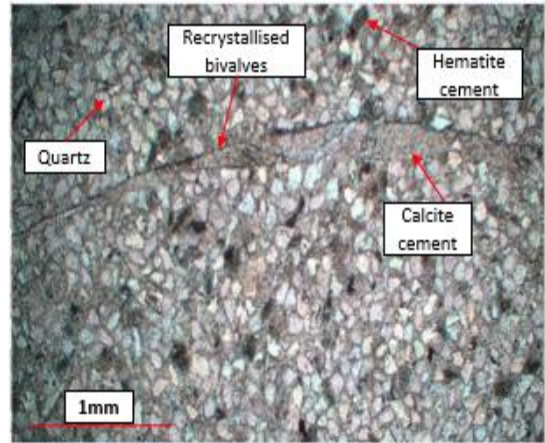


f. Sample 11 (10,048.23ft, 3062.7m)
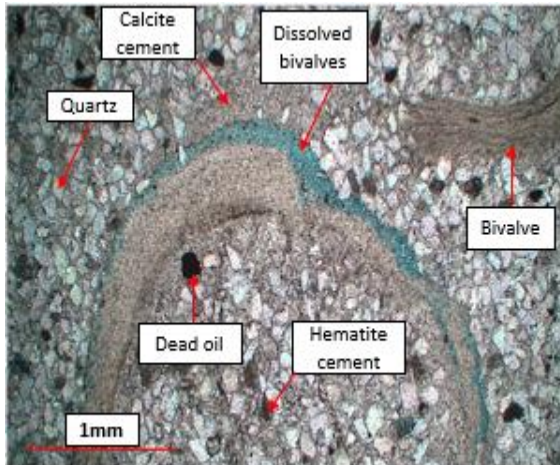


g.   Sample 12 (10,043.6ft, 3061.3m)
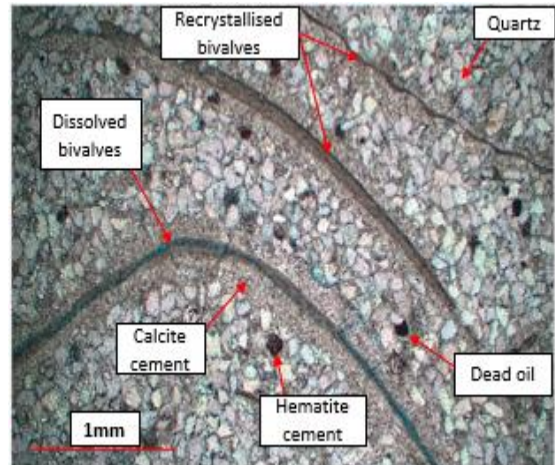


h. Sample 13 (10,035.28ft, 3058.8m)

Figure 19 Samples of Unit 4 at 4X magnification under cross-polarized light.

7.2.4 Unit 4

7.2.4.1 Lithofacies: Conglomerates

Sample 15 (9,970.65ft, 3039.1m) is a sandy conglomerate (Figure 21b), consisting of granule to pebble sized clasts. The grains are rounded to sub-rounded, and moderately well sorted, with minor amounts of fossil fragments. This is mostly grain supported with a minor amount of interstitial matrix. The larger pebbles are composed of a mixture of both opaque dark-grey and white quartz grains under plane-polarized light. These are massive with no orientation of the grains. Dissolution is observed along some of the larger grains. This sample is calcite cemented.

7.2.4.2 Lithofacies: Quartz arenite

Sample 14 (9,986.3ft, 3043.82m) is a quartz arenite (Figure 21a). This sample consists of 99% of quartz grains and 1% of fossil fragments (bivalves). It is comprised of gravel sized quartz grains mixed with silt sized quartz grains. The grains are angular to subangular in shape, poorly sorted, and heavily cemented with calcite. The core sample effervesces with 10% HCl.

Sample 16 (9,964ft, 3037m) is a quartz arenite (Figure 21c). This sample consists of about 100% quartz grains. These are coarse-grained, mostly angular to sub-rounded, with concavo-convex and sutured contacts. This is grain-supported (with no matrix) and mature, with good sorting and rounded grains. These grains are heavily cemented with calcite, with

some quartz overgrowth. The core sample effervesces with 10% hydrochloric acid (HCL) indicating the abundance of calcite cement. No fossil fragments are observed.

Sample 17 (9,948ft, 3032.2m) is a quartz arenite (Figure 21d). This sample consists of ~96% quartz grains and 4% fossil fragments (mostly bivalve fragments sparsely distributed). These are relatively fine-grained in texture. The grains are sub-angular to sub-rounded, mostly with concavo-convex and minor sutured contacts. This is grain-supported and texturally matured (good sorting and sub-rounded grains). Most of the cement observed are quartz overgrowths along the quartz grains. These exhibit fracture porosity with dissolution of some of the bivalve fragments. Migration of dead oil occurred along the fractures. Compaction of sediment grains caused the dissolution of the quartz grains, later precipitated as quartz overgrowths.

Sample 18 (9,940ft, 3029.7m) is a clean quartz arenite (Figure 21e). This lithofacies contain 100% quartz grains. It is coarse-grained in texture, mostly sub-angular to sub-rounded with low sphericity. This is grain-supported and has concavo-convex and sutured grain contacts. It is super mature, well sorted, and with no matrix. There are minor amounts of quartz overgrowths along quartz grains, calcite cement, and few traces of hematite cement. Dissolution appears to be caused by pressure compaction enhancing porosity.

Sample 19 (9,930ft, 3026.7m) is also a clean quartz arenite (Figure 21f). This contains 100% quartz grains. This sample is coarse-grained in texture, mostly sub-angular to sub-rounded with low sphericity. It is grain-supported. The grain contacts are predominantly

concavo-convex and sutured grain contacts. It is super mature, well sorted with no matrix. Minor amounts of quartz overgrowth along quartz grains, calcite cement, and few traces of hematite cement occur in this sample. Dissolution appears to be caused by pressure compaction enhancing porosity.
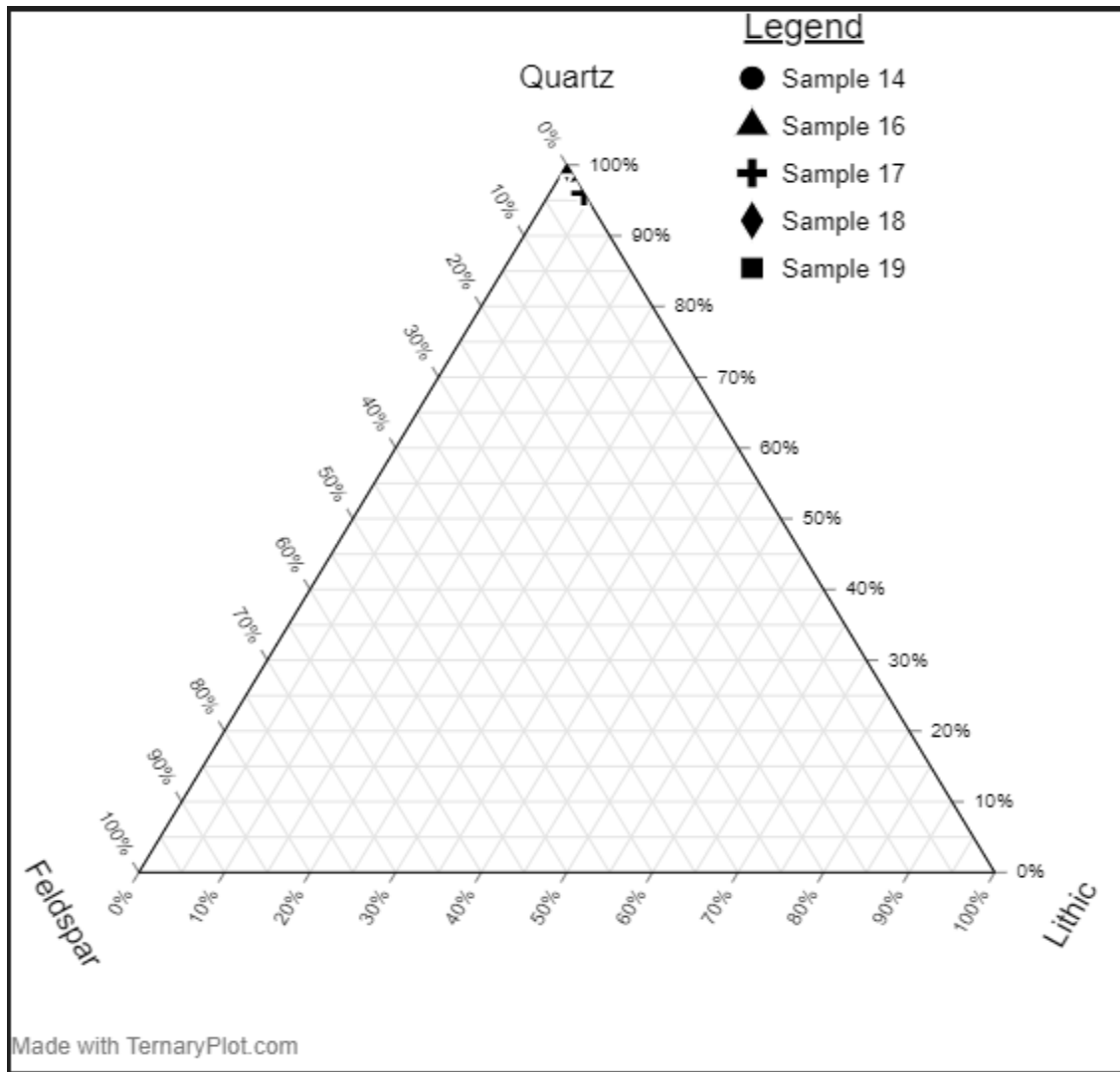


Figure 20 Ternary plot of samples 14, 16, 17, 18 & 19  from Quartz arenite lithofacies of Unit 3.
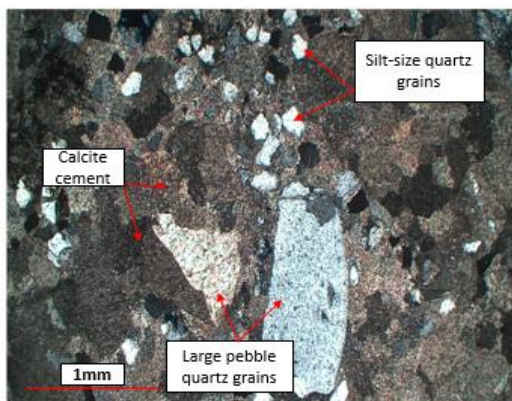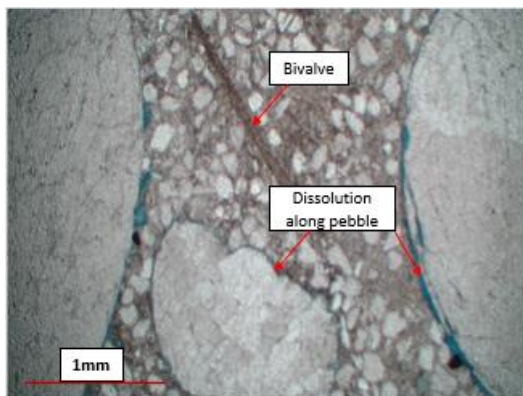
a. Sample 14 (9,986.3ft, 3043.82m)   b. Sample 15 (9,970.65ft, 3039.1m)   c. Sample 16 (9,964ft, 3037m)
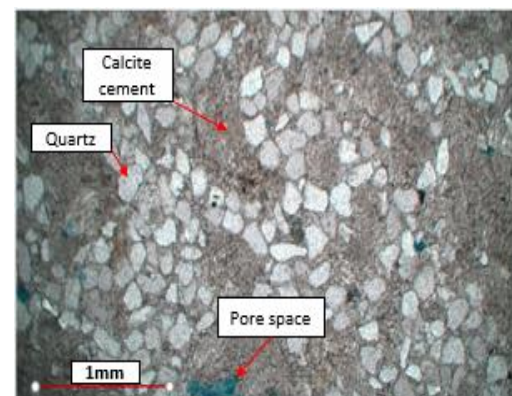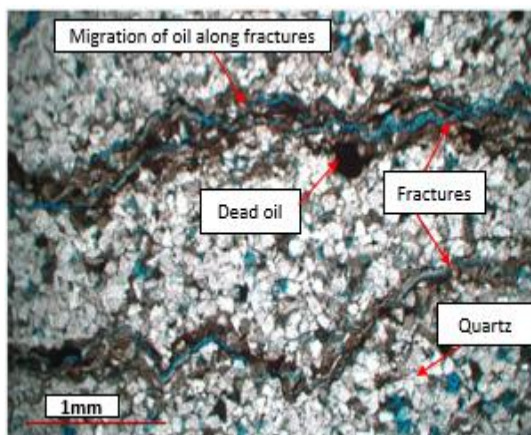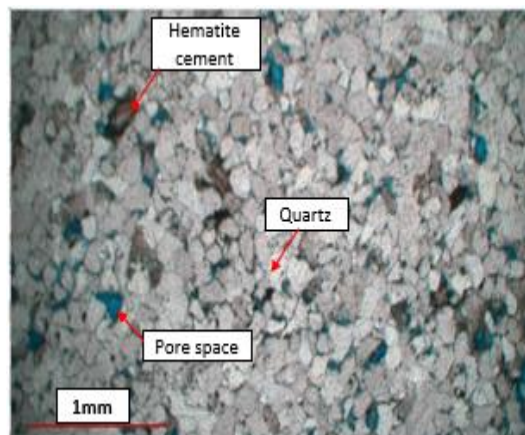
d. Sample 17 (9,948ft, 3032.2m)   e. Sample 18 (9,940ft, 3029.7m)   f. Sample 19 (9,930ft, 3026.7m)
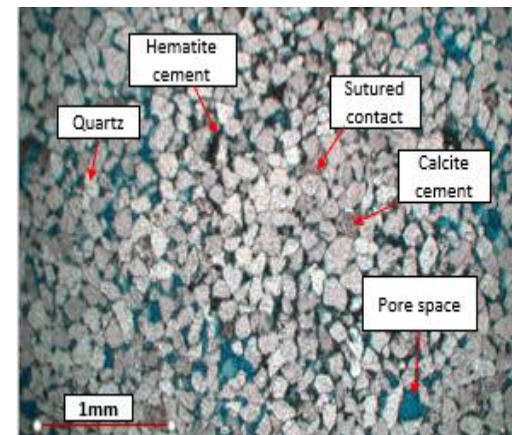
Figure 21 Thin section images of Unit 3 at 4X magnification under cross-polarized light.

7.2.5 Unit 5

7.2.5.1 Lithofacies: Silty mudstone/siltstone

Sample 20 (9,920ft, 3023.6m) is a fossiliferous siltstone (Figure 22a). Abundant bivalve fragments are found throughout the sample. The silt sized grains are comprised primarily of quartz. The grains are mostly rounded floating in a clay matrix. The silt-sized grains fill the pores within the bivalve shells. Hematite nodules occur as iron stained on the bivalve shells. Fractures are found throughout this sample.

Sample 21 (9,917ft, 3022.7m) is a silty mudstone/siltstone (Figure 22b). It is comprised of ~30% - 40% clay minerals and ~50-60% quartz grains. Grains are fine-grained to very fine-grained in size, mostly angular to sub-angular, and well sorted. A few pieces of bivalves and hematite nodules are observed. Generally, this sample is mostly quartz grains in a matrix of clay minerals.

Sample 22 (9,911.25ft, 3021m) is a silty mudstone/siltstone (Figure 22c). It is comprised of ~30% - 40% clay minerals and ~50-60% quartz grains. Grains are fine-grained to very fine-grained in size, mostly angular to sub-angular, and well sorted. A few pieces of bivalves and hematite nodules are observed. This sample mostly contains quartz grains in a matrix of clay minerals.
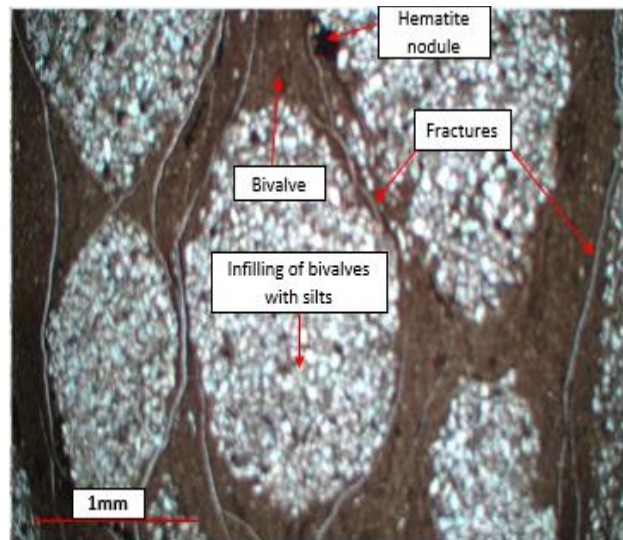
a. Sample 20 (9,920ft, 3023.6m )
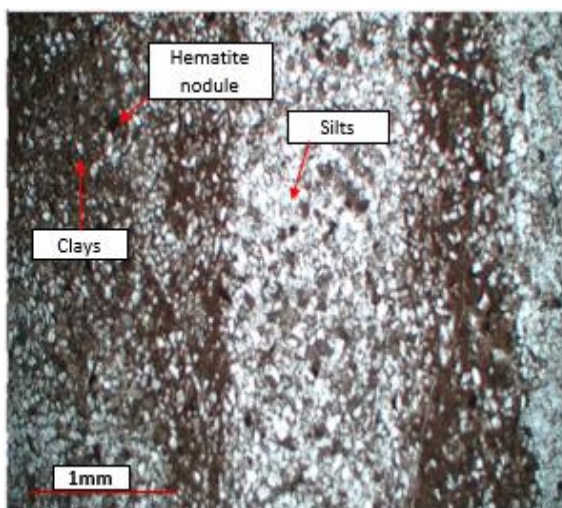


b. Sample 21 (9,917 ft, 3022.7m)
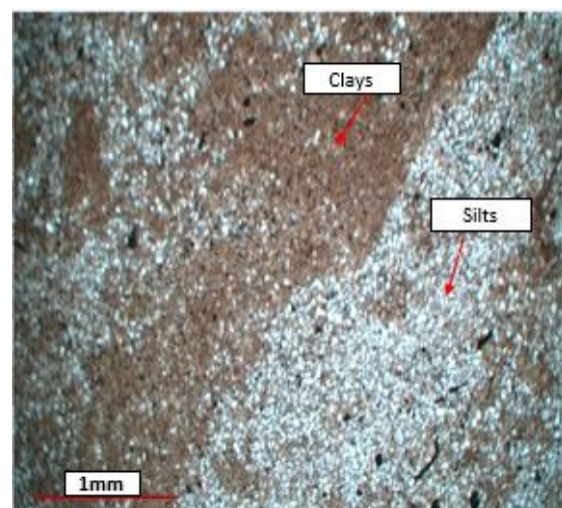


c. Sample 22 (9,911.25 ft, 3021m)

Figure 22 Silty mudstone/siltstone lithofacies of Unit 2 at 4X magnification under cross-polarized light.

7.2.6 Unit 6

7.2.6.2 Lithofacies: Quartz wacke

Sample 23 (9,892ft, 3015.1m) is a fossiliferous quartz wacke (Figure 23a). It consists of about 93% quartz grains and 7% fossil fragments. The quartz grains are coarse-grained, mostly angular, sub-angular to sub-rounded. It is matrix supported, mostly clay-sized grains, with point and concavo-convex grain contacts. The fossils include plant remains and bivalves which are slightly recrystallized. These fossils have weak orientation throughout the sample. The cement consists of quartz overgrowths around the quartz grains and calcite. It slightly effervesces with HCL acid on the cores. This sample is described as immature.

Sample 24 (9,885ft, 3012.9m) is an immature fossiliferous quartz wacke (Figure 23b), similar to sample 23 but contains fewer fossils. This sample contains 95% quartz grains, 2% felspars (microcline and plagioclase) and 3% fossils (bivalves). It is coarse-grained, with angular to sub-angular to sub-rounded grains and low sphericity. The sample is matrix supported with the majority of the clays occurring as the matrix and has undergone slight recrystallization. Some of the bivalves are partly dissolved and filled with clays and quartz grains. Cement consists of quartz, calcite, and hematite cement.

Sample 25 (9,879.92ft, 3011.4m) is a poorly washed bimodal quartz wacke as shown in Figure 23c. This sample consists of ~97% quartz grains, 1% feldspar, and 2% rock fragments (bivalves and chert clasts). It is coarse-grained with a few larger grains,

indicating a bimodal peak. The grains are sub-angular to sub-rounded, with low sphericity. This sample is matrix-supported, with most of the clays occurring as a matrix. The grains are mostly floating in a clay matrix, with a few concave-convex grain contacts and a weak grain orientation (lamination). The cement includes some quartz overgrowths and scattered hematite (red color in thin section). The dark spots are dead oil stains.
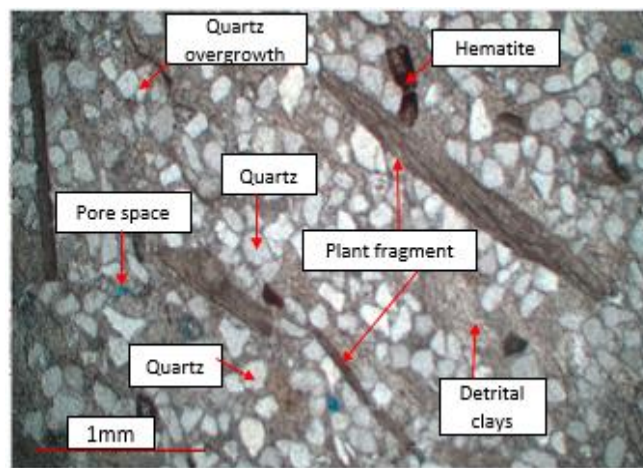


a.     Sample 23 (9,892ft, 3015.1m) under cross-polarized light.



b.   Sample 24 (9,885ft, 3012.9m)  under plane-polarized light.
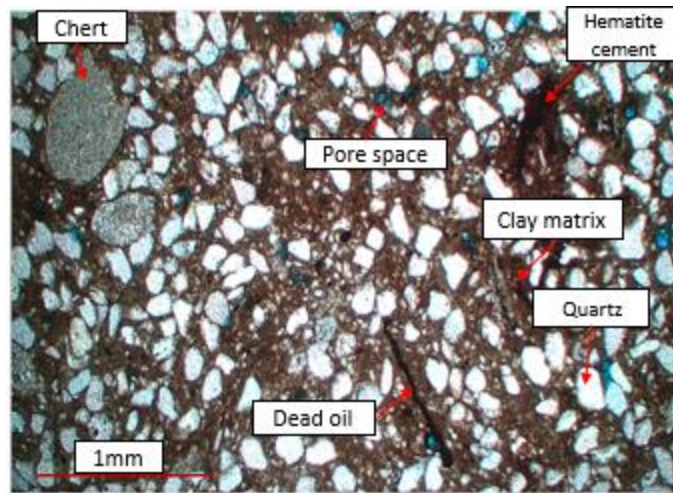
c. Sample 25 (9,879.92ft, 3011.4m) under cross-polarized light.

Figure 23 Samples from sandstone lithofacies of Unit 1 at 4X magnification under cross-polarized and plane-polarized light.
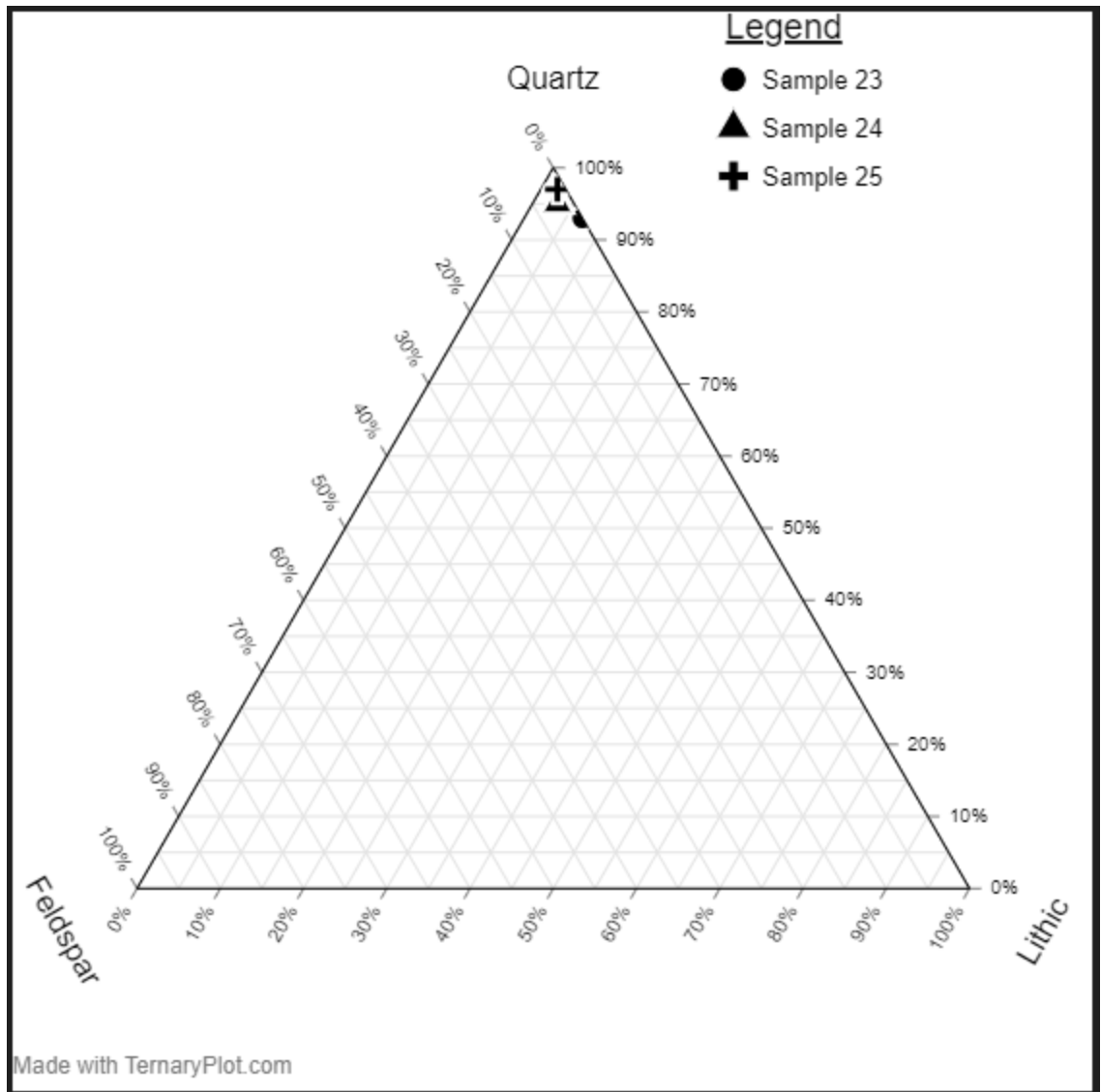
Figure 24 Ternary plot of samples 23, 24 & 25, indicating that the samples are classified as quartz wacke.

7.3 Mineralogy

X-ray powder diffraction data was provided by WD Von Goten Laboratories (2016), previously run on 30 samples throughout the core. The whole rock mineralogy indicates that the primary minerals present in the CVG Sandstones include quartz, calcite, illite/mica/glauconite, and plagioclase. Other minerals in minor amounts include k-feldspar, dolomite, Fe-dolomite/ankerite, and mixed illite-smectite as shown in Figure 25. The illite, mica and glauconite are more abundant in the silty mudstone and quartz wacke lithofacies of Units 5 and 6, respectively, than the other units. Quartz is the dominant mineral in the CVG sandstones. There is an inverse relationship between quartz and calcite; at depths where there is decreased quartz content, the calcite values are very high (50%-100%), and vice versa.

Overall, these are generally classified as "clean'' sandstones with few reactive clay minerals or volcanics if $CO_2$ would be injected into this reservoir. The calcite would be a point of dissolution; however, because the calcite typically is in the form of cement in the sandstone units (section 7.2), $CO_2$ injection could potentially enhance porosity and permeability in the short term (Zhang et al., 2019).
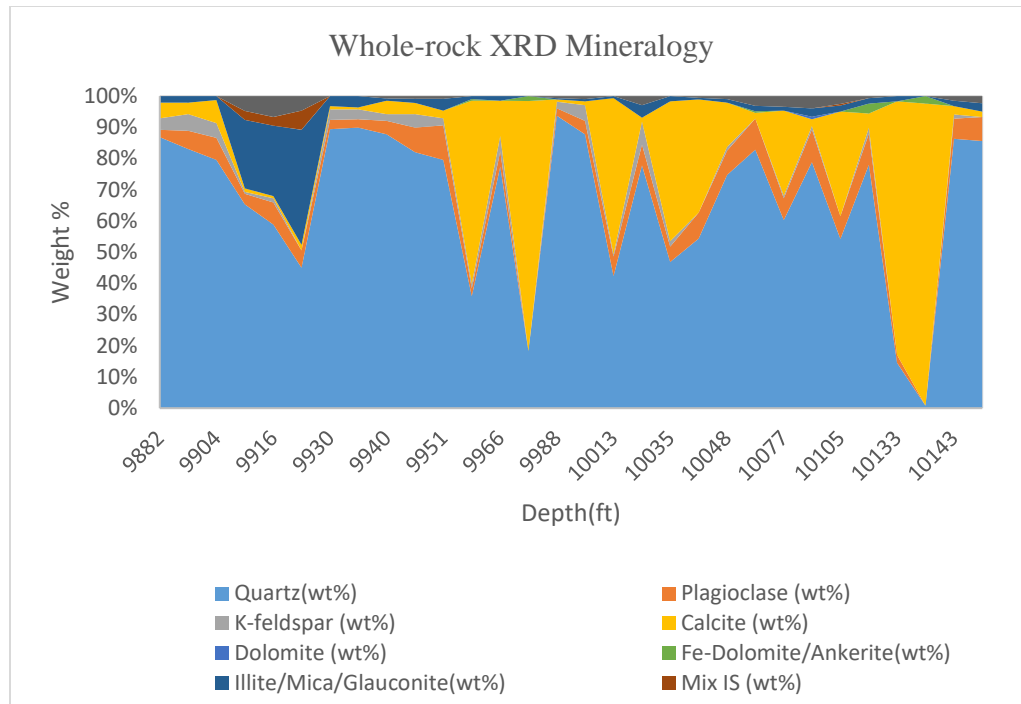
Figure 25 Whole-rock XRD mineralogy versus depth (W.D. Von Gonton Laboratories, 2016).

7.4 Bulk Geochemical Analysis

Si, Ca, K, Al, S, Fe, and Mg are the bulk elements in the Cotton Valley Group Sandstones, and are variable throughout the core, as shown in Figure 28. Here, the focus is mainly on these bulk elements and their mineralogical components.

Generally, the bulk elements represent different proxies including: detrital proxies (Al, K, Si, Mg, Fe, S), in particular the siliciclastic minerals such as quartz, feldspars, micas and clay minerals; carbonate proxies (Ca, Mg), such as calcite and Mg-bearing calcite; and sulphur (S), which could be elemental sulphur or pyrite. The elemental sulphur is a product of pyrite oxidation on the core surface.

Overall, there is a positive linear relationship between the potassium (K%) and aluminium content (Al%) (Figure 26A). This gives an indication that the CVG Sandstones are rich in potassium feldspar/orthoclase ($KAlSi_3O_8$) or illite $(K,H_3O)(Al,Mg,Fe)_2(Si, Al)_4O_{10}((OH)_2(H_2O))$. The aluminum can be attributed to the clay minerals while the potassium can be attributed to both orthoclase and the clay minerals. The XRD indicates minor amounts of potassium feldspar (Figure 25) in the CVG Sandstones, and therefore the potassium (K%) and aluminum (Al%) are attributed to the illite found throughout the formation. Generally, the Si is attributed to the siliciclastic minerals found throughout the core, including quartz, clay minerals, and feldspar. Calcium is attributed primarily to carbonate minerals.

Two trends can be observed between Fe% and S% (Figure 26B). When Fe is High and S is low, the Fe is attributed to illite, chlorite or hematite. However, when both Fe and

S are elevated, this indicates pyrite. Pyrite (FeS$_2$) is in minor amounts throughout the core (< 1%), exceeding 1% in only two samples (Appendix 2) and therefore most of the Fe is concentrated in the clay minerals such as illite and chlorite:

illite (K,H$_3$O)(Al,Mg,Fe)$_2$(Si,Al)$_4$O$_{10}$((OH)$_2$(H$_2$O)),

Chlorite (Mg,Fe)$_3$(Si,Al)$_4$O$_{10}$(OH)$_2$(Mg,Fe)$_3$(OH)$_6$).
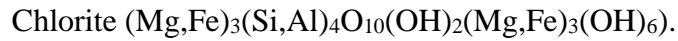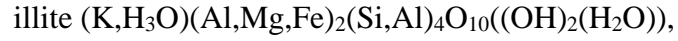
Furthermore, while minor amounts of hematite are found in the thin sections as cement, the XRD did not detect hematite. Hematite generally needs to be present at ~1% or greater to be detected in the XRD (Balsalm et al., 2014). In this study, it is assumed that iron is present either in the clay minerals or as pyrite when sulphur is present.
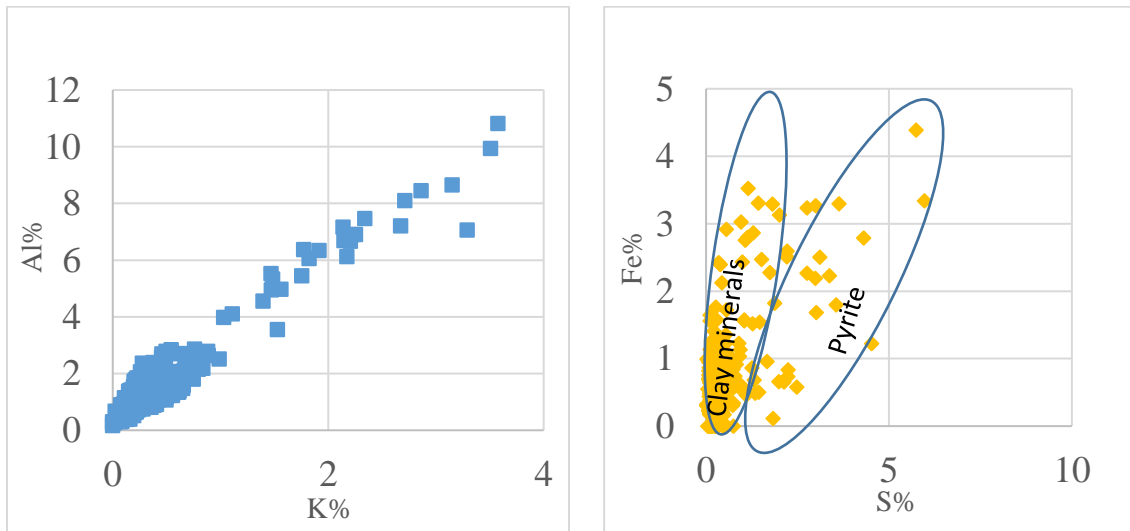


Figure 26 A) Plot of Al (%) versus K (%), B) Plot of Fe (%) versus S (%) depth.

Overall, the calcium content ranged from 0-48% and the magnesium content ranged from 0-2%. Three different trends can be observed when plotting calcium vs magnesium (Figure 27). Based upon the mixing ratios of calcium vs. magnesium, there is primarily calcite (limestone) present in the core where there is an increasing amount of calcium and no magnesium present in the sample. There is also the other extreme where there is a high amount of magnesium, but little to no calcite present in the sample. This is thought to be chlorite because very little to no dolomite is found throughout the samples in XRD or thin sections (Figure 28). Finally, there is a transition zone, where there is some magnesium. This is attributed to Mg-bearing calcites.
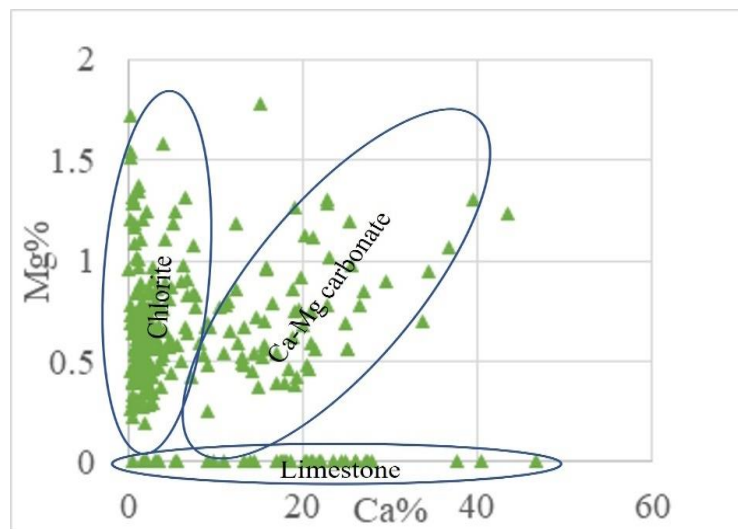


Figure 27 Plot of Mg (%) versus Ca (%).

In Unit 1, sharp increases in K, Al, Fe, Mg and S concentrations are observed where is a silty mudstone/siltstone lithofacies, showcasing the increase in clay minerals in that interval. The concentration of carbonates is lowest at this interval, ranging from 0-5wt%.

In Unit 2, a sharp increase in carbonate content to ~ 48wt% correlating with a lower silica content (5 wt%) is observed. This indicates a carbonate interval/ limestone lithofacies, probably a shallow marine with less detrital influx. Consequently, K, Al, and Fe concentrations are very low (0-5 wt%), indicating fewer clay minerals in this interval. Sulphur content is also relatively low (0-5 wt%), indicating little throughout this section.

Unit 3 and Unit 4 have a similar geochemical variation trend (Si wt% vs Ca wt%). The carbonate content in these units is moderately high, averaging ~25wt%. Other elemental concentrations such as K, Al, Fe, Mg, and S are also generally low (0-5wt%) except at the depths of 10,124ft (3085.8m) in Unit 3, and 9,997ft (3047.1m) in Unit 4. Overall, there are relatively lower concentrations of clay minerals in Unit 3 & 4 except at the depths indicated above. This is confirmed by the XRD (Figure 25) and the general thin section and core descriptions.

The transition from quartz arenites (Unit 4) to silty clay/siltstone lithofacies of Unit 5 (9,912ft - 9,927ft) correlates with a sharp increase in the terrigenous influx of Al, K, Mg, and Fe and decreased calcium content (down to 0 wt.%). The sharp increase in Al, K, Mg, and Fe signifies the input of detrital clays.

Within the quartz wacke interval of Unit 6, it is observed that there is an inverse relationship between silica (Si wt%) and calcium content (Ca wt%) as shown by the XRD

in Figure 25. This is further indicated in XRF data, where increases in Ca correlate with decrease in Si (Figure 28). Also, elemental concentrations of K, Al, Fe, Mg and S are generally very low (0-5 wt%) throughout the interval but are directly proportional to the silica concentration (Si wt%). Overall, this interval contains a large amount of detrital components (quartz and clay minerals) with minor calcite which is most likely in the form of fossils and calcite cement.

The beds throughout the core with increased carbonate content (Ca wt%) are a point of mineral dissolution during carbon dioxide sequestration which could enhance the porosity and permeability of the formation. Clay minerals such as chlorites are triggered by low pH of the brine solution caused by $CO_2$ interactions. This causes dissolution and secondary precipitation of other silicates and carbonates (Zhang et al., 2019).
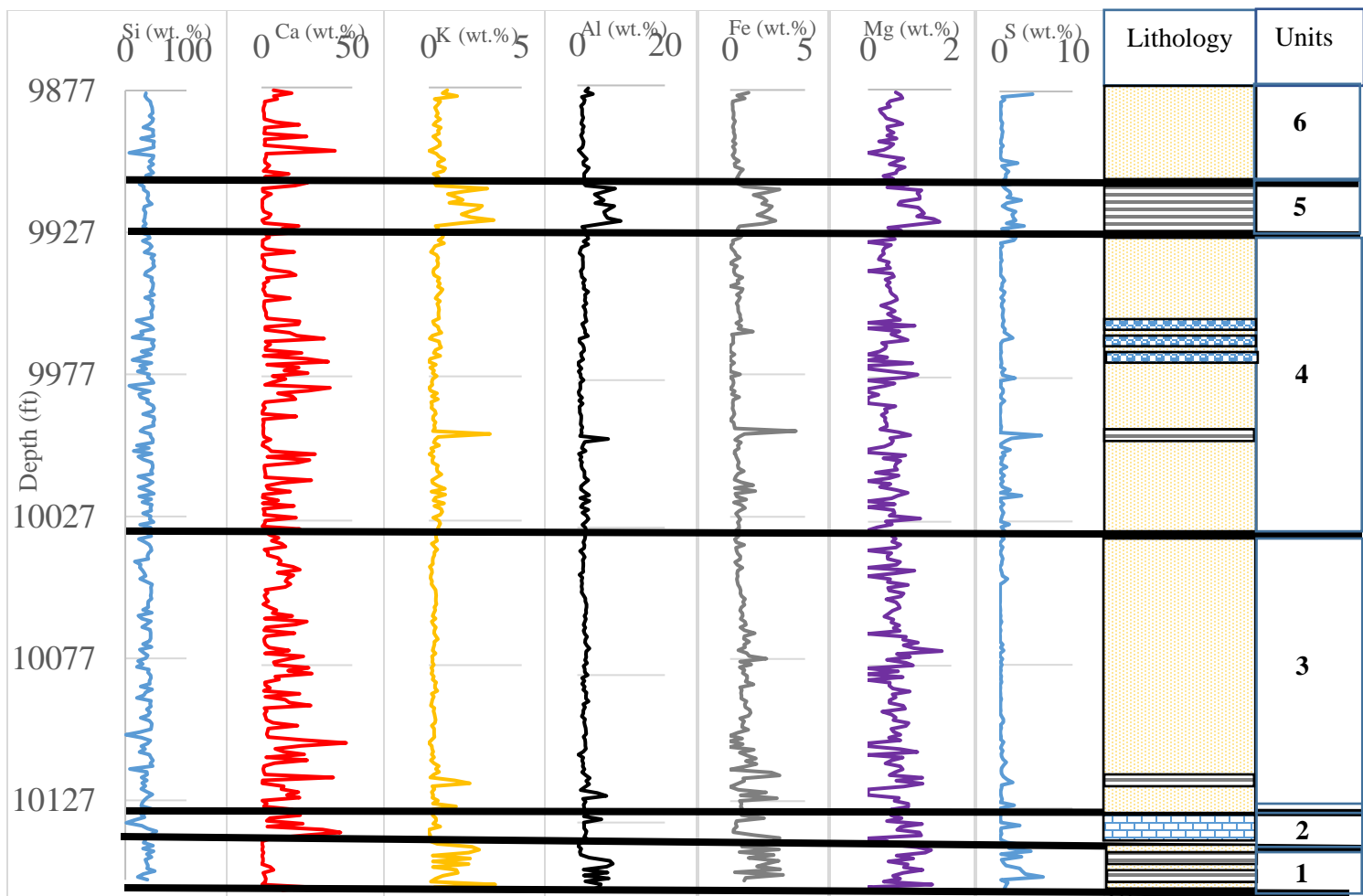
Figure 28 Plot of bulk elements, lithology, and depth of the Worely Estate Core.

7.5 Structure of the Cotton Valley Group Sandstones

Unit 6 is used as a reference datum (horizontal line) for the CVG Sandstones (Figure 29). This is based on the fact that Unit 6 is the top of the chronostratigraphic unit of the cores, and also on the assumption that the tectonic subsidence associated with rifting decreased from the Early Jurassic through to the Late Jurassic-Early Cretaceous, as such had minimal effect on latter sedimentation (Unit 6), hence flat depositional surface with no depositional slopes. The units below the datum line (Unit 1, 2, 3, 4 & 5) were the most affected during/after rifting, which is reflected in the sedimentation and architecture (thickening and thinning trend), creating depositional slopes as seen in Figure 29.

Structure and isopach maps were generated for each unit in the core. Generally, the CVG Sandstones dip from the north-central to the southeastern direction in northern Louisiana (Figures 30). The structure map is contoured at an interval of 25ft (7.62m). Two structural highs are observed, one in the north-central section towards the east Texas boundary, which is associated with two closely spaced wells (API 17-119-21631, 17-119-20355) with a depth of 8850ft (2697.5m) below mean sea level (MSL), and the other towards the far east in the northern Louisiana boundary, around the area of well API 17-027-20830 to a depth of approximately 8900ft (2712.7m) below MSL. These two locations provide closure for a potential structural trap in the area and were once the targets of gas drillers in the region based on production and well locations.

An isolated smaller ridge of approximately 9350ft (2849.8m) below MSL is observed in the south. The top Unit 6 ranged in depths from 8850ft (2697.5m) to 9550ft (3032.8m) below (MSL).
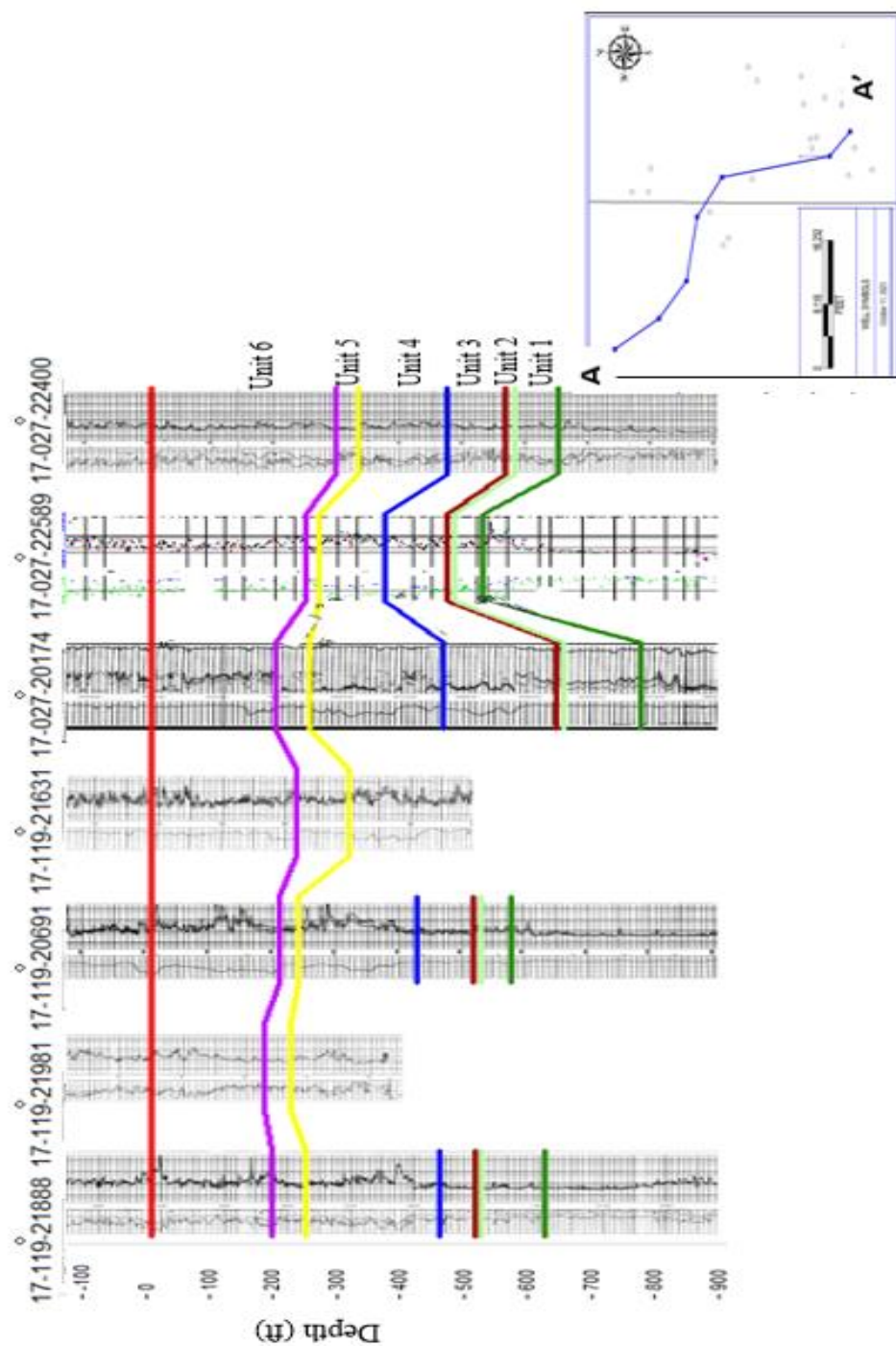
Figure 29 Cross-section A-A' of wells from the northwest to southeast
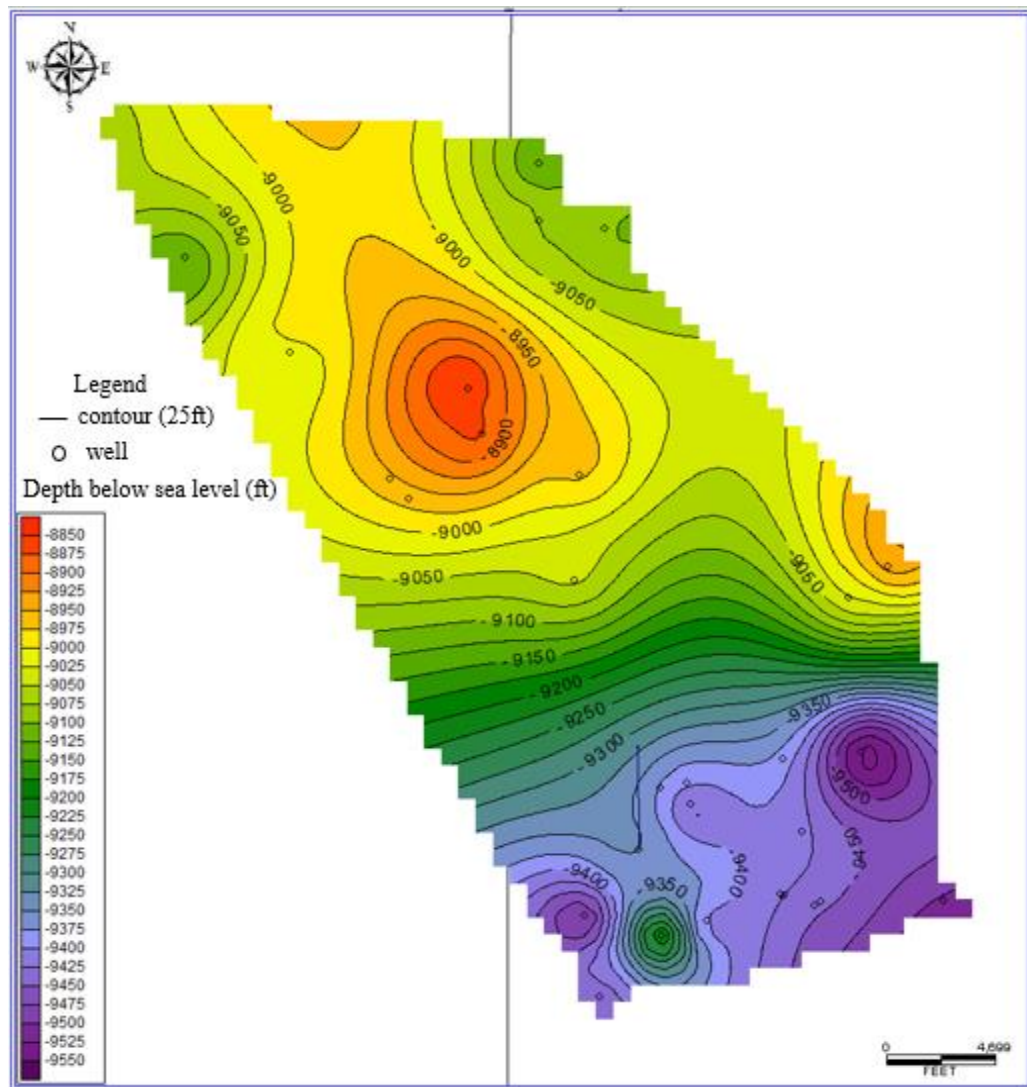
Figure 30 Structural trend of the top of Unit 6.

The base of the CVG Sandstones generally dips from the northwest (East Texas) towards the southeast (northern Louisiana) (Figure 31). However, only one structural high is observed towards the northwest. The base of the CVG Sandstones ranges in depths from

approximately 9,450ft (2880.4m) to 10,150ft (3093.7m) below MSL. These structure maps

of the Cotton Valley Group Sandstones are influenced by subsequent tectonic activities in

the area since deposition of the CVG Sandstones and represent modern structure. Overall,

the Cotton Valley Group Sandstones are located at depths that exceed 8,000ft (2438.4m)

and have available structural maps in the form of a dome (Figure 31) that would enhance

carbon storage, creating closure and a structural trap. The formation is classified as a

"deep" trap and would allow for ideal pressure and temperature conditions to maintain

supercritical $CO_2$ (Bachu, 2003; Bach et al., 2007).
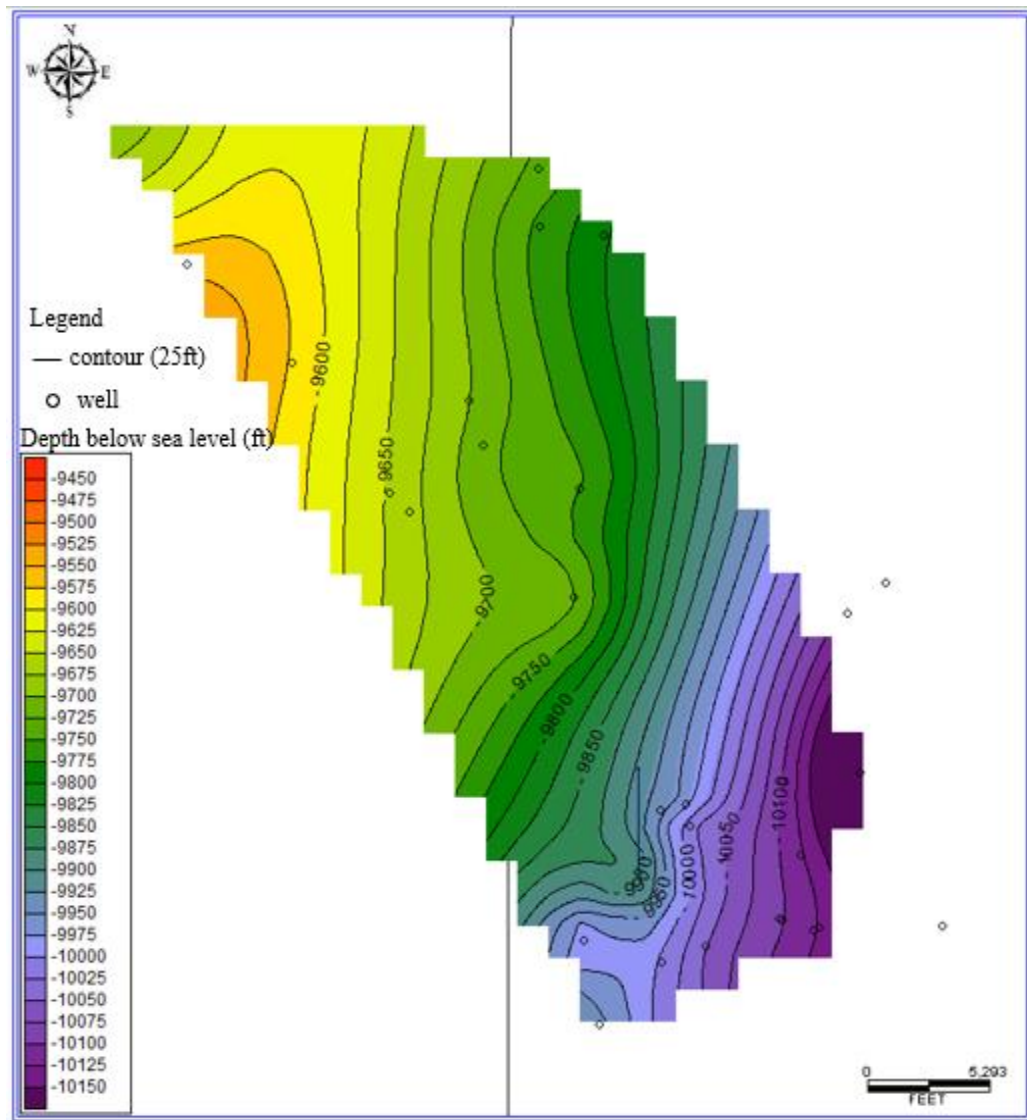
Figure 31 Structural trend for the base Unit 1.

7.6 Isopach maps

Unit 1 isopach map (Figure 32) thickens from the northeast through to the southeast, and thins towards the northwest through to the southwest. The thickness ranges from 165ft (50.3m) to 25ft (7.62).
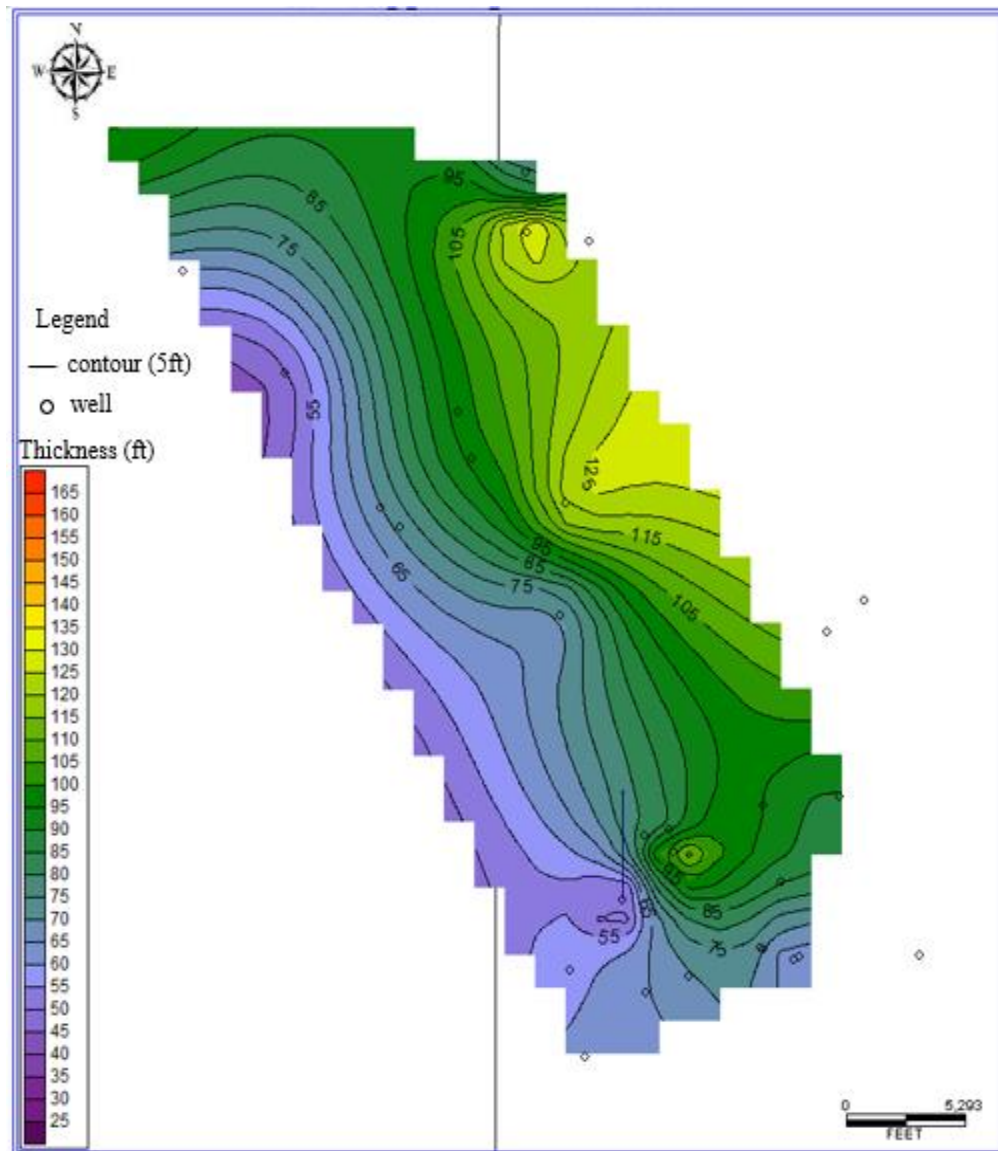


Figure 32 Isopach map of Unit 1.

Unit 2 isopach map (Figure 33) thickens from the center towards the west and towards the south-southeast. Isolated spots of thinning occur in the north and southeast. The thickness ranges from 14.8ft (4.5m) to 7.8ft (2.4m).
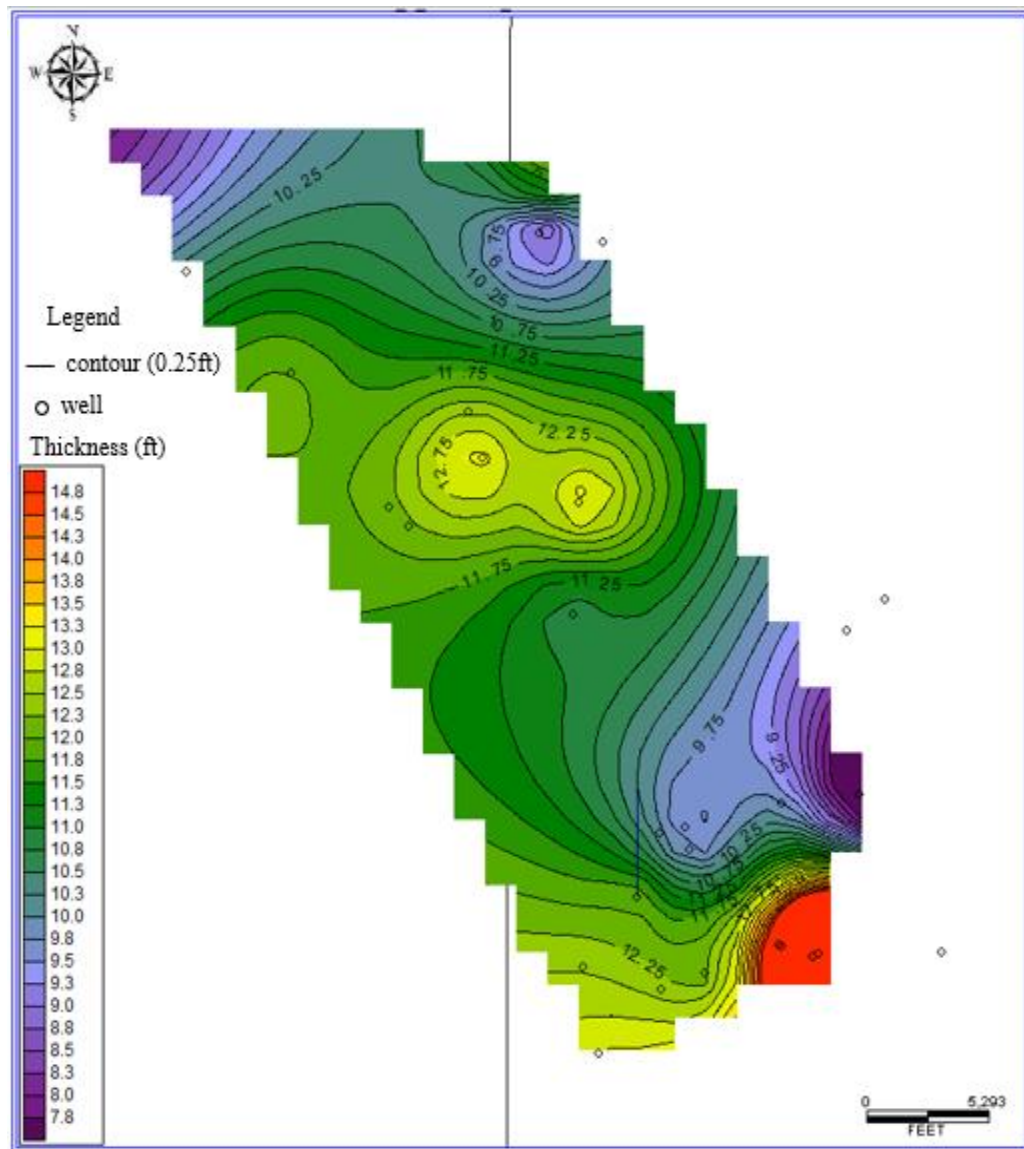


Figure 33 Isopach map of Unit 2.

Unit 3 (Figure 34) shows thickening towards the northeast, and a slight thickening at the southeast, and generally thinning towards the northwest and southwest. Isolated spots of thinning are observed at the south-east, in between the thickening trend. The thickness ranges from 180ft (54.9m) to 40ft (12.2m).
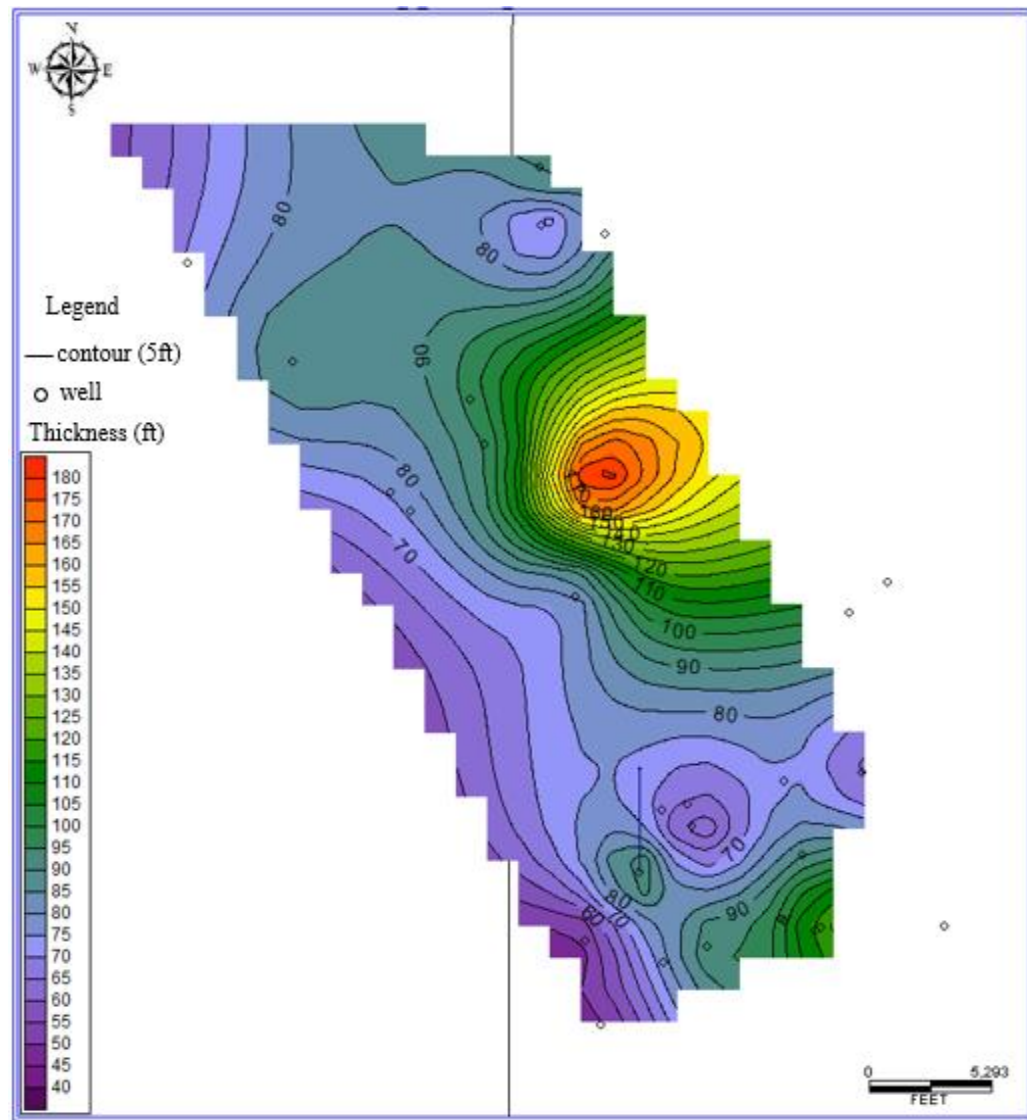


Figure 34 Isopach maps of Unit 3.

Unit 4 isopach map (Figure 35) is thickest at the center, thickens slightly towards the northeast, and thins towards the southeast. The thickness ranges from 380ft (115.8.8m) to 100ft (30.48m).
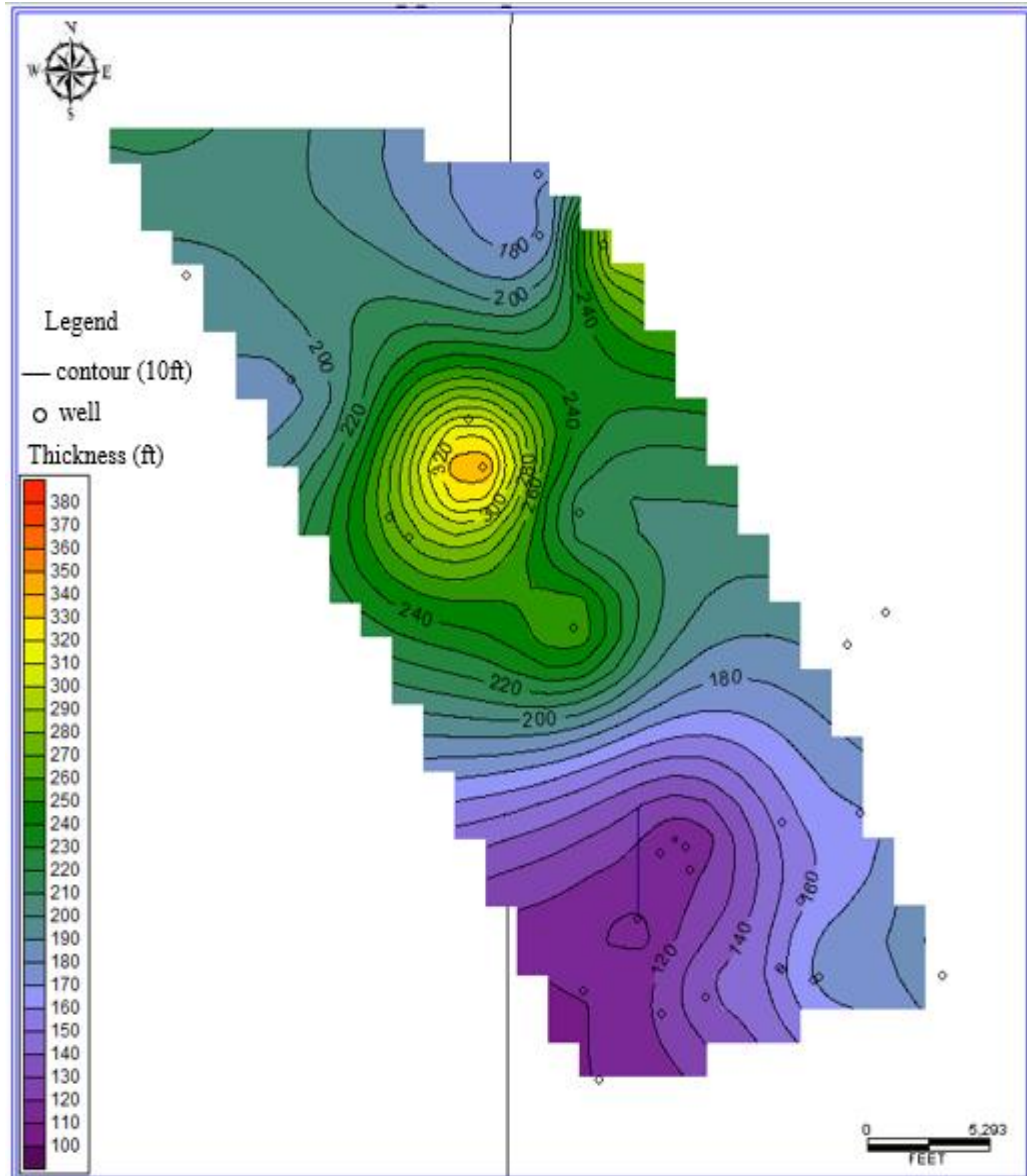


Figure 35 Isopach map of Unit 4.

Unit 5 isopach map (Figure 36) is the thickest in the center and towards the north-east, and thins towards the southeast and the northwest. The thickness of these facies ranges from 74ft (22.6m) to about 18ft (5.5m).
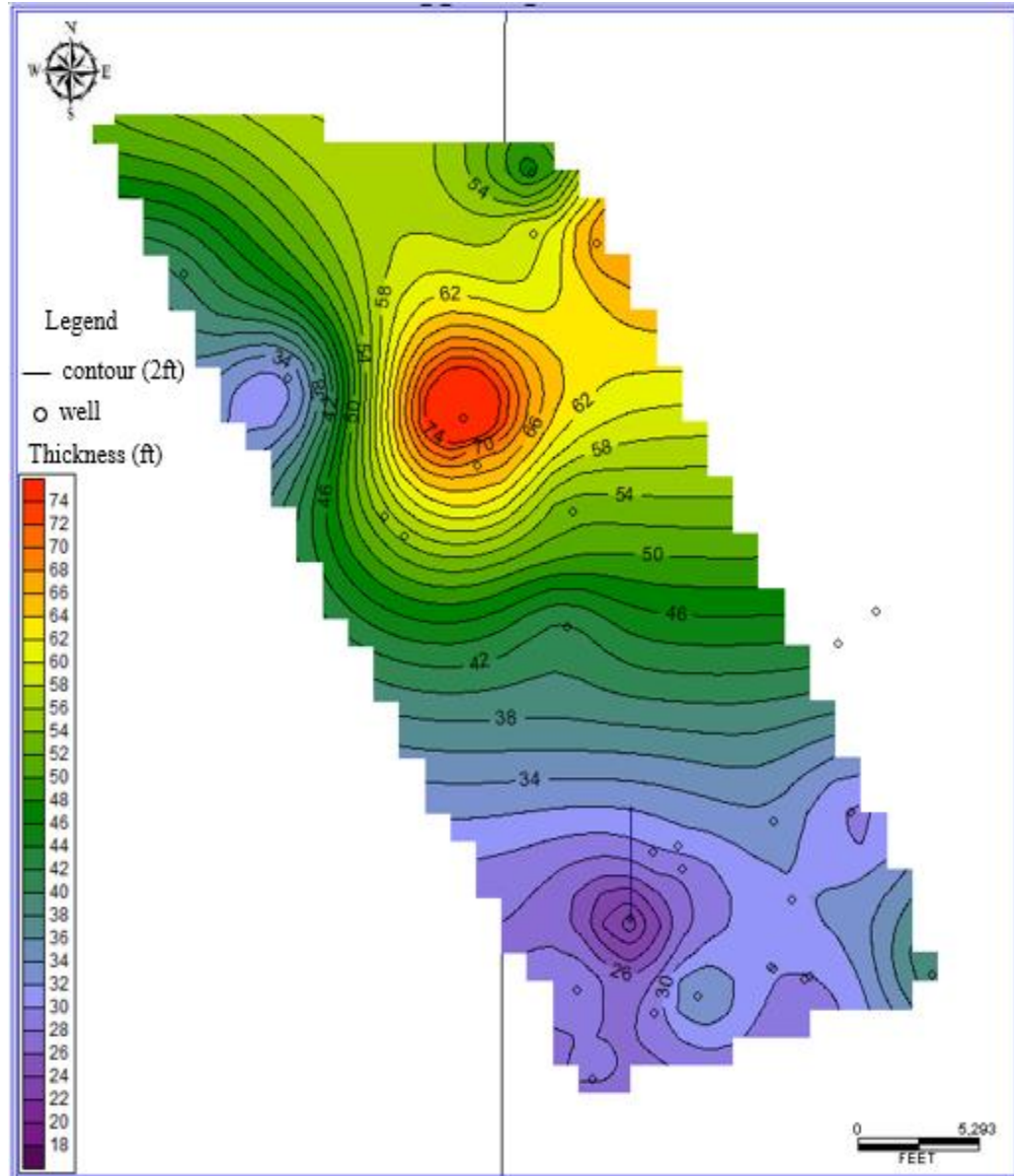


Figure 36 Isopach map of Unit 5.

Unit 6 isopach map (Figure 37) shows a thickening trend towards the south-east and a thinning trend from the center through to the northwest and the northeast. The thickness ranges from 160ft (48.8m) to 440ft (134.1m).
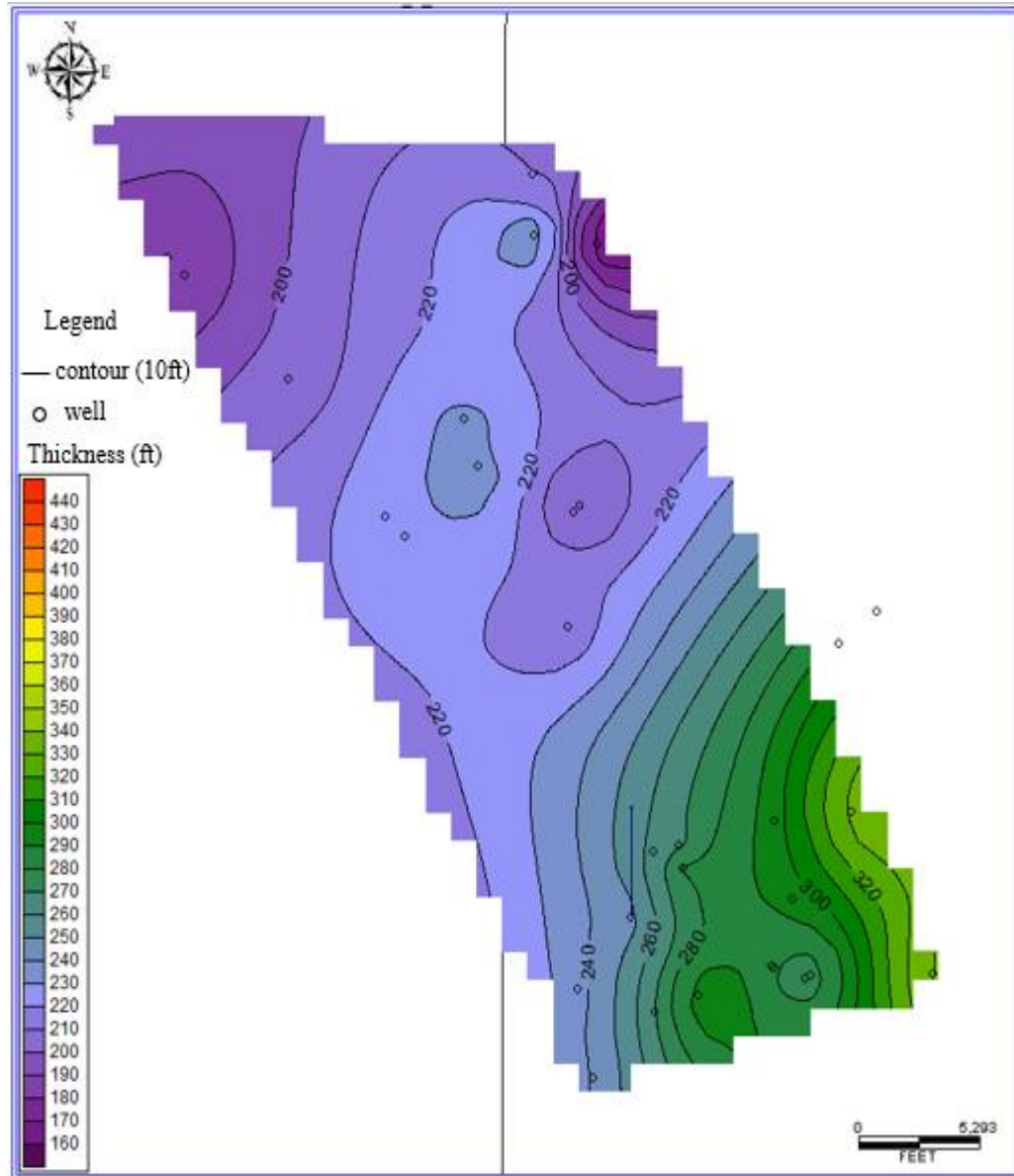


Figure 37 Isopach map of Unit 6.

# 8.0 DISCUSSION

## 8.1 Depositional environment

One of the common features associated with coastlines is the formation of barrier islands, and the northern Gulf of Mexico is no exception. Barrier islands are sand bodies parallel to the coastline, separated from the land by shallow lagoon, estuary or marsh, and commonly dissected by tidal channels or inlets. Barrier islands are well developed on wave-dominated coasts, and associated with low sediment supply and relative sea level rise (Reading, 2009).

In this study, some of the units observed within the Cotton Valley Group Sandstones are reworked barrier islands. The criteria for recognizing barrier island sand bodies in the rock record are discussed below. The transgression and regression of barrier islands create different vertical profiles (Figure 38). In a transgressive barrier island sequence, there is an upward coarsening succession in which coarser grained shoreface and washover sediments become deposited on fine-grained lagoonal sediments, an indication of landward migration of the shoreline (Willis and Moslow., 1994).

Conversely, regressive sequence results in the deposition of fine-grained lagoonal deposits over shoreface sediments (seaward migration of the shoreface) (Willis and Moslow., 1994).
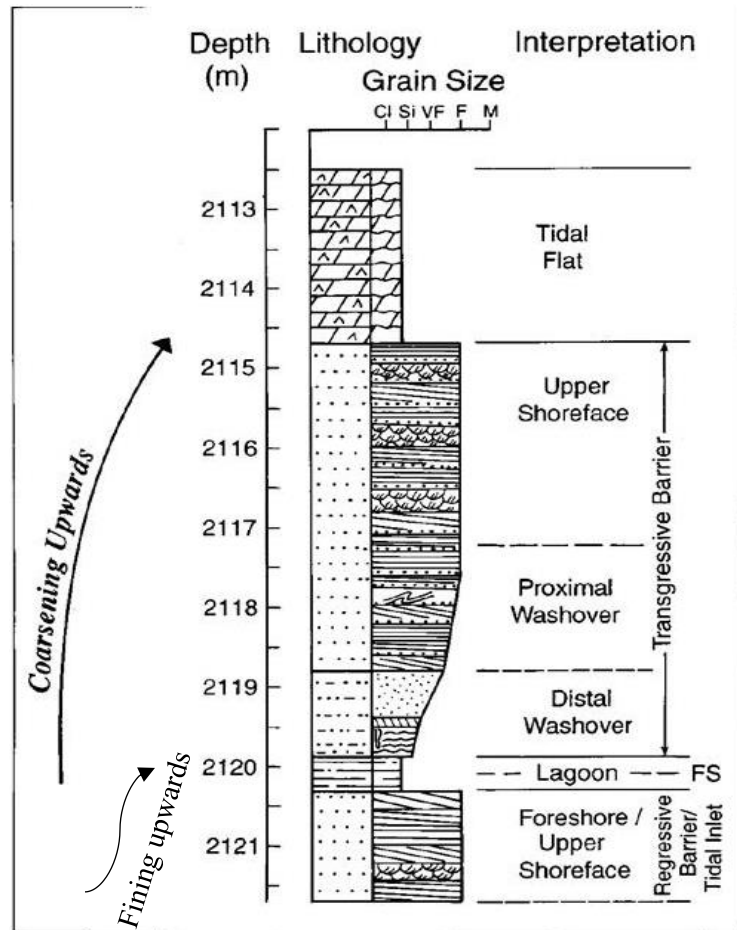
Figure 38 Coarsening upward trend in Halfway Formation transgressive barrier island sand bodies. The interval below 2120.4m shows regressive barrier island deposits (Modified from Willis and Moslow, 1994).

The Worley Estate Core records the rise and fall of sea level in a coastal environment during the deposition of the CVG. The depositional environments in the study area include tidal flats, lagoons, reworked barrier islands, and reefal slope (Figure 39). Overall, the CVG Sandstones in this study consist of a regressive sequence where siltstones/silty mudstones

of lagoonal deposit (Unit 5) overlie reworked barrier island sand deposits (Unit 3 & 4), and capped by a coarser grained tidal deposit.

Unit 1 consists of quartz arenites interbedded with siltstone (Figure 10). These quartz arenites are fine-grained, moderately sorted to well sorted, and are the deposition of a high energy wave-dominated reworked barrier island. The silty-mudstones were deposited during flooding of the coastal environment. This was followed by a rise in sea level to a shallow marine environment, evidenced by the deposition of wackestone in Unit 2, in reef slope adjacent to the barrier islands. This is characterized by an abundance of whole fossils (bivalves) and pellets. The random occurrence of silty quartz grains rip-up clasts at shallow depths (Sample 5) may be the result of storm depositions.

The wackestone in Unit 2 is overlain by the quartz arenites of Units 3 and 4. The interpretations of Unit 3 and Unit 4 are also deposition from a wave-dominated, reworked barrier island, a high-energy environment that washed away most of the fine-grained matrix leaving quartz mineral grains. The occurrence of thin laminated siltstones within these units indicate deposition during periodic rises in sea level or flooding events. Unit 3 is genetically related to Unit 4; however, Unit 3 is heavily calcite cemented throughout its depth (Figure 25). The calcite cementation is thought to have been sourced locally from fossils, and diagenetic, which is explained in Section 8.2 below. The occurrence of conglomerates (large rounded pebbles of quartz) lithofacies intervals within Unit 4 may be attributed to intermittent fluvial inputs with high depositional energy.

Unit 5 is interpreted to be deposited in a low-energy, lacustrine environment called the Hico Lagoon, located behind the barrier islands in Unit 4 (Dyman and Condon, 2006). These silts and clays were washed inland into the lagoon during the periods of high tides. The southward regression of the Terryville barrier island complex gave rise to the expansion of the Hico lagoon behind the barrier southwards (Thomas and Mann, 1966), and consequently the deposition of lagoon siltstones over the reworked barrier islands sandstones.

These silty and clay-rich units abruptly transition into the quartz wacke of Unit 6. Unit 6 is interpreted also as a tidal flat environment characterized by herringbone cross-stratifications with coarser grains compared to the underlying unit. Herringbone cross-stratifications are associated with modern tidal flat environments, on a shallow marine shelf. These have bidirectional current flows where the cross beds are oriented in opposite directions to each other indicating current reversals (Dalrymple et al., 1990).

In regressive or prograding tidal settings, there is a change in grain sizes from coarser grains at the subtidal zones (seawards) to a fining upward sequence in the intertidal zones (landwards); from sands to sand/mud to mud, an indication of a decreasing energy level landwards (Weimer et al., 1982). Therefore, the coarser grained sandstones of Unit 6 can be interpreted as deposition within the subtidal zones of the tidal flat environment.
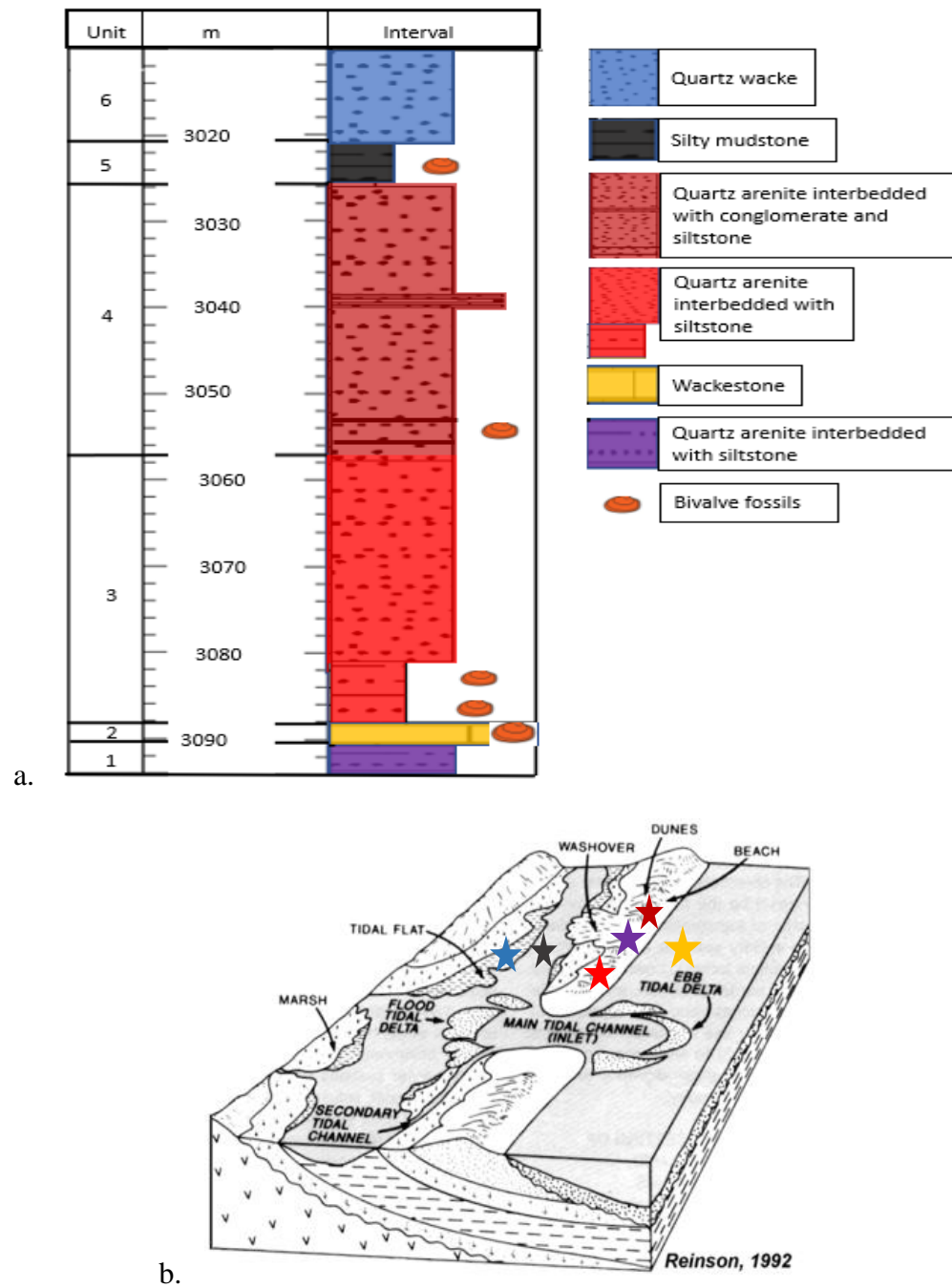
Figure 39 A) Stratigraphic column of the CVG Sandstones. B) Depositional environment (Modified from Reinson, 1992).

8.2 Diagenetic History

Diagenesis is prevalent throughout the Worley Estate core. The earliest phase of diagenesis includes bioturbation of sediments and soft sediment deformation during/after burial giving a mottled appearance from the cores (Figure 15). This was followed by the compaction of sediments as a result of overburden sediment loading, which resulted in fractures and dissolution of fossils and mineral grains at contact boundaries, and later cementation of quartz, calcite, hematite, and recrystallization of bivalves and the clay matrix.

Quartz cementation is thought as the first cement to precipitate in the pore spaces. It is observed as an overgrowth enclosing the individual quartz grain boundaries where they occur (Samples 2, 10, 18). The sources of silica for quartz cement may be locally derived from the pressure dissolution of quartz minerals at contact boundaries or infiltration of groundwater saturated with silica through the pore spaces (Boggs, 2012). Pressure dissolution is a result of the overburden pressure on the individual mineral grain contacts.

Calcite cementation is the second diagenetic cement to precipitate. Calcite cement was most prevalent in the mid to lower portions of the cores (Units 1, 2,3,4) as seen from the XRD data (Figure 25). The calcite cements were observed as pore fillings between the detrital grains and as patchy layers in thin sections (Samples 12, 14, 16). The sources of calcium may be attributed to marine pore-waters, dissolution of bivalve shells, and

limestone beds, which provided free calcium ions for precipitation within the pore spaces between the grains, and also enclosing some of the bivalve shells.

Thirdly, hematite cementation proceeds calcite cementation. This is observed as an iron-stained cement in the clay matrix, and disseminated within calcite cements in thin sections of Samples 8, 23, & 25. In some cases, hematite nodules or cemented pellets were also observed (Figure 22a). Hematite cements are derived from the oxidation of iron-bearing minerals such as biotite in oxic pore waters. Hematite cements indicate an oxidizing environment during diagenesis (Ulmer-Scholle et al., 2014).

The fourth diagenetic process is the simultaneous recrystallization of clay minerals and bivalve shells. The clays in the CVG Sandstones are comprised of both detrital and authigenic clays. Some of the clays have been slightly recrystallized, and partially filled the dissolved bivalves and intergranular pores as discrete aggregates, and as pore-bridging cement completely filling the pore spaces as shown in thin sections (Figures 22 & 23). The rise in sea level (flooding event) is attributed as the main source of detrital clays and silts input. The sources of authigenic clay minerals may be attributed to the transformation of precursor clay minerals, and from direct precipitation from pressure solutions through the pore spaces and fractures. Authigenic clay minerals such as illite and chlorite also occurred as thin films within the intergranular and moldic pores (Sample 24). Chlorite coating has minimal effect on the preservation of porosity. A minor amount of silts were derived from storm deposition as evidenced in sample 5.

The last diagenetic phase is the maturation of organic matter into hydrocarbons. This is observed as the dead oil sparsely distributed in some samples (1, 2, 6 & 17). One notable observation is the migration/flowing of dead oil along open fractures in Sample 6 (10124.8ft, 3086m) and Sample 17 (9948ft, 3032.15m).
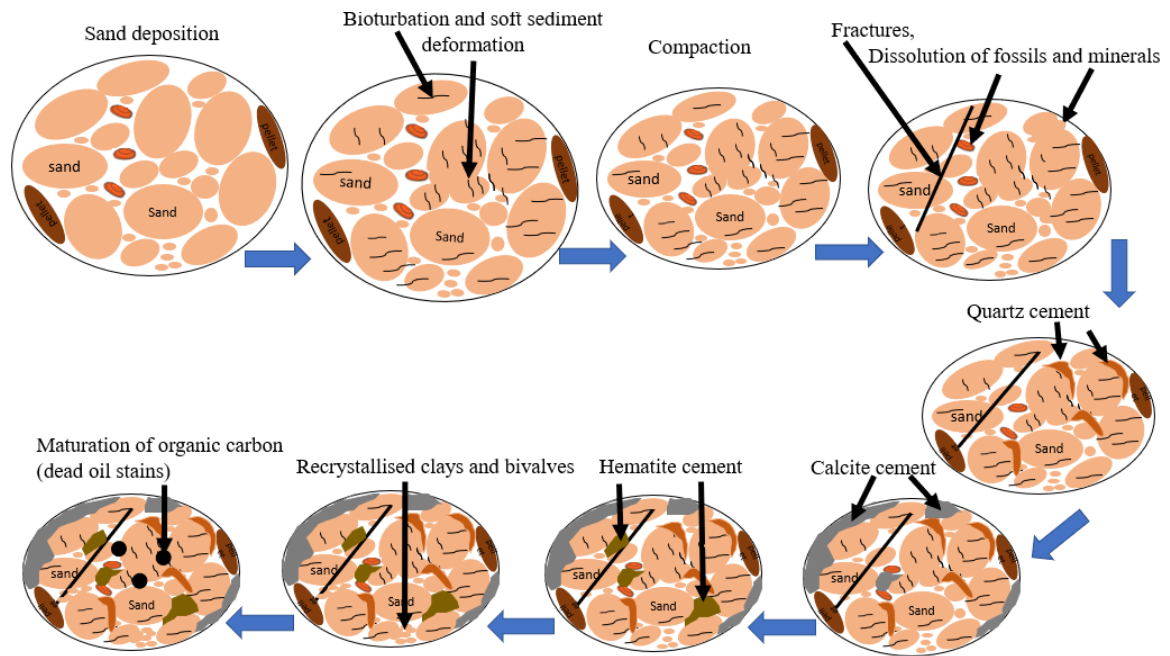


Figure 40 Diagenetic model of the CVG Sandstone.

The diagenetic evolution of the wackestone unit (Unit 2) involves the compaction of silty fossiliferous pelletal/fossiliferous wackestones followed by secondary sparry calcite cement filling in the pore spaces, and later dissolution of fossils resulting in secondary pores (moldic pores).

8.3 Controls on Reservoir Quality

The reservoir quality within the CVG Sandstones is a combination of depositional environment and diagenetic influence. The CVG Sandstones show tight reservoir characteristics as noted by the core analysis, petrology, porosity, and permeability data. The porosity ranged from 0.8% to 14.5%. The permeability is generally very low ranging from 0.003md to 2.04md. There is a positive correlation between porosity and permeability as shown in Figure 41.
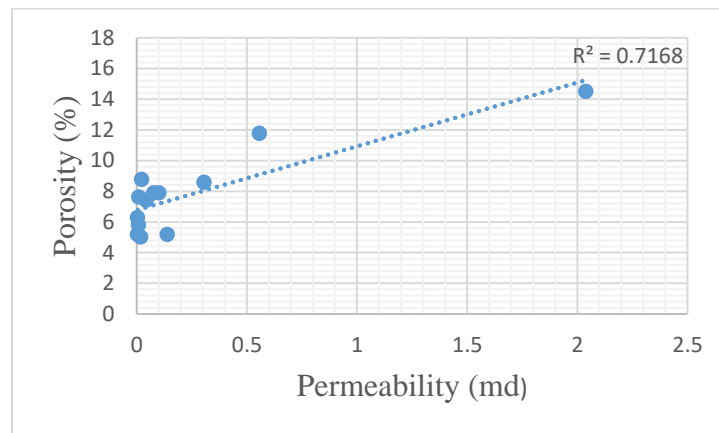


Figure 41 Plot of porosity vs permeability.

The controls on porosity and permeability appear to vary throughout the core. Unit 6 porosity is controlled mainly by the detrital clay matrix as shown in thin sections of Samples 23, 24 & 25 (Figure 23). Overall, diagenesis is thought to be the main influence on the reservoir quality in the deeper units (Units 1, 2, 3 & 4). Calcite cementation is the main factor altering porosity and permeability, with minor amounts of hematite cement, quartz overgrowth, and clay minerals in these units. Calcite cementation is inversely related

to the total porosity; intervals heavily cemented by calcite had low porosity and vice-versa (Figure 42). Samples 12, 13, 14 & 16 are excellent examples of this in thin section (Figures 19 & 20). On the contrary, quartz shows a positive correlation with total porosity (Figure 43). Quartz cementation constituted a minor amount of cementation in the CVG Sandstones compared to calcite cement. Quartz also shows an inverse relation with calcite content (Figure 44).

Although authigenic clay minerals such as chlorite have been suggested to enhance or preserve porosity by preventing the overgrowth of quartz cement by authors such as Hillier et al. (1996), on the contrary, there is no strong correlation between chlorite and porosity preservation in the Cotton Valley Group Sandstones as shown in Figure 45. The porosity within the CVG Sandstones was mostly of secondary origin in nature owing to the development of fractures and moldic pores (dissolution).
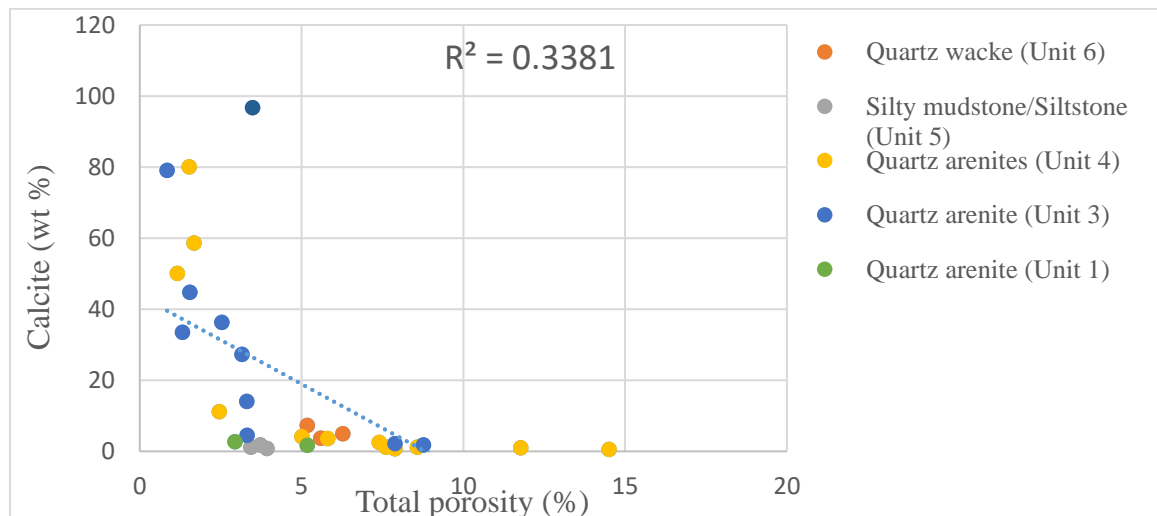


Figure 42 Plot of calcite vs porosity.
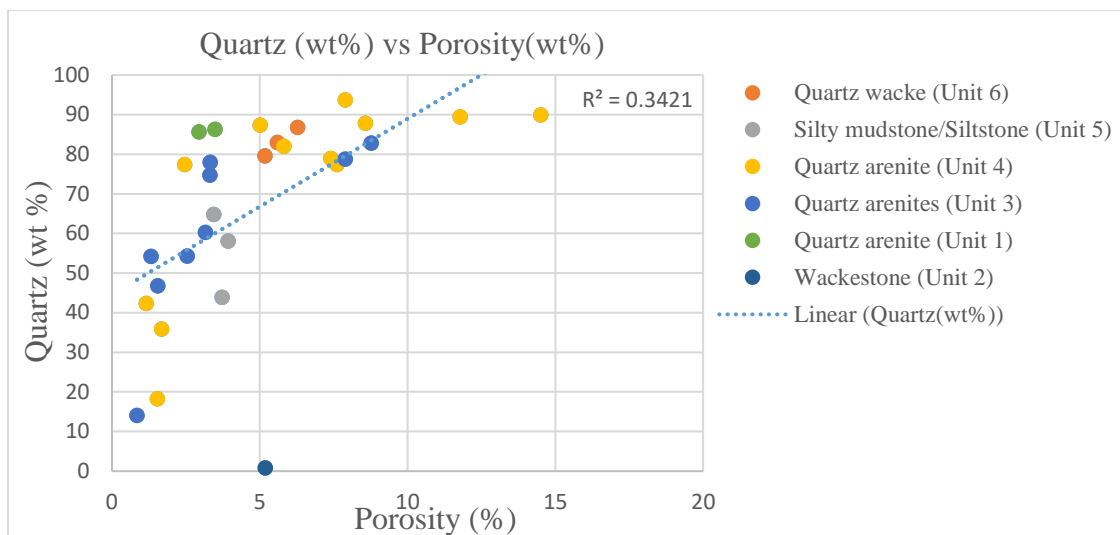
Figure 43 Plot of quartz vs porosity.
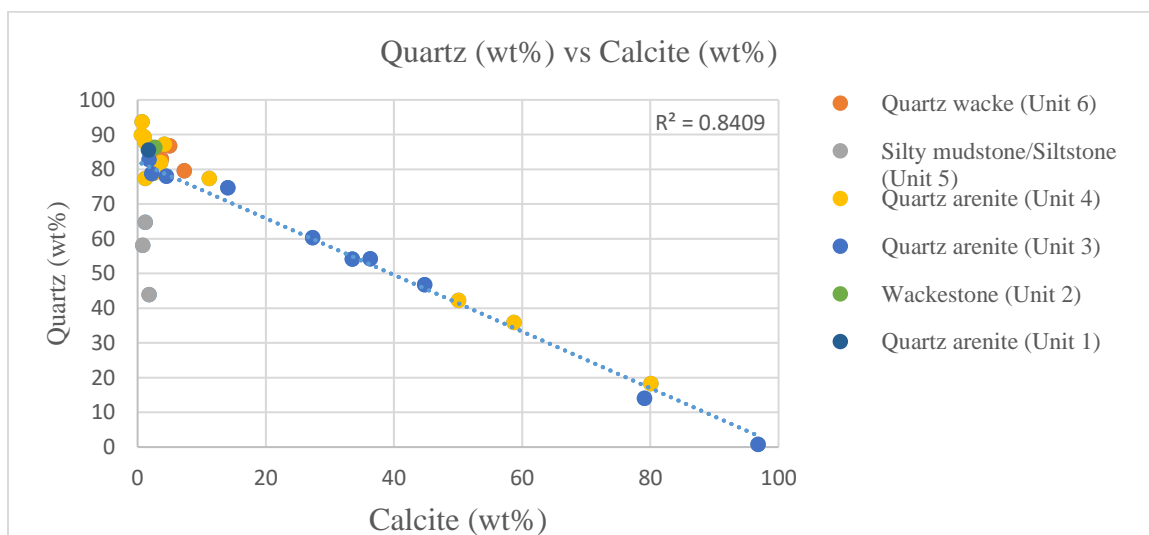


Figure 44 Plot of quartz (wt%) vs calcite (wt%).
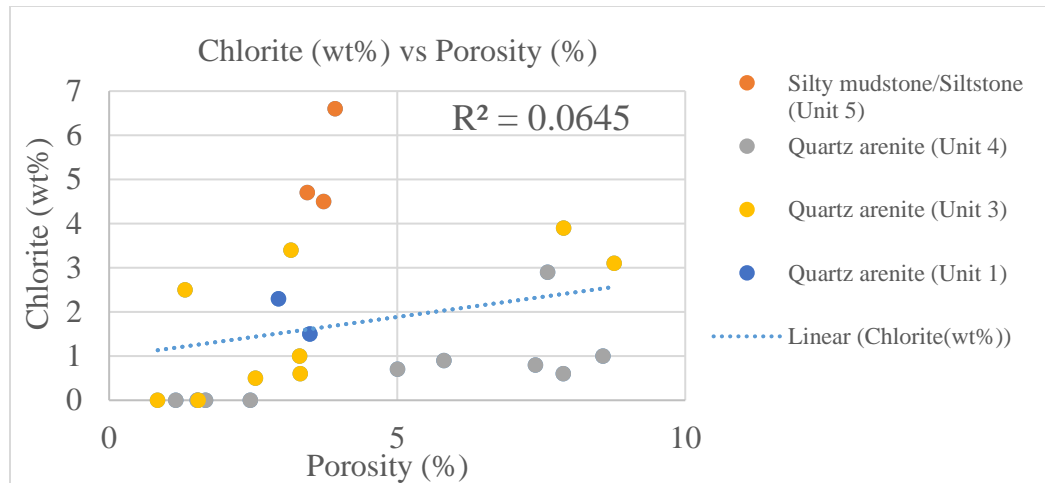
Figure 45 Plot of chlorite vs porosity.

Overall, Unit 4 is regarded as the best reservoir unit in the study area. It has the highest average porosity and permeability values (7.85% and 1.025md respectively). Furthermore, it is texturally mature and contains relatively low calcite cement and clay content, which will result in little reaction with $CO_2$ within the unit.

8.4 Implications for Carbon Sequestration

Chadwik et al., (2008) characterized reservoir properties into positive indicators and cautionary indicators for $CO_2$ storage. Positive indicators are those with these specifications; depth (>1000m, <25000m), reservoir thickness (> 50m), porosity (>20%), permeability (>500mD), salinity ($100g^{-1}$) and uniform stratigraphy. Cautionary indicators are those below or above these specifications. $CO_2$ storage capacity and injectivity are directly dependent on the porosity and permeability values (Raza et al., 2016).

The CVG Sandstones are not excellent reservoirs for potential carbon storage and injectivity as they do not satisfy the recommended threshold for porosity and permeability, classifying the formations as "cautionary". The CVG Sandstones satisfy the threshold limit for reservoir depth (>1000m) and thickness (> 50m).

$CO_2$ containment in the subsurface is dependent on the thickness of the sealing formation. It is classified as a positive indicator if the seal thickness is greater than 100m, and a cautionary indicator if less than 20m (Raza et al., 2016). The potential seal of the CVG Sandstones in this study area is Unit 5 with a thickness of less than 20m, and as such, does not satisfy the recommended sealing threshold.

Solubility trapping is dependent on salinity, temperature and pressure of the reservoir. Raza et al. (2016) classified positive indicators if it has low salinity, low temperature gradient and under pressure, and a cautionary indicator if it has high salinity, high temperature gradient and overpressured (high). Dutton et al. (1993) considered the salinity

of the CVG Sandstones high with estimated formation-water salinity on the order of 170,000ppm TDS (169.8g/L). As such it is regarded as cautionary. Lower salinity tends to reduce $CO_2$ mobility and migration thereby enhancing residual and solubility trapping, and good for containment and vice versa for high salinity (Al-Khdheeawi et al., 2018).

Spencer (1987) classified reservoirs with pressures greater than 0.55psi/ft as overpressure and less than 0.55psi/ft as under pressure. The CVG Sandstones have variable pressures across northern Louisiana, with a fluid pressure gradient greater than 0.55psi/ft occurring in northeastern Louisiana (classified as high), and a normal pressure gradient occurring in the blanket sandstones in northwestern Louisiana (Bartberger et al., 2019). The northeastern areas are unfavorable for carbon sequestration.

Smith et al., (1981) indicated that the geothermal gradients in the northern Louisiana ranged from $25^0C/km$ to over $40^0C/km$, with several sites greater than $30^0C/km$. This is considered relatively high as such it is regarded as a cautionary indicator. High geothermal gradients have lower $CO_2$ storage capacity and higher buoyance forces (Bachu, 2003).

Lastly, the CVG Sandstones have a simple mineralogy, it is predominantly composed of quartz minerals with relatively lower concentrations of reactive minerals such as calcite, chlorite, feldspars, and hematite in varying proportions. According to Zhang et al., (2019), this would limit the $CO_2$-brine-sandstone interactions, as such mineral dissolution becomes limited. Quartz is the main mineral interacting with carbonic acid, which is chemically stable.

Overall, the CVG Sandstones are not suitable for carbon storage, injectivity, solubility trapping, and containment based on the threshold of porosity, permeability, seal, salinity, geothermal gradient, pressure, and mineralogy as discussed above.

Table 2: Summary of the CVG Sandstones for potential CCUS (Modified from Chadwick et al., 2008 ; Raza et al., 2016).

| Ideal conditions | Indication | CVG Sandstone | Suitability |
|---|---|---|---|
| Minerals | Mineral trapping | Less Ca, Mg, or Fe-rich minerals | ✗ |
| Depth (>1000m,< 25000) | Storage capacity | >1000m | ✓ |
| Reservoir thickness (> 50m) | Storage capacity | >278ft, 85m | ✓ |
| Porosity (>20%) | Storage capacity | 0.8% to 14.5% | ✗ |
| Seal thickness (>100m) | Containment | <100m | ✗ |
| Permeability (>500mD) | Injectivity | 0.003mD - 2.04mD | ✗ |
| Low salinity | Solubility trapping | 170000ppm TDS (high) | ✗ |
| Under pressure (< 0.55psi) | Solubility trapping | < 0.55psi, > 0.55psi | ✓✗ |
| Low temperature gradient (< 25°C/km) | Solubility trapping | 25°C/km to over 40°C/km | ✗ |

## 9.0 CONCLUSIONS

The paper assessed the reservoir quality, depositional and diagenetic history of the Cotton Valley Group Sandstones in Claiborne Parish, LA for CCUS Potential. The Cotton Valley Group Sandstones are unfavorable for CCUS based on the parameters discussed above. The following can be concluded from this research.

1. The Cotton Valley Group Sandstones are comprised of quartz wacke, silty mudstone, quartz arenites, limestone, and quartz arenites interbedded with silty mudstone/siltstone. The reservoir properties of these units vary with depositional environment and diagenetic effects.

2. The environment ranged from a low-energy depositional environment to a high-energy depositional environment; from modern tidal flats to lagoon to reworked barrier islands and reefal slope. The quartz wacke (Unit 6) was deposited in a tidal flat environment, the silty mudstone with abundant fossils (Unit 5) was deposited in a lagoon (Hico lagoon), the wackestone unit (Unit 2) in a reefal slope, and the quartz arenites as reworked barrier islands (Unit 1, 3 & 4).

3. The porosity within the CVG Sandstones was mainly of secondary origin (moldic and fractures) caused by the dissolution of cement and bivalves, and minor primary intergranular porosity. Porosity and permeability were mainly restricted by clay minerals and calcite cementation. Authigenic minerals such as chlorite have

minimal effect on preserving porosity, with a weak positive correlation with total porosity.

4. Generally, the Cotton Valley Group Sandstones are not suitable for long-term carbon sequestration because it is either heavily infiltrated with detrital clay matrix or cemented by calcite.

9.1 Future Research

There is great potential for future research on this formation. The data for the Cotton Valley Group is very limited. The core data used in this study was obtained from a single well, and some of the wells did not contain enough well logs such as density and neutron logs.

An in-depth study on the carbon sequestration potential would require additional data such as seismic data of the area, and some geochemical modeling experiments to ascertain how some minerals such as calcite cement, clays, and quartz will react with the $CO_2$ gas under variable depths and pressure within the basin.

# 10.0 REFERENCES

Al-Khdheeawi, E. A., Vialle, S., Barifcani, A., Sarmadivaleh, M., Zhang, Y., & Iglauer, S. (2018). Impact of salinity on CO2 containment security in highly heterogeneous reservoirs. *Greenhouse Gases: Science and Technology*, *8*(1), 93-105.

Atwell, B. W., Henk, B., Meendsen, F. C., & Breyer, J. A. (2008). Depositional Setting and Petroleum Production, Gray Sandstone (Upper Jurassic), Cotton Valley Field, Northern Louisiana.

Bachu, S. (2003). Screening and ranking of sedimentary basins for sequestration of $CO_2$ in geological media in response to climate change. *Environmental Geology*, *44*(3), 277-289.

Bachu, S., Bonijoly, D., Bradshaw, J., Burruss, R., Holloway, S., Christensen, N. P., & Mathiassen, O. M. (2007). $CO_2$ storage capacity estimation: Methodology and gaps. International journal of greenhouse gas control, 1(4), 430-443.

Balsam, W., Ji, J., Renock, D., Deaton, B. C., & Williams, E. (2014). Determining hematite content from NUV/VIS/NIR spectra: Limits of detection. American Mineralogist, 99, 2280-2291.

Bartberger, C. E., Dyman, T. S., & Condon, S. M. (2002). Is there a basin-centered gas accumulation in Cotton Valley group sandstones, Gulf Coast Basin, USA?. US Department of the Interior, US Geological Survey.

Boggs, S. (2012). Principles of sedimentology and stratigraphy.

Bryant, E., & Bryant, E. A. (1997). Climate process and change. Cambridge University Press.

Chadwick, A., Arts, R., Bernstone, C., May, F., Thibeau, S., & Zweigel, P. (2008). Best practice for the storage of CO2 in saline aquifers-observations and guidelines from the SACS and $CO_2$ STORE projects (Vol. 14). British Geological Survey.

Christopoulou, M. A., Koutsovitis, P., Kostoglou, N., Paraskevopoulou, C., Sideridis, A., Petrounias, P., & Koukouzas, N. (2022). Evaluation of the $CO_2$ Storage Capacity in Sandstone Formations from the Southeast Mesohellenic trough (Greece). Energies, 15(10), 3491.

Coleman Jr, J. L., & Coleman, C. J. (1981). Stratigraphic, sedimentologic and diagenetic framework for the Jurassic Cotton Valley Terryville massive sandstone complex, northern Louisiana.

Cornelius, S. (2023). Comparison of the Characteristics of Cretaceous Salt Deposition in Brazil with Jurassic Salt Deposition in the Gulf of Mexico.

Dalrymple, R. W., Knight, R. J., Zaitlin, B. A., & Middleton, G. V. (1990). Dynamics and facies model of a macrotidal sand-bar complex, Cobequid Bay—Salmon River Estuary (Bay of Fundy). *Sedimentology*, *37*(4), 577-612.

Duncan, D. W., & Morrissey, E. A. (2011). The Concept of geologic carbon sequestration. US Department of the Interior, US Geological Survey.

Dutton, S.P., Clift, S.J., Hamilton, D.S., Hamlin, H.S., Hentz, T.F., Howard, W.E., Akhter, M.S., and Laubach, S.E, 1993, Major low permeability sandstone gas reservoirs in the continental United States: University of Texas, Bureau of Economic Geology, Report of Investigations No. 211, 221 p.

Dyman, T.S., and Condon, S.M., 2006, Chapter 2. Assessment of undiscovered conventional oil and gas resources--Upper Jurassic-Lower Cretaceous Cotton Valley Group, Jurassic Smackover interior salt basins total petroleum system, in the East Texas basin and Louisiana-Mississippi salt basins provinces: Data Series, DOI: 10.3133/ds69e_chapter2.

Eoff, J.D., Dubiel, R.F., Pearson, O.N., and Whidden, K., 2015, Geologic Framework for the Assessment of Undiscovered Oil and Gas Resources in Sandstone Reservoirs of the Upper Jurassic– Lower Cretaceous Cotton Valley Group, U.S. Gulf of Mexico Region: Gulf Coast Association of Geological Societies, v. 65, p. 93–105.

Eversull, L. G. (1985). Depositional Systems and Distribution of Cotton Valley Blanket Sandstones in Northern Louisiana.

Ewing, T. E. (2001). Review of Late Jurassic depositional systems and potential hydrocarbon plays, northern Gulf of Mexico Basin.

Hardy, R. and Tucker, M., 1988, Techniques in Sedimentology, In Tucker, M.E (Edited) Blackwell Scientific Publications. Oxford London Edinburgh Boston Melbourne, p.191.

Hillier, S. (1995). Erosion, sedimentation and sedimentary origin of clays. In *Origin and Mineralogy of Clays: Clays and the Environment* (pp. 162-219). Berlin, Heidelberg: Springer Berlin Heidelberg.

Hunt, J.M. 1995: Petroleum Geochemistry and Geology, Second edition, 743 pp. W.H. Freeman and Company, New York.

Kelemen, P., Benson, S. M., Pilorgé, H., Psarras, P., & Wilcox, J. (2019). An overview of the status and challenges of $CO_2$ storage in minerals and geological formations. Frontiers in Climate, 1, 9.

Leetaru, H. E., Frailey, S., Morse, D., Finley, R. J., Rupp, J. A., Drahozval, J. A., & McBride, J. H. (2009). Carbon sequestration in the Mt. Simon Sandstone saline reservoir.

Mancini, E.A., Aharon, P., Goddard, D.A., and Barnaby, R., 2006, Basin Analysis and Petroleum System Characterization and Modeling, Interior Salt Basins, Central and Eastern Gulf of Mexico: DOI: 10.2172/884681.

McClain, K. C. (2021). Mineralogical restrictions on porosity in the Taylor Sand of the Cotton Valley Group, Northern Louisiana Salt Basin, Clairborne Parish, Louisiana.

Morales, J. A. (2022). Wave-Dominated Systems I: Barriers and Barrier Islands. In *Coastal Geology* (pp. 207-225). Cham: Springer Nature Switzerland.

National Academies of Sciences Engineering Medicine (2019). Negative Emissions Technologies and Reliable Sequestration: A Research Agenda. Washington, DC: The National Academies Press. Available online at: https://www.nap.edu/catalog/25259/negative-emissions-technologies-and-reliable-sequestration-a-research-agenda.

Petra User's Manual (2011).

Raza, A., Rezaee, R., Gholami, R., Bing, C. H., Nagarajan, R., & Hamid, M. A. (2016). A screening criterion for selection of suitable $CO_2$ storage sites. *Journal of Natural Gas Science and Engineering*, *28*, 317-327.

Reading, H. G. (Ed.). (2009). Sedimentary environments: processes, facies and stratigraphy. John Wiley & Sons.

Reinson, G. E. (1992). Transgressive barrier island and estuarine systems. *Facies models response to sea level change*, 179-194.

Roberts-Ashby, T. L., Brennan, S. T., Buursink, M. L., Covault, J. A., Craddock, W. H., Drake, R. M., ... & Corum, M. D. (2014). Geologic framework for the national assessment of carbon dioxide storage resources—US Gulf Coast. US Geological Survey.

Saucier, A. E., Finley, R. J., Dutton, S. P., & Lin, Z. S. (1985). Geologic framework of the Travis Peak (Hosston) Formation of east Texas and north Louisiana. Finley, RJ, Dutton, SP, Lin, ZS, and Saucier, AE, The Travis Peak (Hosston) Formation: Geologic Framework, Core Studies, and Engineering Field Analysis: University of Texas, Bureau of Economic Geology, [contract report prepared for the Gas Research Institute under contract no. 5082-211-0708].

Sawyer, D.S., Buffler, R.T., and Pilger, Jr., R.H., 1991, The crust under the Gulf of Mexico, in A. Salvadore, ed., The Gulf of Mexico Basin: decade of North American Geology, Boulder, GSA, p. 53-72.

Smith, D. L., Dees, W. T., & Harrelson, D. W. (1981). Geothermal conditions and their implications for basement tectonics in the Gulf Coast margin.

Snæbjörnsdóttir, S. Ó., Sigfússon, B., Marieni, C., Goldberg, D., Gislason, S. R., & Oelkers, E. H. (2020). Carbon dioxide storage through mineral carbonation. Nature Reviews Earth & Environment, 1(2), 90-102.

Spencer, C.W., 1987, Hydrocarbon generation as a mechanism for overpressuring in Rocky Mountain region: American Association of Petroleum Geologists Bulletin, v. 71, no. 4. p. 368–388.

Thomas, W. A., & Mann, C. J. (1966). Late Jurassic depositional environments, Louisiana and Arkansas. *AAPG Bulletin*, *50*(1), 178-182.

Ulmer-Scholle, D. S., Scholle, P. A., Schieber, J., & Raine, R. J. (2014). A color guide to the petrography of sandstones, siltstones, shales and associated rocks (Vol. 109). Tulsa, OK, USA: American Association of Petroleum Geologists.

UNFCCC (2015). Paris Agreement. In Conference of the Parties COP 21 (Paris), 25.

Wang, X., Wang, X., Hu, W., Wan, Y., Cao, J., Lv, C., ... & Cui, M. (2017). Supercritical CO2-involved water–rock interactions at 85°C and partial pressures of 10–20 MPa: Sequestration and enhanced oil recovery. *Energy Exploration & Exploitation*, *35*(2), 237-258.

Weimer, R. J., Howard, J. D., & Lindsay, D. R. (1982). Tidal flats and associated tidal channels: part 1.

Weltje, G.J., Tjallingii, R., 2008, Calibration of XRF core scanners for quantitative geochemical logging of sediment cores: Theory and application, Earth and Planetary Science Letters, v. 274, p. 423-438.

Willis, A. J., & Moslow, T. F. (1994). Stratigraphic setting of transgressive barrier-island reservoirs with an example from the Triassic Halfway Formation, Wembley Field, Alberta, Canada. *AAPG bulletin*, *78*(5), 775-791.

Xu, T., Apps, J. A., & Pruess, K. (2004). Numerical simulation of $CO_2$ disposal by mineral trapping in deep aquifers. *Applied geochemistry*, *19*(6), 917-936.

Xu, T., Apps, J. A., & Pruess, K. (2005). Mineral sequestration of carbon dioxide in a sandstone–shale system. Chemical Geology, 217(3-4), 295-318.

Zhang, L., Wang, Y., Miao, X., Gan, M., & Li, X. (2019). Geochemistry in geologic $CO_2$ utilization and storage: A brief review. Advances in Geo-Energy Research, 3(3), 304-313.

Zhang, K., Sang, S., Liu, C., Ma, M., & Zhou, X. (2019). Experimental study the influences of geochemical reaction on coal structure during the CO2 geological storage in deep coal seam. *Journal of Petroleum Science and Engineering*, *178*, 1006-1017.

## 11.0 APPENDICES

Appendix 1: XRF data

| Depths (ft) | Si% | Ca% | K% | Al% | S% | Fe% | Mg% |
|---|---|---|---|---|---|---|---|
| 9877.95 | 33.62563 | 6.603315 | 0.989217 | 2.517161 | 4.5262 | 1.223268 | 0.664401 |
| 9878.95 | 32.17362 | 16.54525 | 0.747524 | 1.80413 | 0.369904 | 0.478876 | 0.786402 |
| 9879.95 | 35.54994 | 6.77493 | 1.529704 | 3.560746 | 0.712591 | 0.980697 | 0.829476 |
| 9880.95 | 40.74688 | 8.735859 | 0.319075 | 1.041741 | 0.109415 | 0.167776 | 0.532397 |
| 9881.95 | 42.12487 | 1.747826 | 0.61982 | 1.701736 | 0.234379 | 0.154876 | 0.461574 |
| 9882.95 | 43.67768 | 1.860526 | 0.486837 | 1.493226 | 0.114946 | 0.171658 | 0.535616 |
| 9883.95 | 44.24109 | 1.10767 | 0.334638 | 0.863164 | 0.155621 | 0.1813 | 0.279313 |
| 9884.95 | 44.82668 | 1.054188 | 0.409156 | 1.134746 | 0.197257 | 0.227096 | 0.312586 |
| 9885.95 | 39.60515 | 1.421127 | 0.494813 | 1.076908 | 0.123124 | 0.233427 | 0.392917 |
| 9886.95 | 45.75663 | 1.412475 | 0.391381 | 1.104659 | 0.182871 | 0.187529 | 0.440011 |
| 9887.95 | 44.10523 | 1.669461 | 0.61508 | 1.395985 | 0.408495 | 0.339776 | 0.682251 |
| 9888.95 | 39.02243 | 7.718445 | 0.379483 | 1.123154 | 0.334279 | 0.245244 | 0.825036 |
| 9889.95 | 29.32945 | 20.81952 | 0.258906 | 0.909255 | 0.269546 | 0.175649 | 0.464495 |
| 9890.95 | 45.64559 | 1.784967 | 0.649446 | 1.484816 | 0.442829 | 0.253717 | 0.478458 |
| 9891.95 | 45.31634 | 1.71493 | 0.497458 | 1.196903 | 0.356915 | 0.241116 | 0.617882 |
| 9892.95 | 46.35395 | 1.445785 | 0.557588 | 1.314486 | 0.352538 | 0.312826 | 0.463261 |
| 9893.95 | 25.44468 | 24.84696 | 0.236389 | 0.81025 | 0.202119 | 0.309226 | 0.684056 |
| 9894.95 | 47.27131 | 1.81168 | 0.425194 | 1.074228 | 0.1294 | 0.176747 | 0.269064 |
| 9895.95 | 45.79167 | 1.955057 | 0.599357 | 1.40275 | 0.499433 | 0.369215 | 0.606752 |
| 9896.95 | 46.84005 | 1.684178 | 0.598526 | 1.368748 | 0.148075 | 0.180948 | 0.522337 |
| 9897.95 | 29.40771 | 19.17619 | 0.357002 | 1.171608 | 0.225941 | 0.312911 | 0.381467 |
| 9898.95 | 6.712286 | 40.44882 | 0.020588 | 0.300873 | 0.150847 | 0.290635 | 0 |
| 9899.95 | 46.23931 | 2.580945 | 0.405069 | 0.911584 | 0.141523 | 0.163044 | 0.3652 |
| 9900.95 | 45.27291 | 2.637353 | 0.546695 | 1.524174 | 0.341022 | 0.273212 | 0.84882 |
| 9901.95 | 39.64835 | 1.715737 | 0.835119 | 2.187128 | 2.482198 | 0.582272 | 0.684323 |
| 9902.95 | 45.59788 | 1.869963 | 0.503349 | 1.401599 | 0.324987 | 0.284399 | 0.519979 |
| 9903.95 | 37.91932 | 4.355025 | 0.491335 | 1.40349 | 0.747325 | 0.341671 | 0.884894 |
| 9904.95 | 41.0534 | 2.695119 | 0.887098 | 2.644622 | 1.252751 | 0.865442 | 0.702028 |
| 9905.95 | 45.52691 | 1.167179 | 0.794625 | 2.160703 | 0.83709 | 0.661698 | 0.676036 |
| 9906.95 | 33.64222 | 14.93664 | 0.252695 | 1.563092 | 0.911815 | 0.576253 | 0.368407 |

Continued

| Depths (ft) | Si% | Ca% | K% | Al% | S% | Fe% | Mg% |
|---|---|---|---|---|---|---|---|
| 9907.95 | 46.32204 | 1.954101 | 0.521187 | 1.58028 | 0.533071 | 0.441516 | 0.60782 |
| 9908.95 | 32.50091 | 14.50278 | 0.381798 | 1.559413 | 2.231058 | 0.736571 | 0 |
| 9909.95 | 23.3221 | 25.5142 | 0.296763 | 1.391084 | 0.441915 | 0.518896 | 0.977148 |
| 9910.95 | 30.18808 | 18.43612 | 0.399338 | 1.904369 | 0.822566 | 0.918175 | 0.459648 |
| 9911.95 | 30.15458 | 0.592384 | 3.151436 | 8.654249 | 1.432146 | 3.305691 | 1.281518 |
| 9912.95 | 36.94533 | 0.741488 | 1.913836 | 6.350625 | 1.519801 | 2.473721 | 1.184521 |
| 9913.95 | 37.64995 | 5.29618 | 1.029482 | 3.986301 | 1.044592 | 1.561592 | 1.238092 |
| 9914.95 | 35.56679 | 2.068038 | 1.471116 | 4.954314 | 2.98716 | 2.190211 | 1.24217 |
| 9915.95 | 37.63315 | 0.304334 | 1.823615 | 6.066144 | 0.996348 | 2.435619 | 0.777638 |
| 9916.95 | 43.20423 | 0.424432 | 1.108635 | 4.111384 | 0.430833 | 2.124518 | 0.727175 |
| 9917.95 | 31.45733 | 0.379776 | 2.863464 | 8.455131 | 1.133409 | 2.800835 | 1.206677 |
| 9918.95 | 29.95099 | 0.711425 | 2.671746 | 7.215427 | 2.212543 | 2.596685 | 1.284682 |
| 9919.95 | 33.39793 | 1.258849 | 2.17359 | 6.130482 | 1.743477 | 2.279545 | 1.343963 |
| 9920.95 | 32.28128 | 5.107443 | 1.770582 | 6.383037 | 1.876171 | 1.822074 | 1.180095 |
| 9921.95 | 31.6855 | 4.062465 | 2.251949 | 6.907413 | 2.206052 | 2.511808 | 1.574934 |
| 9922.95 | 30.00188 | 0.255778 | 3.505231 | 9.946685 | 0.953352 | 3.029085 | 1.715401 |
| 9923.95 | 33.89598 | 1.436674 | 1.753471 | 5.454902 | 3.372042 | 2.230951 | 1.102865 |
| 9924.95 | 29.14738 | 20.42076 | 0.361122 | 1.134539 | 0.346258 | 0.617501 | 0.482754 |
| 9925.95 | 36.64775 | 11.33313 | 0.511061 | 1.745503 | 1.33823 | 0.488434 | 0.800077 |
| 9926.95 | 24.46135 | 24.43233 | 0.274677 | 1.08137 | 0.3001 | 0.524293 | 0 |
| 9927.95 | 37.44537 | 2.643025 | 0.792173 | 2.297649 | 2.247243 | 0.834368 | 0.564163 |
| 9928.95 | 39.7599 | 4.156957 | 0.734794 | 2.510766 | 1.992322 | 0.661714 | 0.645039 |
| 9929.95 | 28.40565 | 0.607571 | 0.521491 | 1.469313 | 0.140012 | 0.183522 | 0 |
| 9930.95 | 39.46449 | 0.682999 | 0.819488 | 2.486115 | 0.402813 | 0.199136 | 0.554622 |
| 9931.95 | 43.24175 | 0.53054 | 0.325743 | 0.937888 | 0.058027 | 0 | 0.400071 |
| 9932.95 | 38.91021 | 2.374488 | 0.240485 | 0.7198 | 0.175604 | 0.14307 | 0.35528 |
| 9933.95 | 31.37283 | 18.04005 | 0.115263 | 0.533854 | 0.205514 | 0.309956 | 0.386846 |
| 9934.95 | 47.61222 | 0.425468 | 0.414701 | 1.325234 | 0.165355 | 0.393044 | 0.303028 |
| 9935.95 | 42.44865 | 0.341723 | 0.511556 | 1.230381 | 0.346444 | 0.643448 | 0.259403 |
| 9936.95 | 46.67118 | 1.701492 | 0.438306 | 1.303155 | 0.088943 | 0.258857 | 0.504848 |
| 9937.95 | 45.34834 | 1.440908 | 0.498271 | 1.31576 | 0.119173 | 0 | 0.450956 |
| 9938.95 | 47.47288 | 1.188549 | 0.474346 | 1.269606 | 0.19553 | 0.458762 | 0.532335 |
| 9939.95 | 41.70227 | 3.316113 | 0.277414 | 0.768571 | 0.190191 | 0.246634 | 0 |
| 9940.95 | 33.85252 | 15.55893 | 0.232782 | 0.956679 | 0.09257 | 0.258866 | 0.581628 |
| 9941.95 | 31.61288 | 18.94625 | 0.292691 | 1.015426 | 0.45825 | 0.361397 | 0.622404 |

Continued

| Depths (ft) | Si% | Ca% | K% | Al% | S% | Fe% | Mg% |
|---|---|---|---|---|---|---|---|
| 9942.95 | 44.00531 | 2.921311 | 0.569426 | 1.765189 | 0.676143 | 0.819983 | 0.421044 |
| 9943.95 | 42.28381 | 3.924139 | 0.467756 | 1.312782 | 0.365246 | 0.481077 | 0.528185 |
| 9944.95 | 45.65525 | 1.200947 | 0.593441 | 1.597228 | 0.380932 | 0.565644 | 0.446064 |
| 9945.95 | 45.06973 | 1.84967 | 0.494518 | 1.402854 | 0.182465 | 0 | 0.532607 |
| 9946.95 | 44.162 | 0.758304 | 0.74812 | 2.523663 | 0.736066 | 0.846937 | 0.533574 |
| 9947.95 | 41.04921 | 1.833108 | 0.629222 | 1.802561 | 0.533751 | 0.74523 | 0.571973 |
| 9948.95 | 47.1553 | 2.3129 | 0.472581 | 1.806942 | 0.224287 | 0.456216 | 0.671887 |
| 9949.95 | 32.55837 | 15.65128 | 0.362115 | 1.722931 | 0.59583 | 0.669915 | 0.698668 |
| 9950.95 | 44.3494 | 1.624251 | 0.597755 | 2.078787 | 0.341166 | 0.561532 | 0.546261 |
| 9951.95 | 42.03787 | 1.518578 | 0.453112 | 1.395181 | 0.274176 | 0.428545 | 0.317396 |
| 9952.95 | 45.81831 | 1.223001 | 0.5272 | 1.791487 | 0.530013 | 0.519284 | 0.516566 |
| 9953.95 | 44.63048 | 1.834297 | 0.550012 | 1.87829 | 0.490304 | 0.519313 | 0.641466 |
| 9954.95 | 41.99351 | 2.66874 | 0.522583 | 1.749702 | 0.428989 | 0.540659 | 0.479001 |
| 9955.95 | 43.41752 | 2.50792 | 0.516914 | 1.925844 | 0.450167 | 0.657507 | 0.607562 |
| 9956.95 | 43.43639 | 3.211947 | 0.553339 | 2.070919 | 0.598405 | 0.655965 | 0.76853 |
| 9957.95 | 18.61073 | 21.02135 | 0.215232 | 1.071945 | 0.461184 | 0.740265 | 0 |
| 9958.95 | 28.22373 | 20.33409 | 0.291601 | 1.407331 | 0.398588 | 0.401411 | 1.123753 |
| 9959.95 | 41.326 | 2.144325 | 0.50518 | 1.790071 | 0.792523 | 0.740346 | 0 |
| 9960.95 | 45.57474 | 2.103963 | 0.534887 | 1.771655 | 0.643316 | 0.549068 | 0.75659 |
| 9961.95 | 25.83766 | 15.50157 | 0.672821 | 2.40715 | 1.267563 | 1.518935 | 0.557463 |
| 9962.95 | 28.64465 | 19.48153 | 0.194463 | 0.523216 | 1.831993 | 0.115899 | 0.757068 |
| 9963.95 | 11.78933 | 34.43913 | 0.051076 | 0.493399 | 0.453776 | 0.21274 | 0.950288 |
| 9964.95 | 47.33651 | 2.33911 | 0.553385 | 1.235096 | 0.161442 | 0.205339 | 0.339513 |
| 9965.95 | 43.24099 | 4.876889 | 0.590576 | 1.483686 | 0.176298 | 0.220033 | 0.439353 |
| 9966.95 | 46.86283 | 2.261236 | 0.655665 | 1.591366 | 0.155657 | 0 | 0.41561 |
| 9967.95 | 44.66911 | 2.310233 | 0.356429 | 0.812654 | 0.271011 | 0 | 0.282284 |
| 9968.95 | 26.41563 | 22.02726 | 0.276601 | 0.984951 | 0.101344 | 0 | 0 |
| 9969.95 | 42.06535 | 1.219387 | 0.61186 | 1.341317 | 0.162064 | 0.287754 | 0.461178 |
| 9970.95 | 25.37499 | 24.96522 | 0.085428 | 0.320029 | 0.236284 | 0 | 0 |
| 9971.95 | 11.91358 | 36.75609 | 0 | 0.312649 | 0.297063 | 0 | 1.062631 |
| 9972.95 | 42.61495 | 3.129781 | 0.377136 | 0.950524 | 0.099315 | 0.275212 | 0 |
| 9973.95 | 24.00994 | 20.54457 | 0.07405 | 0.312795 | 0.747293 | 0 | 0 |
| 9974.95 | 34.25183 | 12.65941 | 0.281316 | 0.763413 | 0.329037 | 0 | 0.58816 |
| 9975.95 | 20.24097 | 25.43489 | 0.202452 | 0.735627 | 0.457947 | 0 | 1.189301 |
| 9976.95 | 39.18714 | 6.170245 | 0.429456 | 1.407527 | 2.12899 | 0.65781 | 0.895903 |

Continued

| Depths (ft) | Si% | Ca% | K% | Al% | S% | Fe% | Mg% |
|---|---|---|---|---|---|---|---|
| 9977.95 | 36.41051 | 13.26399 | 0.202769 | 0.644537 | 0.048978 | 0 | 0 |
| 9978.95 | 43.46669 | 6.793362 | 0.164432 | 0.691353 | 0.195515 | 0.194548 | 0.634564 |
| 9979.95 | 46.40934 | 1.936532 | 0.196384 | 0.692302 | 0.147781 | 0.228675 | 0.399681 |
| 9980.95 | 6.724277 | 37.68517 | 0.018805 | 0.271383 | 0.496541 | 0.172186 | 0 |
| 9981.95 | 16.63621 | 26.03074 | 0.097125 | 0.459711 | 0.493848 | 0 | 0 |
| 9982.95 | 40.05882 | 9.041906 | 0.448417 | 1.124517 | 0.179983 | 0.310345 | 0.252949 |
| 9983.95 | 22.83361 | 16.88563 | 0.157575 | 0.401735 | 0.222366 | 0.119859 | 0 |
| 9984.95 | 24.82219 | 18.72596 | 0.488959 | 1.220274 | 0.69827 | 0.611013 | 0 |
| 9985.95 | 37.1277 | 1.869285 | 0.133837 | 0.526817 | 0.211694 | 0.208388 | 0 |
| 9986.95 | 35.63038 | 0.740477 | 0.176857 | 0.538095 | 0.088612 | 0.185133 | 0.660812 |
| 9987.95 | 45.00192 | 1.924391 | 0.139533 | 0.550203 | 0.121669 | 0.20104 | 0.405579 |
| 9988.95 | 47.37881 | 0.618598 | 0.340028 | 0.889404 | 0.133198 | 0.163459 | 0.453763 |
| 9989.95 | 44.59691 | 0.519573 | 0.38129 | 0.882575 | 0.072704 | 0.232105 | 0.332115 |
| 9990.95 | 29.0247 | 19.26213 | 0.235032 | 0.829805 | 0.103094 | 0.289029 | 0.423035 |
| 9991.95 | 46.66338 | 0.883549 | 0.229869 | 0.770566 | 0.145079 | 0.180181 | 0.409045 |
| 9992.95 | 47.73528 | 1.32193 | 0.363387 | 1.159187 | 0.141182 | 0 | 0.451444 |
| 9993.95 | 45.11623 | 0.783491 | 0.282493 | 0.894401 | 0.255277 | 0.235147 | 0.457243 |
| 9994.95 | 46.87132 | 1.079117 | 0.332672 | 1.045896 | 0.189942 | 0.270013 | 0.296469 |
| 9995.95 | 31.09988 | 0.997952 | 0.217256 | 0.648765 | 0.009823 | 0.304894 | 0.738263 |
| 9996.95 | 24.67283 | 0.900172 | 3.290214 | 7.063227 | 5.742135 | 4.390734 | 1.01775 |
| 9997.95 | 40.95397 | 1.383605 | 0.499382 | 1.731987 | 1.669703 | 0.961101 | 0.536073 |
| 9998.95 | 41.23161 | 4.990736 | 0.348369 | 1.277054 | 0.869311 | 0.593115 | 0.603571 |
| 9999.95 | 45.47168 | 0.992981 | 0.273554 | 1.035858 | 0.229247 | 0.339359 | 0.561641 |
| 10000.95 | 44.80079 | 0.52229 | 0.546186 | 1.920537 | 0.19509 | 0.722876 | 0.392454 |
| 10001.95 | 18.98756 | 3.640162 | 0.130282 | 0.386435 | 1.43539 | 0.503981 | 0 |
| 10002.95 | 38.7645 | 5.34282 | 0.261318 | 0.946821 | 0.408422 | 0.579587 | 0 |
| 10003.95 | 13.72173 | 29.50794 | 0.040439 | 0.621631 | 0.725815 | 0.308813 | 0.896842 |
| 10004.85 | 43.03666 | 3.282454 | 0.273578 | 1.129614 | 0.14138 | 0.285553 | 0.569549 |
| 10004.95 | 41.45782 | 3.898536 | 0.23213 | 0.959358 | 0.44301 | 0.34656 | 0.374605 |
| 10005.95 | 21.4155 | 26.50455 | 0.186395 | 0.904062 | 0.299055 | 0.416436 | 0.781253 |
| 10006.95 | 28.93471 | 20.04104 | 0.203839 | 1.091976 | 0.215786 | 0.506077 | 0.674517 |
| 10007.95 | 43.49993 | 1.549865 | 0.489072 | 1.641501 | 0.982976 | 0.586795 | 0.642189 |
| 10008.95 | 44.59814 | 1.574711 | 0.422411 | 1.64843 | 0.222236 | 0.514556 | 0.704506 |
| 10009.95 | 44.96758 | 2.002728 | 0.451548 | 1.660422 | 0.179289 | 0.549946 | 0.189981 |
| 10010.95 | 41.80138 | 2.292031 | 0.67377 | 2.500795 | 0.642804 | 0.913407 | 0.738626 |

Continued

| Depths (ft) | Si% | Ca% | K% | Al% | S% | Fe% | Mg% |
|---|---|---|---|---|---|---|---|
| 10011.95 | 44.14799 | 1.928339 | 0.420965 | 1.597412 | 0.170229 | 0.527135 | 0.512606 |
| 10012.95 | 21.13861 | 27.44746 | 0.16744 | 0.835839 | 0.485265 | 0.373703 | 0 |
| 10013.95 | 35.63304 | 11.08085 | 0.207626 | 0.810796 | 0.185764 | 0.297661 | 0.542004 |
| 10014.95 | 44.85567 | 2.810658 | 0.471353 | 1.684676 | 0.403872 | 0.740706 | 0.287422 |
| 10015.95 | 38.11454 | 3.50082 | 0.86949 | 2.675881 | 1.463679 | 1.543217 | 0.668769 |
| 10016.95 | 22.70947 | 15.78573 | 0.137836 | 0.691838 | 0.150069 | 0.316505 | 0.953049 |
| 10017.95 | 36.91908 | 0.964503 | 0.881418 | 2.790565 | 3.012309 | 1.685789 | 0.71852 |
| 10018.95 | 46.72634 | 0.717333 | 0.358796 | 1.302387 | 0.15762 | 0.360391 | 0.5663 |
| 10019.95 | 22.96881 | 9.196735 | 0.246998 | 0.840215 | 0.118042 | 0.448689 | 0 |
| 10020.95 | 42.16174 | 0.715859 | 0.814631 | 2.536615 | 0.590241 | 1.072796 | 0.644163 |
| 10021.95 | 28.04247 | 17.96768 | 0.296582 | 1.163794 | 0.185113 | 0.249253 | 0 |
| 10022.95 | 43.27446 | 1.049662 | 0.659802 | 2.117082 | 0.34266 | 0.756848 | 0.611301 |
| 10023.95 | 40.93318 | 1.776886 | 0.720736 | 2.573276 | 0.569166 | 0.998938 | 0.634514 |
| 10024.95 | 42.40877 | 1.226493 | 0.608828 | 1.968531 | 0.367928 | 0.614772 | 0.521222 |
| 10025.95 | 28.78428 | 19.04026 | 0.243161 | 1.20113 | 0.245585 | 0.393022 | 1.258858 |
| 10026.95 | 41.38125 | 2.181813 | 0.53067 | 1.840951 | 0.149758 | 0.555738 | 0.430551 |
| 10027.95 | 39.99786 | 1.810162 | 0.619856 | 2.060145 | 1.314061 | 0.682134 | 0.576599 |
| 10028.95 | 46.0233 | 0.439871 | 0.530351 | 1.531713 | 0.234473 | 0.500167 | 0.225643 |
| 10029.95 | 24.31876 | 21.0892 | 0.47345 | 1.861662 | 0.582666 | 0.580007 | 0 |
| 10030.95 | 41.3241 | 2.47986 | 0.551735 | 1.67166 | 0.943165 | 0.614493 | 0.62361 |
| 10031.95 | 42.64467 | 4.601091 | 0.383229 | 1.371451 | 0.157541 | 0.35219 | 0.564434 |
| 10032.95 | 36.36138 | 9.419658 | 0.400917 | 1.613813 | 0.607539 | 0.660823 | 0.665327 |
| 10033.95 | 42.14239 | 5.648563 | 0.435341 | 1.586553 | 0.24815 | 0.542542 | 0.580235 |
| 10034.95 | 22.40119 | 11.13993 | 0.166872 | 0.649787 | 0.02823 | 0.31806 | 0.780037 |
| 10035.95 | 31.89898 | 13.30138 | 0.306822 | 1.300554 | 0.448315 | 0.410952 | 0.669597 |
| 10036.95 | 38.92686 | 1.697871 | 0.452674 | 1.729595 | 0.264389 | 0.938246 | 0 |
| 10037.95 | 41.99063 | 3.600023 | 0.305999 | 1.266974 | 0.107229 | 0.39651 | 0.559211 |
| 10038.95 | 42.9636 | 3.451107 | 0.300516 | 1.36191 | 0.288604 | 0.436318 | 0.470651 |
| 10039.95 | 37.84603 | 9.163786 | 0.227617 | 1.356172 | 0.454537 | 0.511912 | 0.477991 |
| 10040.95 | 36.37205 | 10.59435 | 0.212092 | 1.334207 | 0.351119 | 0.689301 | 0.768776 |
| 10041.95 | 37.53698 | 9.128579 | 0.227966 | 1.390012 | 0.298065 | 0.66288 | 0.689826 |
| 10042.95 | 15.45317 | 17.42601 | 0.050775 | 0.487247 | 0.023386 | 0.330796 | 0 |
| 10043.95 | 25.0671 | 21.0792 | 0.160261 | 1.164578 | 0.195721 | 0.478658 | 1.118541 |
| 10044.95 | 23.87284 | 8.820207 | 0.179183 | 0.988733 | 0.342599 | 0.825949 | 0.66621 |
| 10045.95 | 28.14567 | 17.60399 | 0.115339 | 1.090813 | 0.414729 | 0.516038 | 0 |

Continued

| Depths (ft) | Si% | Ca% | K% | Al% | S% | Fe% | Mg% |
|---|---|---|---|---|---|---|---|
| 10068.95 | 416459.4 | 16209.98 | 2968.68 | 20588.4 | 743.86 | 9505.74 | 12018.39 |
| 10069.95 | 41.61773 | 2.331869 | 0.29683 | 1.937066 | 0.44558 | 0.926788 | 0.853608 |
| 10070.95 | 39.60675 | 4.14783 | 0.257627 | 2.068096 | 0.177316 | 1.271724 | 1.100184 |
| 10071.95 | 29.20258 | 15.13915 | 0.209861 | 1.789525 | 0.565794 | 0.942925 | 1.773393 |
| 10072.95 | 42.77383 | 1.901168 | 0.356396 | 2.256893 | 0.109623 | 0.989233 | 0.69721 |
| 10073.95 | 23.66864 | 23.01835 | 0.181078 | 1.427597 | 0.044232 | 0.551377 | 1.012524 |
| 10074.95 | 29.46737 | 14.13317 | 0.209269 | 1.673084 | 0.422196 | 1.116301 | 0.45389 |
| 10075.95 | 36.80378 | 6.756985 | 0.198391 | 1.724803 | 0.146776 | 1.260032 | 0.91056 |
| 10076.95 | 33.68764 | 7.603213 | 0.275437 | 2.368303 | 0.346385 | 2.424072 | 1.078389 |
| 10077.95 | 20.96548 | 25.933 | 0.149159 | 1.088917 | 0.133249 | 0.655756 | 0 |
| 10078.95 | 28.70323 | 14.70613 | 0.208979 | 1.629836 | 0.216279 | 1.40833 | 0.722525 |
| 10079.95 | 19.03888 | 27.79227 | 0.136142 | 1.080827 | 0.091507 | 0.654133 | 0 |
| 10080.95 | 38.32476 | 7.57996 | 0.274778 | 1.700457 | 0.270344 | 0.954984 | 0.835134 |
| 10081.95 | 37.03523 | 9.708873 | 0.205782 | 1.391478 | 0.191914 | 0.845136 | 0 |
| 10082.95 | 41.54116 | 1.962719 | 0.394538 | 2.13002 | 0.294682 | 1.135421 | 0.525458 |
| 10083.95 | 41.97816 | 2.079071 | 0.327406 | 1.959447 | 0.112194 | 1.137346 | 0.51234 |
| 10084.95 | 39.52393 | 4.72527 | 0.326058 | 1.977443 | 0.12143 | 1.043729 | 0.595686 |
| 10085.95 | 39.80578 | 1.229177 | 0.451918 | 2.578297 | 0.110618 | 1.562178 | 1.005258 |
| 10086.95 | 25.34293 | 20.88379 | 0.159487 | 1.392168 | 0.130285 | 0.665957 | 0.59232 |
| 10087.95 | 43.76569 | 2.154985 | 0.262319 | 1.782005 | 0.135736 | 0.789851 | 0.668352 |
| 10088.95 | 33.17548 | 13.09996 | 0.18528 | 1.397722 | 0.254922 | 0.731452 | 0.521214 |
| 10089.95 | 30.53807 | 15.36412 | 0.16198 | 1.338756 | 0.138699 | 0.771463 | 0.517492 |
| 10090.95 | 19.09404 | 27.03837 | 0.119762 | 1.023778 | 0.140545 | 0.74812 | 0.847257 |
| 10091.95 | 42.06105 | 1.572728 | 0.297833 | 1.791519 | 0.131171 | 1.103001 | 0.890571 |
| 10092.95 | 40.44946 | 2.874243 | 0.255977 | 1.559193 | 0.185113 | 0.982631 | 0.345217 |
| 10093.95 | 42.10131 | 1.656518 | 0.300753 | 1.73538 | 0.090581 | 1.019319 | 0.569941 |
| 10094.95 | 35.23097 | 2.262244 | 0.339801 | 1.935048 | 0.298798 | 1.303703 | 0.664977 |
| 10095.95 | 40.43242 | 2.780412 | 0.357657 | 1.954474 | 0.534885 | 1.359306 | 0.611167 |
| 10096.95 | 37.61302 | 6.278995 | 0.32652 | 2.007376 | 0.538107 | 1.230368 | 0.975219 |
| 10097.95 | 25.29111 | 19.76773 | 0.161319 | 1.409199 | 0.152141 | 0.672491 | 0.912277 |
| 10098.95 | 39.2891 | 3.683448 | 0.281798 | 1.761509 | 0.235605 | 0.939132 | 0.560321 |
| 10099.95 | 43.11848 | 3.366018 | 0.282519 | 1.819379 | 0.127569 | 0.8121 | 0.613416 |
| 10100.95 | 42.74044 | 2.881309 | 0.289644 | 1.808957 | 0.117054 | 0.800694 | 0.776338 |
| 10101.95 | 41.75951 | 3.731816 | 0.298177 | 1.948908 | 0.20831 | 1.217949 | 0.508085 |
| 10102.95 | 23.73194 | 22.83739 | 0.147357 | 1.377118 | 0.18361 | 0.50294 | 0.778321 |

Continued

| Depths (ft) | Si% | Ca% | K% | Al% | S% | Fe% | Mg% |
|---|---|---|---|---|---|---|---|
| 10103.95 | 0.945754 | 46.64357 | 0 | 0.256703 | 0.564038 | 0 | 0 |
| 10104.95 | 26.51656 | 21.83551 | 0.163199 | 1.337572 | 0.345772 | 0.79192 | 0 |
| 10105.95 | 40.92983 | 7.620998 | 0.168664 | 1.084288 | 0.157821 | 0 | 0.77173 |
| 10106.95 | 36.62126 | 12.32291 | 0.241156 | 1.390271 | 0.470643 | 0.841108 | 1.183918 |
| 10107.95 | 26.20129 | 23.48752 | 0.158657 | 1.208794 | 0.245627 | 0 | 0 |
| 10108.95 | 32.21871 | 2.606231 | 0.291874 | 1.659292 | 0.289643 | 1.573717 | 0.831913 |
| 10109.95 | 23.19373 | 25.21483 | 0.117534 | 1.081967 | 0.485211 | 0.635595 | 0.563926 |
| 10110.95 | 39.30499 | 7.279528 | 0.265026 | 1.929922 | 0.927663 | 1.133954 | 0.418069 |
| 10111.95 | 41.70651 | 1.418675 | 0.541912 | 2.845395 | 0.556219 | 1.723812 | 0.77743 |
| 10112.95 | 45.44718 | 1.022138 | 0.378817 | 2.062291 | 0.277072 | 1.050244 | 0.832636 |
| 10113.95 | 40.8247 | 1.28516 | 0.559972 | 2.706042 | 0.269635 | 1.763909 | 0.649368 |
| 10114.95 | 44.7218 | 1.89991 | 0.273353 | 1.728191 | 0.279906 | 0.878277 | 0.517584 |
| 10115.95 | 7.232432 | 39.44571 | 0.084287 | 0.744788 | 0.537171 | 0 | 1.303336 |
| 10116.95 | 35.25008 | 0.702025 | 1.395537 | 4.562321 | 1.068335 | 2.755355 | 0.680947 |
| 10117.95 | 35.55321 | 0.456822 | 2.20514 | 6.67537 | 1.814868 | 3.291159 | 1.30821 |
| 10118.95 | 26.72914 | 12.27898 | 0.191551 | 1.33119 | 0.281528 | 0.886927 | 0.853736 |
| 10119.95 | 35.15314 | 10.91557 | 0.308067 | 1.921162 | 0.278343 | 0.92938 | 0 |
| 10120.95 | 27.613 | 20.33771 | 0.161904 | 1.403959 | 0.17985 | 0.466042 | 0 |
| 10121.95 | 32.98976 | 13.99272 | 0.236302 | 1.558878 | 0.156567 | 0 | 0 |
| 10122.95 | 26.10994 | 21.0097 | 0.190372 | 1.542992 | 0.243115 | 0.540406 | 0.743735 |
| 10123.95 | 35.37518 | 0.480007 | 0.487355 | 2.601379 | 0.385278 | 2.395263 | 0.640173 |
| 10124.95 | 44.26361 | 2.963083 | 0.22661 | 1.52759 | 0.150472 | 0.698843 | 0.96851 |
| 10125.95 | 36.04854 | 1.300374 | 1.468541 | 5.536413 | 2.002793 | 3.131213 | 0.966085 |
| 10126.95 | 30.91628 | 16.98409 | 0.223326 | 1.483412 | 0.177359 | 0.650481 | 0.544339 |
| 10127.95 | 27.48491 | 18.82309 | 0.2155 | 1.592055 | 0.242253 | 0.754666 | 0.860592 |
| 10128.95 | 25.97959 | 21.36257 | 0.203957 | 1.571935 | 0.224898 | 0.705698 | 0.556955 |
| 10129.95 | 42.28632 | 4.673856 | 0.380944 | 2.08877 | 0.124798 | 0.832586 | 0.804544 |
| 10130.95 | 43.67359 | 2.85792 | 0.391445 | 1.904593 | 0.149667 | 0.736426 | 0.456556 |
| 10131.95 | 25.63331 | 22.68224 | 0.24402 | 1.572713 | 0.195271 | 0.770139 | 1.299468 |
| 10132.95 | 31.39969 | 3.2942 | 0.618613 | 2.707563 | 2.759041 | 2.267226 | 0.786372 |
| 10133.95 | 14.67775 | 33.70056 | 0.023256 | 0.676806 | 0.259898 | 0.424883 | 0.701181 |
| 10134.95 | 1.644835 | 43.46503 | 0 | 0.169439 | 0.192697 | 0.369062 | 1.234482 |
| 10135.95 | 27.0347 | 22.903 | 0.073698 | 0.910285 | 0.307848 | 0.440698 | 1.279823 |
| 10136.95 | 36.54216 | 5.708208 | 0.038512 | 0.553136 | 0.061864 | 0.228999 | 0 |
| 10137.95 | 50.94783 | 0.460938 | 0.078899 | 0.800914 | 0.194275 | 0.213168 | 0.471752 |

Continued

| Depths (ft) | Si% | Ca% | K% | Al% | S% | Fe% | Mg% |
|---|---|---|---|---|---|---|---|
| 10138.95 | 43.01713 | 0.327808 | 0.456894 | 2.699507 | 1.045786 | 1.575342 | 0.45063 |
| 10139.95 | 32.20213 | 0.848129 | 2.338581 | 7.478767 | 3.629617 | 3.296258 | 1.166368 |
| 10140.95 | 32.94584 | 0.306543 | 2.709745 | 8.103217 | 1.29195 | 2.864364 | 1.513482 |
| 10141.95 | 29.70556 | 1.148112 | 2.146744 | 6.690223 | 4.308455 | 2.788894 | 1.375326 |
| 10142.95 | 45.07396 | 0.301612 | 0.211226 | 1.434647 | 0.231094 | 0.779666 | 0.684783 |
| 10143.95 | 29.03637 | 0.793523 | 2.22425 | 6.908469 | 2.994596 | 3.269246 | 1.086904 |
| 10144.95 | 46.09378 | 0.864749 | 0.225116 | 1.494271 | 0.295695 | 0.618933 | 0.488281 |
| 10145.95 | 35.33018 | 0.193132 | 2.138303 | 7.164198 | 0.551539 | 2.917013 | 0.950724 |
| 10146.95 | 43.00828 | 4.905804 | 0.224591 | 1.8534 | 0.896335 | 1.231632 | 0.863836 |
| 10147.95 | 32.86681 | 6.618919 | 1.482492 | 5.346447 | 2.757843 | 3.234871 | 1.314154 |
| 10148.95 | 34.61012 | 1.032732 | 1.561903 | 4.978226 | 3.109458 | 2.505222 | 0.847837 |
| 10149.95 | 36.96797 | 1.817467 | 0.759037 | 2.871629 | 3.553178 | 1.798435 | 0.602506 |
| 10150.95 | 35.62833 | 2.481156 | 0.371766 | 2.400923 | 5.970536 | 3.341334 | 0.767784 |
| 10151.95 | 48.26519 | 2.178224 | 0.108362 | 1.156971 | 0.222366 | 0.322327 | 0.375716 |
| 10152.95 | 29.27137 | 0.323688 | 3.576091 | 10.81999 | 1.153316 | 3.526652 | 1.541289 |
| 10153.95 | 20.19915 | 27.14853 | 0.307486 | 1.73391 | 0.91287 | 1.033677 | 0 |
| 10154.95 | 36.29083 | 11.69138 | 0.26288 | 1.616349 | 0.690715 | 0.936096 | 0.643756 |

Appendix 2: XRD data

| Depth (ft) | Quartz (wt%) | Plagioclase (wt%) | K-feldspar (wt%) | Calcite (wt%) | Pyrite (wt%) | Dolomite (wt%) | Fe-Dolomite/Ankerite (wt%) | Illite/Mica/Glauconite (wt%) | Mix IS (wt%) | Chlorite (wt%) | Total Clays (wt%) |
|---|---|---|---|---|---|---|---|---|---|---|---|
| 9882.18 | 86.8 | 2.4 | 3.7 | 5 | | | | 2.1 | | 0 | 2.1 |
| 9888.35 | 83 | 5.9 | 5.3 | 3.7 | | | | 2.1 | | 0 | 2.1 |
| 9904 | 79.6 | 7 | 4.8 | 7.3 | | | | 1.3 | | 0 | 1.3 |
| 9913.1 | 64.8 | 3.3 | 0.6 | 1.2 | | | | 21.7 | 2.9 | 4.7 | 29.3 |
| 9916.2 | 58.1 | 7 | 1.3 | 0.8 | | | | 22.2 | 2.8 | 6.6 | 31.6 |
| 9922.1 | 43.9 | 5.4 | 0 | 1.8 | | | | 36 | 6 | 4.5 | 46.5 |
| 9930.4 | 89.4 | 3 | 3.4 | 1 | | | | 3.2 | | 0 | 3.2 |
| 9930.9 | 89.9 | 2.7 | 3.2 | 0.6 | | | | 3.6 | | 0 | 3.6 |
| 9939.9 | 87.3 | 4.3 | 2.2 | 4.2 | 0.6 | | | 0.8 | | 0.7 | 1.5 |
| 9945.9 | 82 | 7.9 | 4.3 | 3.6 | | | | 1.3 | | 0.9 | 2.2 |
| 9951.36 | 78.9 | 11 | 2.2 | 2.5 | | | | 3.8 | | 0.8 | 4.6 |
| 9963.25 | 35.9 | 2.4 | 1.5 | 58.7 | 2.1 | | 0.5 | 1 | | 0 | 1 |
| 9965.59 | 77.4 | 4.9 | 5 | 11.2 | | | | 1.5 | | 0 | 1.5 |
| 9986.4 | 18.3 | 0 | 0 | 80.1 | 2.9 | | 1.6 | 0 | | 0 | 0 |
| 9987.88 | 93.7 | 2.4 | 2.1 | 0.7 | 0.6 | | | 0.5 | | 0.6 | 1.1 |
| 9992.67 | 87.8 | 4.3 | 5 | 1.2 | | | | 0.7 | | 1 | 1.7 |
| 10012.55 | 42.3 | 6.3 | 0.7 | 50.1 | 0.6 | | | 0.6 | | 0 | 0.6 |
| 10024.88 | 77.4 | 6.7 | 7.3 | 1.2 | | | | 4 | | 2.9 | 6.9 |
| 10035.1 | 46.8 | 5 | 1.7 | 44.8 | | | | 1.7 | | 0 | 1.7 |
| 10043.4 | 54.3 | 8.3 | 0 | 36.3 | 0.5 | | | 0.6 | | 0.5 | 1.1 |
| 10048.11 | 74.7 | 7.8 | 1.3 | 14.1 | | | | 1.1 | | 1 | 2.1 |
| 10069.49 | 82.8 | 10 | 0 | 1.8 | | | 0.5 | 1.8 | | 3.1 | 4.9 |
| 10076.79 | 60.3 | 7 | 0.8 | 27.3 | 0.5 | | | 1.2 | | 3.4 | 4.6 |
| 10093.62 | 78.8 | 10.5 | 1.1 | 2.2 | | 0.8 | | 2.7 | | 3.9 | 6.6 |
| 10105.13 | 54.2 | 7.3 | 0 | 33.5 | 0.8 | | | 2 | 0.5 | 2.5 | 5 |
| 10124.5 | 78 | 10 | 1.9 | 4.5 | 0.7 | | 3.2 | 1.8 | | 0.6 | 2.4 |
| 10133.31 | 14.1 | 2.5 | 0 | 79.1 | 2.9 | | | 1.6 | | 0 | 1.6 |
| 10134.68 | 0.8 | 0 | 0 | 96.8 | | | 2.4 | 0 | | 0 | 0 |
| 10143.43 | 86.3 | 6.5 | 1.3 | 2.7 | | | | 1.7 | | 1.5 | 3.2 |
| 10150.1 | 85.6 | 7.7 | 0 | 1.7 | | | | 2.7 | | 2.3 | 5 |

Appendix 3: Well data

| API_UWI | Latitude | Longitude | Latitude_BH | Longitude_BH | TVD_FT |
|---|---|---|---|---|---|
| 17-119-20691 | 32.92135 | -93.268992 | 32.92135 | -93.268992 | 12000 |
| 17-027-22020 | 32.89426 | -93.228761 | 32.89426 | -93.228761 | 9400 |
| 17-027-20830 | 32.8962 | -93.184686 | 32.896196 | -93.184686 | 9500 |
| 17-027-01931 | 32.85589 | -93.19374 | 32.855892 | -93.19374 | 11967 |
| 17-027-22022 | 32.85677 | -93.19939 | 32.856771 | -93.19939 | 9437 |
| 17-027-22400 | 32.8536 | -93.209763 | 32.8536 | -93.209763 | 10650 |
| 17-027-22265 | 32.94423 | -93.234181 | 32.944226 | -93.234181 | 12000 |
| 17-119-20355 | 32.91184 | -93.241868 | 32.911836 | -93.241868 | 12400 |
| 17-119-21631 | 32.91713 | -93.24384 | 32.917129 | -93.24384 | 9778 |
| 17-027-20761 | 32.89249 | -93.19003 | 32.892488 | -93.19003 | 9500 |
| 17-027-22589 | 32.87436 | -93.21971 | 32.862029 | -93.219496 | 10600 |
| 17-027-20220 | 32.93649 | -93.22484 | 32.936485 | -93.22484 | 11445 |
| 17-027-20849 | 32.85414 | -93.226986 | 32.854135 | -93.226986 | 9500 |
| 17-119-21981 | 32.93275 | -93.283926 | 32.932752 | -93.283926 | 10000 |
| 17-027-22384 | 32.87011 | -93.212794 | 32.870108 | -93.212794 | 10600 |
| 17-027-01932 | 32.85609 | -93.176441 | 32.856092 | -93.176441 | 10507 |
| 17-119-21888 | 32.95108 | -93.296196 | 32.951078 | -93.296196 | 11825 |
| 17-027-22260 | 32.9374 | -93.234061 | 32.9374 | -93.234061 | 12000 |
| 17-027-20808 | 32.85167 | -93.216077 | 32.851669 | -93.216077 | 9580 |
| 17-027-20174 | 32.90689 | -93.228141 | 32.906886 | -93.228141 | 12500 |
| 17-027-20851 | 32.84438 | -93.224736 | 32.844378 | -93.224736 | 10280 |
| 17-027-21468 | 32.86758 | -93.212138 | 32.867581 | -93.212138 | 10650 |
| 17-027-21527 | 32.87403 | -93.188217 | 32.87403 | -93.188217 | 10750 |

Appendix 4: Point Count data on thin section.

| Sample No. | Depth (ft) | Depth (m) | Calculated (Quartz, Feldspar & Rock fragment) | | | |
|---|---|---|---|---|---|---|
| | | | Quartz % | Feldspar % | Rock fragment (%) | |
| 1 | 10149.8 | 3093.6 | 99 | 1 | 0 | |
| 2 | 10143.29 | 3091.7 | 99 | 1 | 0 | |
| 7 | 10104.98 | 3080 | 95 | 0 | 5 | |
| 8 | 10089.3 | 3075.2 | 90 | 0 | 10 | |
| 9 | 10076.68 | 3071.4 | 95 | 0 | 5 | |
| 10 | 10069.6 | 3069.2 | 100 | 0 | 0 | |
| 11 | 10048.23 | 3062.7 | 97 | 0 | 3 | |
| 12 | 10043.6 | 3061.3 | 94 | 1 | 6 | |
| 13 | 10035.28 | 3058.8 | 93 | 2 | 5 | |
| 14 | 9986.3 | 3043.82 | 99 | 0 | 1 | |
| 15 | 9970.65 | 3039.1 | 98 | 0 | 2 | |
| 16 | 9964 | 3037 | 100 | 0 | 0 | |
| 17 | 9948 | 3032.2 | 96 | 0 | 4 | |
| 18 | 9940 | 3029.7 | 100 | 0 | 0 | |
| 19 | 9930 | 3026.7 | 100 | 0 | 0 | |
| 23 | 9892 | 3015.1 | 93 | 0 | 7 | |
| 24 | 9885 | 3012.9 | 95 | 2 | 3 | |
| 25 | 9879.92 | 3011.4 | 97 | 1 | 2 | |
| **Sample No.** | **Depth (ft)** | **Depth (m)** | **Calculated (Fossils, Intraclasts, Pellets & Oolites)** | | | |
| | | | Fossils % | Intraclasts % | Pellets % | Oolites % |
| 4 | 10134.52 | 3089 | 95 | | 5 | |
| 5 | 10133.2 | 3088.6 | 90 | | 10 | |
| **Sample No.** | **Depth (ft)** | **Depth (m)** | **Calculated (Silts and clay)** | | | |
| | | | Silt % | Clay % | | |
| 3 | 10138.5 | 3090 | 90 | 10 | | |
| 6 | 10124.8 | 3086 | 90 | 10 | | |
| 20 | 9920 | 3023.6 | 90 | 10 | | |
| 21 | 9917 | 3022.7 | 60 | 30%-40% | | |
| 22 | 9911.25 | 3021 | 60 | 30%-40% | | |

## 12.0 VITA

Frederick Owusu graduated from Mfantsipim School in Cape-coast, Ghana. He gained admission to the University of Ghana in August 2008, to earn a Bachelor of Science degree in Geology. During undergraduate studies, he worked as a Geology intern at AngloGold Ashanti Mines, Iduapriem-Tarkwa. After undergraduate studies, he worked as a Teaching Assistant at the University of Ghana. Frederick enrolled in the Geology Masters program at Stephen F. Austin State University and graduated in May 2024.

Permanent Address: House no 24, Jonfiah Street, West Anaji, Takoradi.

Style Manual: GSA

This thesis was typed by Frederick Owusu